IRAS

SMALL SCALE STRUCTURE

CATALOG

Prepared under the supervision of the
Joint IRAS Science Working Group (JISWG)

The Joint IRAS Science Working Group was composed of:

G. Neugebauer	1977-1984	Co-chairman 1977-1984
R. J. van Duinen	1977-1982	Co-chairman 1977-1982
H. J. Habing	1977-1984	Co-chairman 1982-1984

H. H. Aumann	1977-1984	T. de Jong	1977-1984	P. R. Wesselius	1982-1984
D. A. Beintema	1977-1984	F. J. Low	1977-1984	B. Baud	1982-1984
N. Boggess	1977-1984	P. L. Marsden	1977-1984	C. A. Beichman	1982-1984
J. Borgman	1977-1981	S. R. Pottasch	1977-1983	T. N. Gautier	1982-1984
P. E. Clegg	1977-1984	B. T. Soifer	1977-1984	S. Harris	1982-1984
F. C. Gillett	1977-1984	R. G. Walker	1977-1984	G. K. Miley	1982-1984
M. G. Hauser	1977-1984	J. P. Emerson	1977-1984	F. M. Olnon	1982-1984
J. R. Houck	1977-1984	E. Raimond	1979-1984	E. T. Young	1982-1984
R. E. Jennings	1977-1984	M. Rowan-Robinson	1979-1984		

IRAS

SMALL SCALE STRUCTURE

CATALOG

Catalog Prepared by

George Helou

and

D. W. Walker

Introduction Edited by

George Helou

PREFACE

The attached Introduction describes the Small Scale Structure Catalog and is being released in a preliminary version, as the Catalog itself is being released in the tape version. A hard-bound version of this document and the Catalog itself will be released in 1986.

Any reader who finds errors in the text or the Catalog is requested to communicate such errors promptly to:

George Helou
IPAC, 100-22
California Institute of Technology
Pasadena, California 91125

TABLE OF CONTENTS

INDEX OF TABLES

INDEX OF FIGURES

I. INTRODUCTION

The primary mission of the Infrared Astronomical Satellite (IRAS) was to conduct a sensitive and unbiased survey of the sky in four wavelength bands at 12, 25, 60, and 100 μm. Launched in January 1983, IRAS ceased operations in November 1983 after having successfully surveyed 96% of the sky. The IRAS mission, the data processing, and the products are described in detail in the *Explanatory Supplement to the IRAS Catalogs and Atlases* (*Vol. I* of this series), with which the reader is assumed to be familiar. References to chapters and sections in the *Supplement* are given here prefixed with Suppl., e.g., Suppl.I.A.

Results from the IRAS survey are presented in various forms depending primarily on the angular scale of interest. They include a catalog of infrared point sources (the Point Source Catalog), the present Small Scale Structure Catalog (hereafter the SSS Catalog or the Catalog), and an atlas of absolute surface brightness images of the infrared sky (the Sky Brightness Images). The Point Source Catalog contains some 250,000 entries resulting from a search for spatially unresolved sources in the survey data. At the other extreme, the Sky Brightness Images display the large scale appearance of the sky with a resolution of 4′. The SSS Catalog attempts to fill the gap by listing sources resolved in any band up to a maximum size of 8′, aiming in particular at an adequate description of the infrared emission from objects such as galaxies, planetary nebulae or compact HII regions. Given the complexity of the infrared sky and the infinite variety of source shapes, the scope of a SSS Catalog remains by necessity vaguely defined, quite apart from technical problems posed by the specifics of telescope design and operation. This introduction describes the Catalog and the manner in which it was constructed, discusses the uncertainties in the various quantities listed, and gives a statistical overview of the sources in the Catalog.

The Small Scale Structure Catalog contains 16,740 sources which point out directions on the sky where IRAS resolved emission on the scale of 2′ to 8′, in at least one of the four bands, in a reliable and unconfused manner. Although the objective was to find intuitively acceptable "small extended sources", the Catalog entries are in fact defined by excursions in sky brightness detectable above the local baseline on spatial scales smaller than about 8′, excluding point sources. The Catalog lists for each entry and in each band separately: a position accurate to about one arcminute (rms); a flux density accurate to 50% (rms) overall, and better at high signal to noise ratios; a rough indicative size if a point source is present at the same location; and a variety of warning and processing flags. Completeness in the Catalog is not estimated since it varies with position on the sky as a function of source density and number of survey coverages. Fewer than 3% of the Catalog entries are unreliable. Almost all of these are weak point sources broadened by radiation hits or detector noise.

In spite of every effort to select only resolved, well-defined, and isolated sources for inclusion in the Catalog, a few problems remain. At low signal to noise ratios, the processor may have erred in deciding whether a source is resolved or not. Many entries, mostly at 60 and 100 μm refer only to emission features that are details in larger structures known as Galactic cirrus. Naturally, some close double and multiple point sources appear in the Catalog. There is also some evidence for flux densities at 12 and 25 μm being overestimated by 0.5 to 1 Jy. The greatest amount of caution perhaps is required in interpreting the *absence* of an entry in this Catalog, in one or in all bands. Incompleteness is a complex function

of band, brightness, and location so an absence does not necessarily imply the lack of detectable extended emission in any band.

While Small Scale Structure cannot be defined or measured with the same finality as point sources, Catalog entries always represent correlated and confirmed events in the detector output, making them valuable pointers to the IRAS images and raw data. The SSS processor has distilled from the survey a wide variety of objects and provided reasonable estimates of their parameters, but if a detailed shape description, or a more accurate position, flux, or size are needed, it is necessary to go back to the fundamental reference, the raw detector output.

The algorithms used to detect and measure the entries in this Catalog are described in Suppl.V.E, and summarized in Chapter II. Chapter III examines the detection processing to assess the types of sources detected and the influence of noise on their reliability. Chapter IV describes the strategy used to select the most reliable sources for the Catalog from the larger pool of confirmed detections. Chapter V provides an overview of the statistical properties of the Catalog, a comparison with other IRAS data products, and estimates for the accuracy of the measured quantities. Chapter VI discusses reliability and completeness. Chapter VII details the formats of the printed and machine-readable versions of the Catalog.

II. PROCESSING AND CALIBRATION OVERVIEW

Detections at spatial scales larger than the point source response of IRAS were used to locate and measure stationary, unconfused emission resolved by the detectors but smaller than 8′. As described in Suppl.V.E, the data stream from each detector was scanned with zero-sum square-wave filters in order to identify candidate detections (*source detection*). Confirmation was sought for each candidate detection on another detector along the same scan track a few seconds later (*seconds confirmation*). All confirmed detections within roughly a 36 hour period were assembled to construct a model of the source (*source construction and hours confirmation*). An effort was then made to discard sources that were confused, larger than 10′, or fragments of larger structures (*cluster analysis*). Survey coverages of the same area of the sky made by the satellite weeks or months apart were treated identically then used to enforce the third confirmation requirement (*weeks confirmation*). Each of the four bands was also treated separately and identically, and counterparts for weeks-confirmed sources in one band were sought among confirmed sources in the other bands (*band merging*). Entries were finally selected for inclusion in the Catalog based on their total flux and their confirmation history at the hours and weeks level (*final source selection*).

The basic design of SSS detection processing in the IRAS data was analogous to Point Source processing, but with reduced spatial resolution and no shape discrimination. More radical differences between SSS and Point Source processing intervened beyond source recognition. *Hours confirmation* was two-dimensional. *Cluster analysis deleted* potential sources in crowded regions. *Weeks confirmation* and *band merging* were carried out in reverse order to Point Source processing, thus accounting for the absence of upper limits in non-detected bands.

A. Source Detection

As detailed in Suppl.V.E.1, calibrated detector data were repeatedly compressed to retain only progressively lower spatial frequencies, and passed at every iteration through an eight point, symmetric, zero-sum filter. When the filter was applied to the original detector output, it enhanced sources about 1′ wide at 12 and 25 μm, sources about 2′ wide at 60 μm, and sources about 4′ at 100 μm. At each iteration each pair of consecutive samples in the data was averaged and the resulting stream was passed through the filter. This averaging procedure was carried out four times for the 12 and 25 μm data, three times for the 60 μm data, and twice for the 100 μm data. Thus, at 12 and 25 μm, enhanced sources were approximately 2′, 4′, 8′ and 16′ wide after each iteration. At 60 μm, they were 4′, 8′ and 16′ wide. At 100 μm, they were 8′ and 16′ wide. Note that the technique of compressing the stream then applying the same filter is equivalent to using a filter that is twice as wide, but applying it only at every other data point. While increasing the computational speed, the technique decreases the spatial resolution in the filtered data by a factor of 2 at each iteration.

Noise in each filtered data stream was estimated using a simple linear noise estimator. The median of the first 50 maxima in an observation was used as the initial estimate. This estimate was updated at each maximum thereafter by reducing (or increasing) the estimate by multiplication (or division) by a constant if the maximum was greater (or less) than the noise. This constant was 0.95 for the 12, 25, and

60 μm bands, and 0.9 for the 100 μm band. Maxima in the filtered data streams whose post-filter signal to noise ratios exceeded a threshold of 2.0 were saved for comparison processing. Since the actual signal to noise ratio is 1.83 times the post-filter ratio, the actual signal to noise threshold for accepting candidate detections was about 3.66 (This threshold is erroneously quoted as 3 in Suppl.V.E.1)

The comparison processing proceeded from the least compressed filtered data stream (narrowest detections) to the most compressed. Comparisons were made only between maxima in two consecutive data streams, and only if the maxima were separated by no more than five samples of the less compressed data stream. The detection with the largest maximum was chosen as the best representation of the source. Point sources and sources with a characteristic size of 16′ or greater were not passed on to the confirmation processing step. Note that the comparison scheme allowed multiple detections at the same position from the same detector, as long as the detections were not in consecutive data streams. For example, at 12 and 25 μm both 2′ and 8′ detections could be registered from the same detector at the same position, possibly corresponding to the superposition of two sources of different widths.

An additional scheme was used to attempt to separate superpositions of sources. If the maxima between consecutive (in the compression sequence) filtered data streams were "slowly varying", i.e. the amplitude decreased more slowly than a threshold value of 0.67 per compression step, then the series of maxima was marked as a slowly varying chain and the last maximum in the sequence was selected as the best representation of the source. As implemented, this technique could only produce 8′ wide sources in the 12 and 25 μm bands, and produced nothing in the 60 and 100 μm bands. Note that a bright point source would have produced a sequence of detections decreasing in amplitude by a factor 2 at each consecutive compression step.

B. Subsequent Processing

Only potential detections that were seconds confirmed (Suppl.V.E.2) were considered for further processing. Each detection was assigned a solid angle defined by the detector width in the cross-scan direction and its template width (2′, 4′, or 8′) in the scan direction. Positional overlap between two detections from two different detectors was the only condition for *seconds confirmation.* No confirmation in the strict sense of Point Source processing was sought at the hours time-scale.

Using the sizes assigned to those detections, a model for the source was constructed by piecing together all overlapping detections from the same band and the same hours-confirming coverage (Suppl.V.E.3). The model consisted of a representation of the intensity distribution on a grid with 1′ square pixels. If the source was found to be clearly bounded, contained well within the grid, and above the threshold values of signal to noise ratio and confirmation level (see Suppl.V.E.3 for a definition), it was added to the file of intermediate small extended sources (FISES). The minimum confirmation level requirement usually implies a confirmation requirement at the hours time scale. The only quantities kept from the model were: total flux from the zero'th moment, centroid position from the first moments, and major, minor diameters and orientation from the diagonalized matrix of second moments. These diameters would eventually be interperted as the positional uncertainty for the source (see V.C.3).

Cluster analysis processing (Suppl.V.E.4) was then applied to FISES in an effort to verify that its entries were well-defined and relatively isolated. Clusters of entries at the same wavelength and from the

same hours confirming coverage were identified and merged; if the resulting source exceeded about 10′ in diameter it was rejected from further processing.

Thus only small clusters and isolated entries were considered for *weeks confirmation* (Suppl.V.E.5), which required both positional and flux agreement. When sources were merged in *cluster analysis* or *weeks confirmation*, their fluxes, positions, and positional uncertainty matrices were combined in an extension of the original definitions of these quantities. *Band merging* (Suppl.V.E.6) operated on the weeks-confirmed sources with the same positional agreement requirement used in *weeks confirmation.* Occasionally, the processing led to a source containing more than one component from the same band (see Suppl.V.E.6 for details); these complications were resolved during *final source selection* for the Catalog.

The thresholds used in each of *cluster analysis*, *weeks confirmation* and *band merging* were chosen to enhance reliability (Suppl.V.E.7). *Final source selection* was applied next as discussed in detail in Chapter IV; its purpose was to select for inclusion in the Catalog sources with repeatability or fluxes indicating higher reliability.

Table II.B.1 gives an overview of the processing in terms of the number of entries involved at each step, at each of the four wavelengths. The last line, labeled "merged", gives the number of sources into which sources in the individual bands were combined. The percentages of FISES entries discarded by *cluster analysis* were 34%, 32%, 51%, and 34% respectively at 12, 25, 60, and 100 μm. The percentages of surviving sources or small clusters rejected by *weeks confirmation* were 75%, 73%, 55%, and 42%, respectively.

TABLE II.B.1 Processing Overview

Band	---------- Number of Entries after Each Step ----------			
	Seconds Confirmation	*Cluster Analysis*	*Weeks Confirmation*	*Final Selection*
12μm	116,342	65,957	7,160	3,071
25μm	124,464	71,543	8,057	3,762
60μm	226,400	87,365	16,789	8,334
100μm	154,959	82,039	19,549	10,882
Merged			39,355	16,740

C. Calibration Philosophy

Chapter VI of the Supplement presents a detailed description of the calibration procedure for the IRAS data, including the Small Scale Structure Catalog (Suppl.VI.B.2). In summary, the amplitude of the extended detections multiplied by the filter width in arcminutes was interpreted as the integral of the signal above the baseline. The total signal computed after *source construction* was treated like signal from a point source, except for a uniform correction to account for the variation of responsivity with source

size. As discussed in Suppl.IV.A, detector responsivity is a function of the duration for which the detector is exposed to a source. This dwell time dependence (Figure Suppl.IV.A.4.1) was obtained from data where point sources were scanned by the telescope at varying speeds. By analogy, extended sources scanned at the survey rate caused a response characteristic of a longer dwell time since they illuminated each detector for a longer time than a point source. Using Figure Suppl.IV.A.4.1, 10% and 8% increases in responsivity were assumed at 12 and 25 μm, respectively, corresponding to sources typically four times wider than the nominal point source template. The uncertainties resulting from such a uniform correction disregarding size variations are negligible compared with the photometric uncertainties due to the detection and source assembly schemes. As indicated by Figure Suppl.IV.A.4.2, a similar correction could not be defined at 60 and 100 μm.

Note that the flux densities appearing in the SSS Catalog are obtained from the fluxes in the IRAS bands assuming $\nu \times f_\nu$ = constant (Suppl.VI.C). In order to obtain the actual flux density at the nominal wavelength in each band, numbers in the Catalog must be corrected according to the prescription in Suppl.VI.C, or by using Table Suppl.VI.C.6 which is reproduced at the end of this volume.

III. ANALYSIS OF DETECTION PROCESSING

This chapter discusses the results of numerical simulations aimed at understanding the properties of the SSS *source detection* processor. The simulations attempt to describe in broad terms what features in a detector stream would be recognized as candidate extended sources. They show the full width at half maximum (FWHM) of extended sources recognized by *source detection* is a strong function of their shape (III.A). The narrowest sources recognized have a FWHM ranging from 20% to 50% wider than a point source. The largest sources recognized have a FWHM ranging from 6′ to 10′. Pairs of point sources lined up in the scan direction and separated by roughly 1′ to 5′ could be detected as a single extended source (III.B). Gaussian detector noise, alone or combined with weak point sources, could cause extended detections (III.C). These spurious detections occurred with a sufficiently low frequency that they could be cleaned out of the Catalog in the course of *final source selection.* The effects of radiation hits were not simulated, although they are an important source of spurious detections.

The figures in this Chapter show simulation results for the 12 and 25 μm bands only, but can be scaled exactly to obtain the results for the other bands. To read results at 60 μm, all scales in arcminutes should be multiplied by two, remembering that detections were kept only from the data streams compressed once or twice ($\lesssim 8'$). For 100 μm, all scales should be multiplied by four remembering that detections were kept only from the once compressed data stream ($\sim 8'$). The slight variations in the detailed shape of point source response from band to band are negligible and are not considered here.

A. Response to Extended Sources

For this simulation, sources were assumed to have simple shapes (Gaussian, triangle, exponential, square wave) in the scan direction and to be thin in the cross-scan direction; the assumed source shape was convolved with the telescope point spread function then fed into the detection processor as noiseless detector output. The response of the processor is illustrated in Figure III.A.1 for a Gaussian and Figure III.A.2 for a square wave shape, respectively. Figures III.A.1 and III.A.2 show the amplitude of a source in the filtered data streams at each level of compression, as a function of the width of a source with constant peak amplitude. A heavy line indicates the range of spatial extents where an amplitude would constitute an accepted detection in the given filter. Because the simulated source has a total flux proportional to its width, the amplitude from one filter level to the next remains roughly constant. For the same reason, filter amplitude rises linearly as long as the filter is wider than the source and thus contains most of the emission. The amplitude is accepted as a detection just as source and filter become of comparable width at which point the amplitude starts underestimating the total emission in the source. The departure of the filter amplitude from a straight line in the range where a detection is accepted from that filter defines a fundamental limit on the photometric accuracy, since flux estimation is based on these detection amplitudes. The largest under-estimation possible is on the order of 50%. This effect is evidently over-shadowed by other, random errors in flux estimation. For a discussion of final photometric uncertainties, see V.C.1.

As may be seen on Figure III.A.2, detections from a narrow filter can appear even when a square wave source is wider than that filter; these detections are due to the sharp corners leading and trailing the

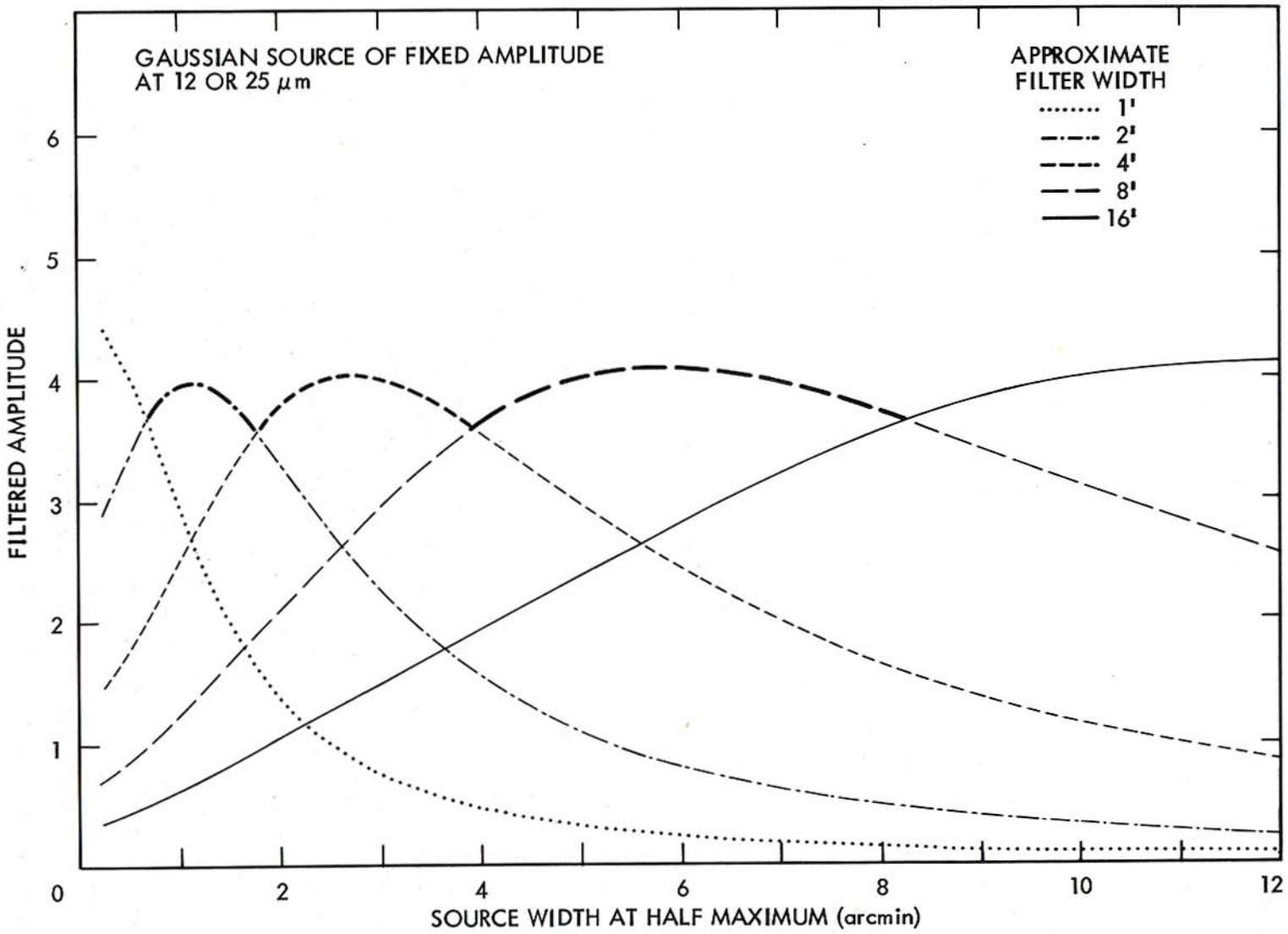

Figure III.A.1 Response of SSS *source detection* processor as a function of the intrinsic full width at half maximum of a Gaussian shaped source. The different lines refer to the variously filtered data streams that each enhance sources of a particular spatial extent. The thicker lines show the range of source extents that would result in a detection in a given filtered data stream. As discussed in the text, the horizontal scale is correct for 12 and 25 μm, but must be doubled for 60 μm detections and quadrupled for 100 μm detections.

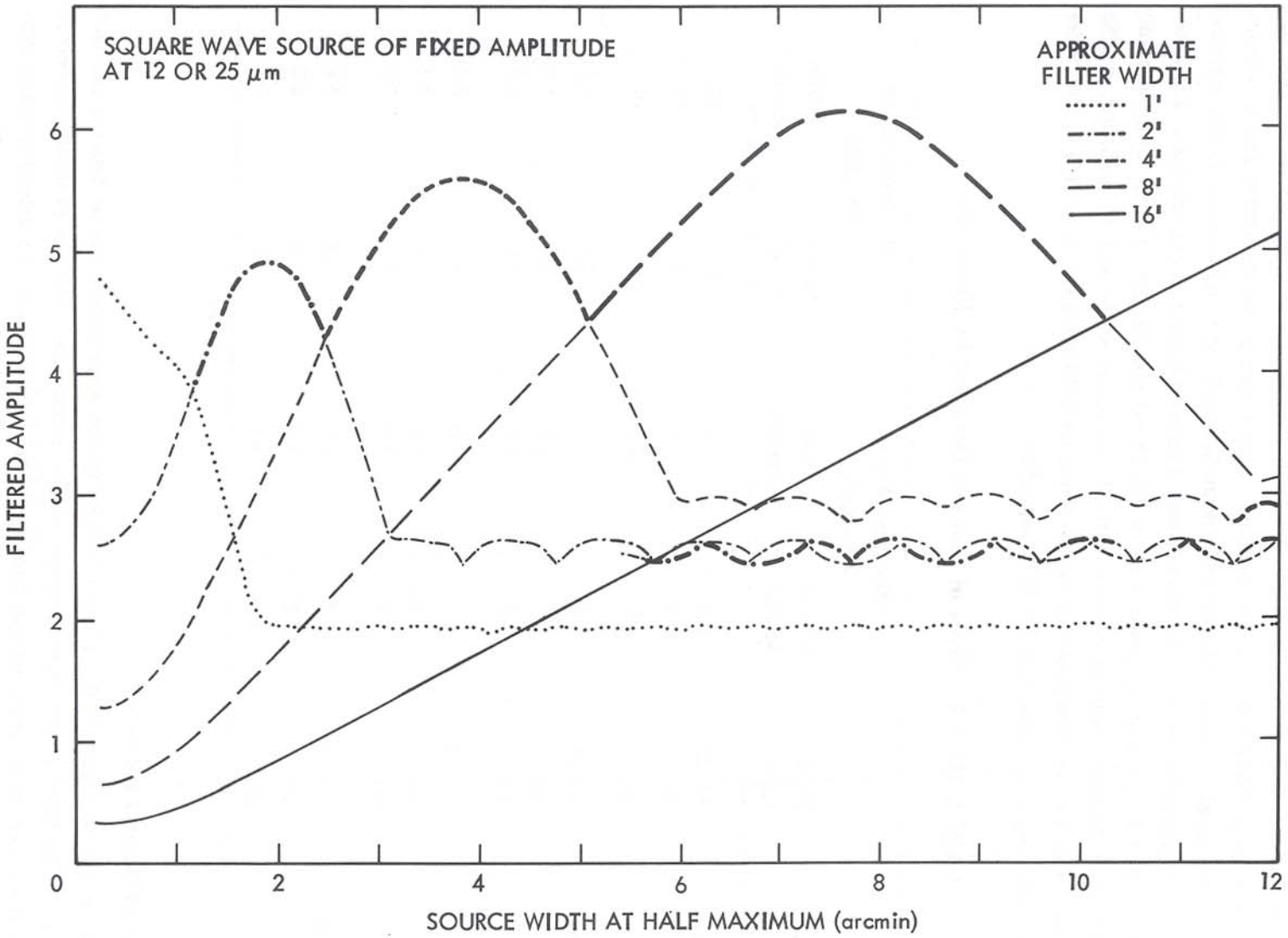

Figure III.A.2 Response of SSS *source detection* processor as a function of the intrinsic full width at half maximum of a square wave shaped source. See caption for Fig. III.A.1 for details.

source. These detections are repeatable and could confirm to become examples of Catalog entries that refer to details in larger structures.

Table III.A.1 summarizes the results of the detection simulations; it shows for each shape the minimum and maximum FWHM that can be detected. Under each of the minimum and maximum headers, the columns labeled "Source Model" and "Beam-Smeared" refer respectively to the intrinsic source width and the source width after convolution with a detector's point source response. The latter has a FWHM of 0.8′, 0.8′, 1.6′ and 3.2′ respectively at 12, 25, 60 and 100 μm. Clearly, minimum and maximum FWHM of detectable sources depends critically on source shape and, in particular, on the existence of wings as in the case of exponential shape. Minimum FWHM ranges from 20% to 50% wider than the point source response. Maximum FWHM ranges from 6′ to 10′.

TABLE III.A.1 Sizes of Sources Detected by Processor

		Minimum Width FWHM(′)		Maximum Width FWHM(′)	
Source Shape	Band (μm)	Source Model	Beam-Smeared	Source Model	Beam-Smeared
Square Wave	12, 25	1.2	1.2	10.	10.
	60	2.3	2.3	10.	10.
	100	4.6	4.7	10.	10.
Triangular	12, 25	0.9	1.1	7.7	8.1
	60	1.7	2.2	7.6	8.4
	100	3.5	4.5	7.5	8.5
Gaussian	12, 25	0.7	1.0	8.3	8.3
	60	1.3	1.9	7.9	8.1
	100	2.7	3.9	7.1	7.5
Exponential	12, 25	0.4	1.0	5.8	6.2
	60	0.8	1.9	5.4	6.2
	100	1.5	3.8	4.6	6.5

B. Response to Double Point Sources

As may be seen on Figure III.B.1, a pair of closely spaced point sources can be detected as a small extended source. The figure illustrates the response of the processor as a function of separation between two noiseless point sources of equal strength lined up in the scan direction. An extended source detection can be returned with the point sources located less than one arcminute apart. The maximum separation still causing an extended detection varies between 4′ and 5.5′ depending on the band. Similar simulations show that as the ratio of amplitudes between the two point sources increases, the range of

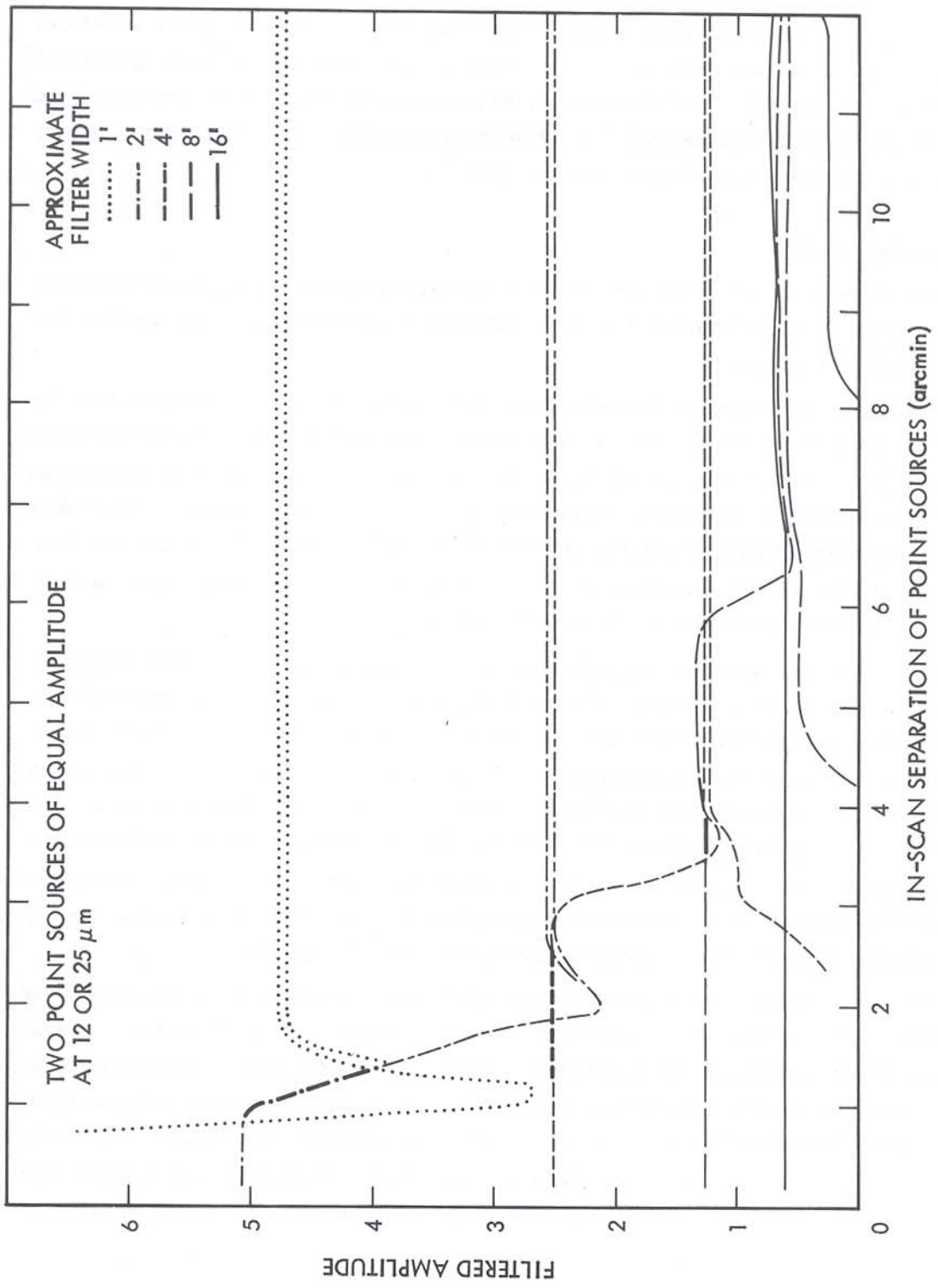

Figure III.B.1 Response of SSS *source detection* processor to two equal point sources as a function of separation between them. See caption for Fig. III.A.1 for details.

separations allowing extended detections shrinks until it is negligible for a ratio of 10 to 1.

Based on the results of this simulation, the following necessary but insufficient conditions were derived that would apply in the case of a pair of point sources detected as an extended source: (i) the two point sources are within 5′ of each other in the scan direction, and positioned on either side of the "extended source"; (ii) they are within 5′ of each other in the cross-scan direction and on either side of the "extended source", so a single detector can pick both of them up in a single scan. These conditions were used to flag sources in the course of *final source selection* (IV.B.2.e).

C. Noise Induced Detections

The behavior of the processor in the presence of noise was also tested, using a Gaussian (white) noise component; it was estimated that the $1/f$ noise contribution to the 8′ filtered data was less than 10%, and could therefore be neglected.

In the first test, when a data stream of simulated pure noise was fed through the processor, with the post-filter signal to noise ratio threshold set at 2.0, the processor returned 0.66, 0.66, 0.51, and 0.36 detections per minute of data (or 3.85° of sky) at 12, 25, 60, and 100 μm, respectively. Because of their random nature, these spurious detections were weeded out by the multiple confirmation requirements: disregarding all other thresholds, at most 100 spurious weeks-confirmed sources could have resulted at 12 and 25 μm, less than ten at 60 μm, and none at 100 μm. These remaining spurious sources would be discarded by *final selection* processing (Chapter IV).

The second test was an attempt to determine how frequently a point source combined with noise would be detected as a small extended source. When a weak point source was introduced into the simulated noise data stream described above and the data was fed through the detection processor, a clear enhancement in the number of spurious detections was found. This enhancement peaked for sources with a signal to noise ratio of three to four, and vanished for sources with a ratio of seven or more. This class of spurious detections is harder to deal with for they repeat at the same positions and could pass the confirmation requirements more frequently. The simulations showed however that a faint point source generated an extended detection only once out of every six or seven times it was scanned; this made it possible to find selection rules that weeded out these spurious detections (Chapter IV).

Probably the worst cause of spurious detections was radiation hits. Like Gaussian noise, they could cause false detections due to two hits in succession or could combine with point sources to cause extended detections; these detections were not, however, limited to low flux levels. Radiation hits also tended to add artificially to the flux in a detection, especially because the detection with (locally) maximal amplitude was chosen; this meant that hits were preferentially accepted rather than rejected. Moreover, their effects could be felt more heavily in certain areas of the sky (See Suppl.III.C and Suppl.IV.A.6) which were always surveyed while the satellite was likely to be subjected to a high density of radiation hits.

IV. FINAL SOURCE SELECTION

A. Problems and Their Solutions

A.1 Overview

Along with the versatility required of a detection algorithm for sources of unspecified shape, the Small Scale Structure processor possessed the undesirable property of allowing through spurious detections resulting from processing artifacts or instrumental effects. These spurious entries had to be eliminated by a careful selection of the sources to appear in the final Catalog. *Final selection* processing was constrained to use the limited information available in the intermediate file of small extended sources (FISES) (Suppl.V.E.3 and II.B) while attempting to remove unreliability which had its roots in the earliest stages of *source detection* processing.

As described in Chapter II, the *source detection* processor located sources by seeking maximum amplitude over both time (position) and frequency (filter width). This made the processor extremely susceptible to error in the presence of radiation hits (Suppl.IV.A.6), liable to detect as extended structure weak point sources combined with noise, and biased toward flux over-estimation. Particularly important differences from the point source detection processor that resulted in low reliability were:

(i) lack of template fitting,

(ii) multiple filter search (II.A, Suppl.V.E.1),

(iii) lack of strict requirement for *hours confirmation* (II.B, Suppl.V.E.3),

(iv) relaxed positional requirement and absence of flux or size test at *seconds confirmation* (II.B, Suppl.V.E.2), and

(v) low thresholds leaning towards completeness at the expense of reliability in the *source detection* and *source construction* algorithms (Suppl.V.E.1, 2, and 3).

A.2 Manifestations of Unreliability

Most spurious detections were rejected at *weeks confirmation* (II.B), but the list of weeks-confirmed, band merged sources still required a final processing step to remove unreliable entries. One class of problem entries, optical cross-talk, was flagged but not removed at the detection level; cross-talk removal is discussed in IV.B.2.a below. The other main class of problems, noise induced detections, was anticipated on the basis of the simulations in III.C to be mainly of two kinds: detections of noise and radiation hits confirmed with more of the same, and weak point sources broadened by noise and radiation hits. While there was no simple way to recognize them individually, these unreliable entries manifested themselves in statistically useful patterns:

i) Too many entries at ecliptic poles

All-sky plots of the positions of the *weeks confirmed* sources showed high concentrations at both ecliptic poles, the areas with the greatest number of repeat coverages by the IRAS survey. The excess entries contained few weeks confirming sightings (two or three) compared to the actual number of survey coverages in their area (often six or more). Upon closer examination they proved to be unreliable entries,

i.e. false sources or weak broadened point sources. Redundant coverage at the poles had increased the probability for noise induced detections to overlap and eventually to weeks confirm. The specific signature of these noise induced entries was a low ratio, denoted N/M, of observed number (N) to expected number (M) of sightings. This observation inspired the repeatability test in *final selection* (IV.B.2.b). The final Catalog shows no unusual concentration at the poles.

ii) Low number of detections

Noise induced entries were often found to have a low number of seconds-confirmed detections per hours-confirming sighting, again a result of their origin in a stochastic process. Thus the test for a minimum number of detections per sighting was introduced (IV.B.2.c).

iii) Low fluxes

The group of unreliable entries defined by low N/M was also characterized by low fluxes, as would be expected from noise induced detections; 95% of the flux densities in this group at 12 μm and high Galactic latitudes were below 3 Jy, compared to about 55% for intermediate and high N/M populations. The additional caution required when dealing with low flux sources was translated into the flux test (IV.B.2.d).

A.3 Threshold Selection

While it was clear that entries with low N and high M were unreliable and entries with high N and high M were reliable, the majority of entries under consideration for selection were in neither of these categories. Most candidate sources had 2 weeks-confirming sightings and resided in areas of sky surveyed only two or three times. The properties of this population guided the choice of flux thresholds for *final selection* processing.

At several flux levels in the range of interest, a group of about 30 entries were chosen with $N/M = 2/3$ or $2/2$, in low source density sky at high Galactic latitudes. The raw detector data from scans over these positions were then examined by eye to decide which of these entries would be acceptable for inclusion in the Catalog. The unacceptable fraction of 12 μm entries dropped from about one third at 2 Jy to less than 10% at 3 Jy (see VI.A and Table VI.A.1 for more detail). At the thresholds ultimately selected, 3, 3, 2.5 and 5 Jy at 12, 25, 60 and 100 μm, respectively, unacceptable entries numbered two out of 26 at 12 μm, one out of 20 at 25 μm, two out of 27 at 60 μm, and one out of 29 at 100 μm. While some unreliable entries (point source plus noise) were missed by this choice, increasing the thresholds would have entailed sacrificing many good entries to remove bad ones, in the ratio of about 50 to 1.

Those choices for the thresholds were supported by two independent facts. First, the value adopted for each band corresponded roughly to the flux in an excursion above the baseline with the size of the largest filter width and an amplitude of four times the mean detector noise in that band. Second, most of the entries with $N = 2$ and $M > 4$ had fluxes lower than the thresholds: 92% at 12 μm, 95% at 25 μm, 73% at 60 μm, and about 50% at 100 μm. The drop at the two longer wavelengths was a side effect of *cluster analysis*, discussed in IV.A.4 below, which affected more severely these bands (Suppl.V.E.7).

The thresholds thus established in areas of low source density were extended to more crowded areas by interpreting the threshold as a multiple of the local noise level, dominated by detector noise in areas of

low source density, and by confusion noise in crowded areas. The noise level was estimated from the flux distribution in FISES, which is known to contain mostly spurious detections (Tables Suppl.V.E.1 and II.B.1). In each 1° by 1° ecliptic bin (Suppl.X and Appendix Suppl.X.1) containing more than ten FISES entries in a given band, the threshold was obtained by tripling the flux density corresponding roughly to the 25th percentile of the flux distribution of those entries. In bins with fewer sources, the thresholds at 12, 25, 60 and 100 μm defaulted to 3, 3, 2.5 and 5 Jy, which values would obtain if the flux distribution were constructed for all low source density bins put together. After a threshold value had been assigned to each bin on the sky, the resulting map was smoothed to avoid unusually low thresholds surrounded by high values in adjacent bins. The final threshold maps are shown in Figures IV.A.1-4. Note that the thresholds thus obtained can be quite high in the brightest parts of the Galactic plane, especially at 100 μm.

A.4 Remaining Concerns

As detailed in III.B above, double or multiple point sources could combine to produce small extended sources acceptable for inclusion in the Catalog. The results of the simulations in III.B were used to define a necessary condition for two point sources to generate an extended source detection. A test was then devised to flag Catalog entries for which that necessary condition arose. The test served for flagging purposes only because it could not indicate a sufficient condition when satisfied, nor could it rule out the existence of truly extended emission superposed on the two point sources (IV.B.2.e).

The majority of the sky (72%) was covered three times by the IRAS survey. This was reflected by the majority of IRAS Point Sources (69%) containing three or more hours-confirmed sightings. By contrast, the Small Scale Structure Catalog has only about 50% of its sources weeks-confirmed three or more times. Even at flux levels high above the noise, many sources had three opportunities to hours confirm but succeeded only twice. The basis for this lack of repeatability was found to be in the mechanics of the survey. The first and second coverages had similar scan angles, whereas the third coverage often had a scan angle very different from the first two (Suppl.III). The different scan angle affected the results at two levels:

i) The ability of the *detection* algorithm (II.A and III above) to locate emission depended on scan angle, especially in the cases of thin and elongated sources, double or multiple point sources, diffuse cirrus, or parts of larger structures.

ii) The results of *cluster analysis* also varied as a function of scan angle, mostly in areas dominated by cirrus or complex structure (Suppl.V.E.4 and Suppl.V.E.7.a), such as the Galactic plane at 12 and 25 μm, and most of the sky at 60 and 100 μm. Changes in FISES entries as a function of scan direction caused shifting linkage patterns in clusters; spurious detections added to clusters increased the scatter. Sources very close to some threshold could thus pass it on two out of three trials.

Clearly, all but the most asymmetric small extended sources should have been resolved every time, regardless of scan angle. Catalog entries with high N/M were indeed found to correspond mostly to clean, well-defined sources. Entries with $N/M = 2/3$ were also found to be usually acceptable, suffering mostly from confusing backgrounds. To illustrate this aspect of the Catalog, 16 entries with $N/M = 2/3$, more than 10° away from the Galactic plane, and with more than 10 Jy in flux density at 12 μm, were

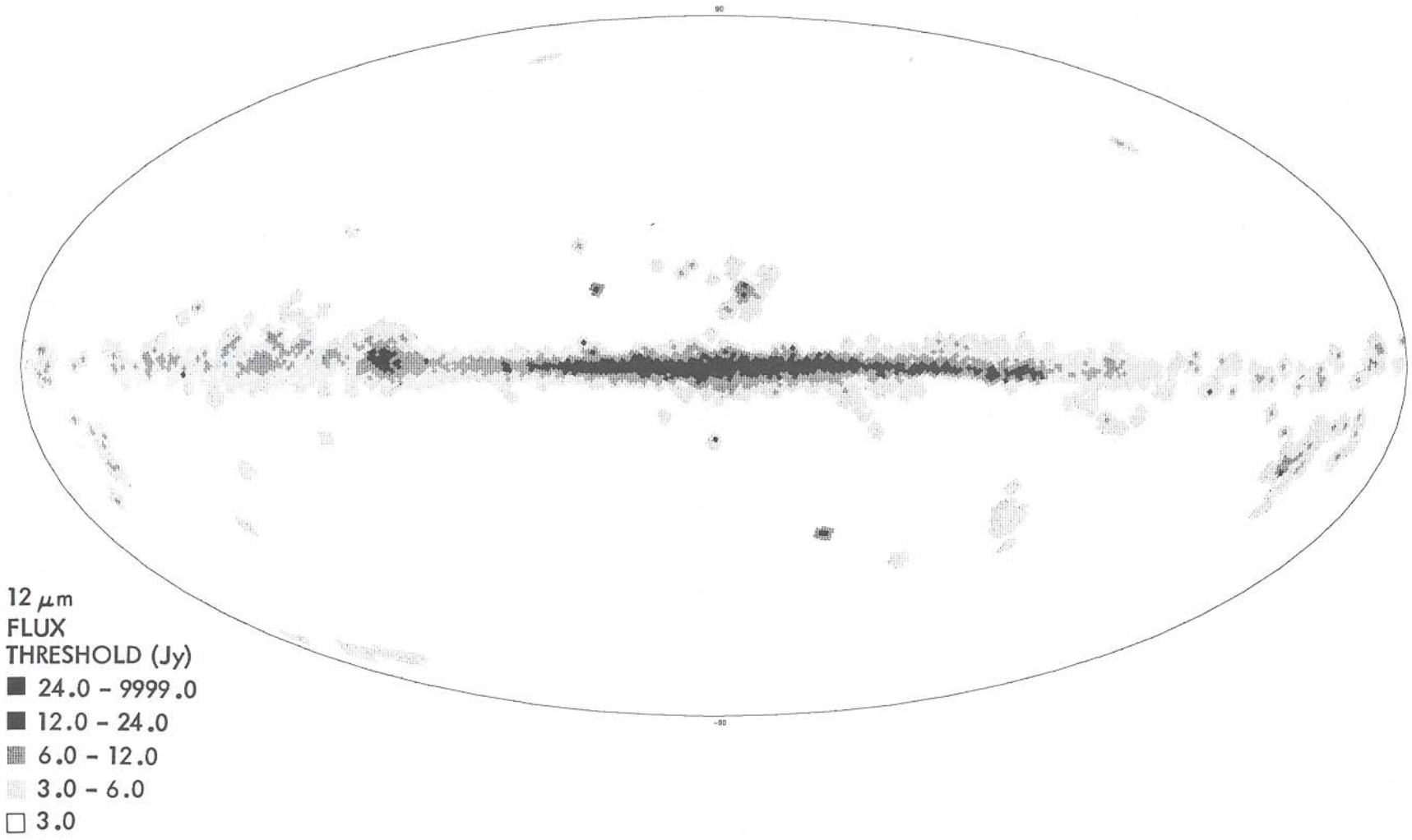

Figure IV.A.1 All-sky maps in Aitoff projection of Galactic coordinates showing the flux density threshold used at 12 μm as part of the flux test.

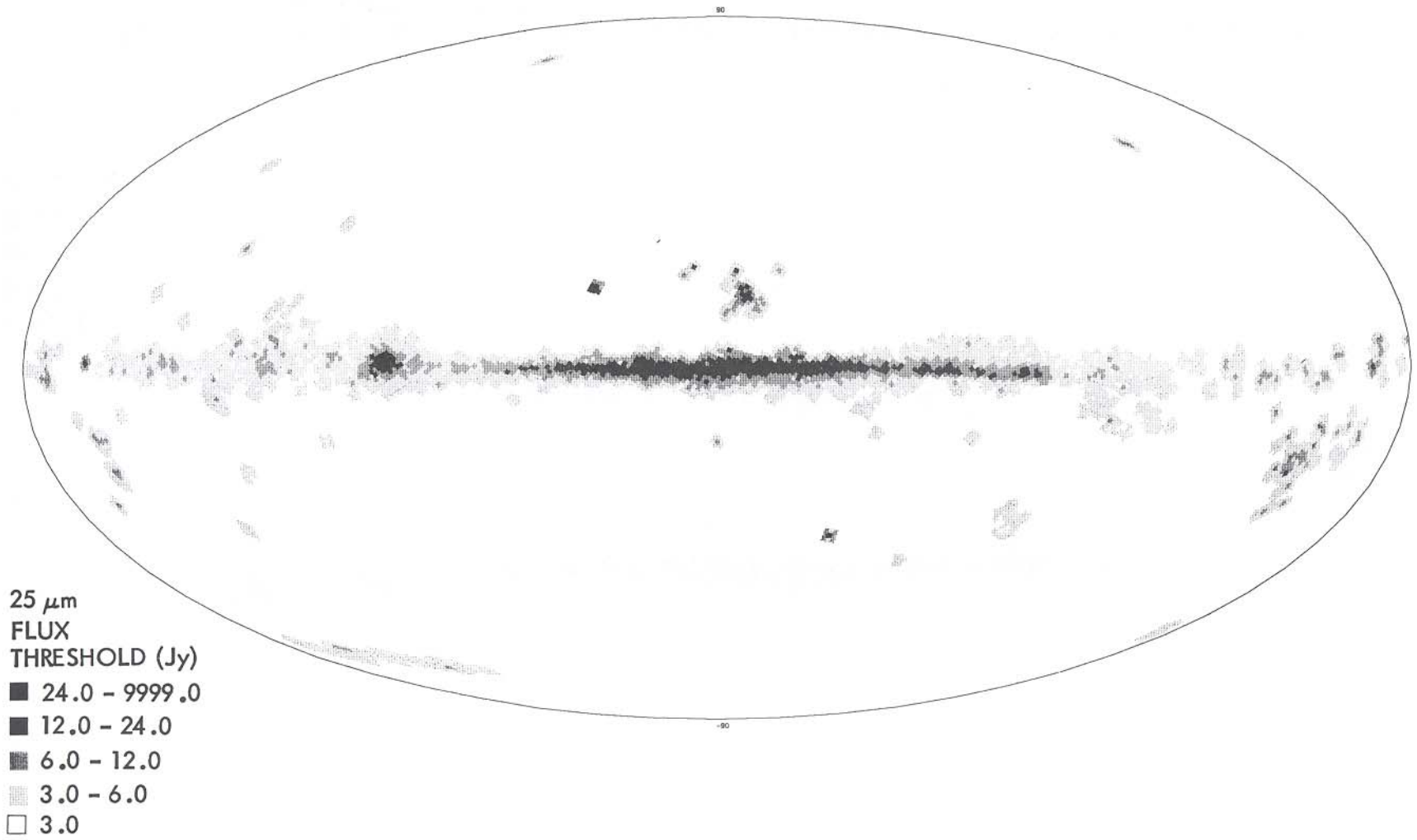

Figure IV.A.2 All-sky maps in Aitoff projection of Galactic coordinates showing the flux density threshold used at 25 μm as part of the flux test.

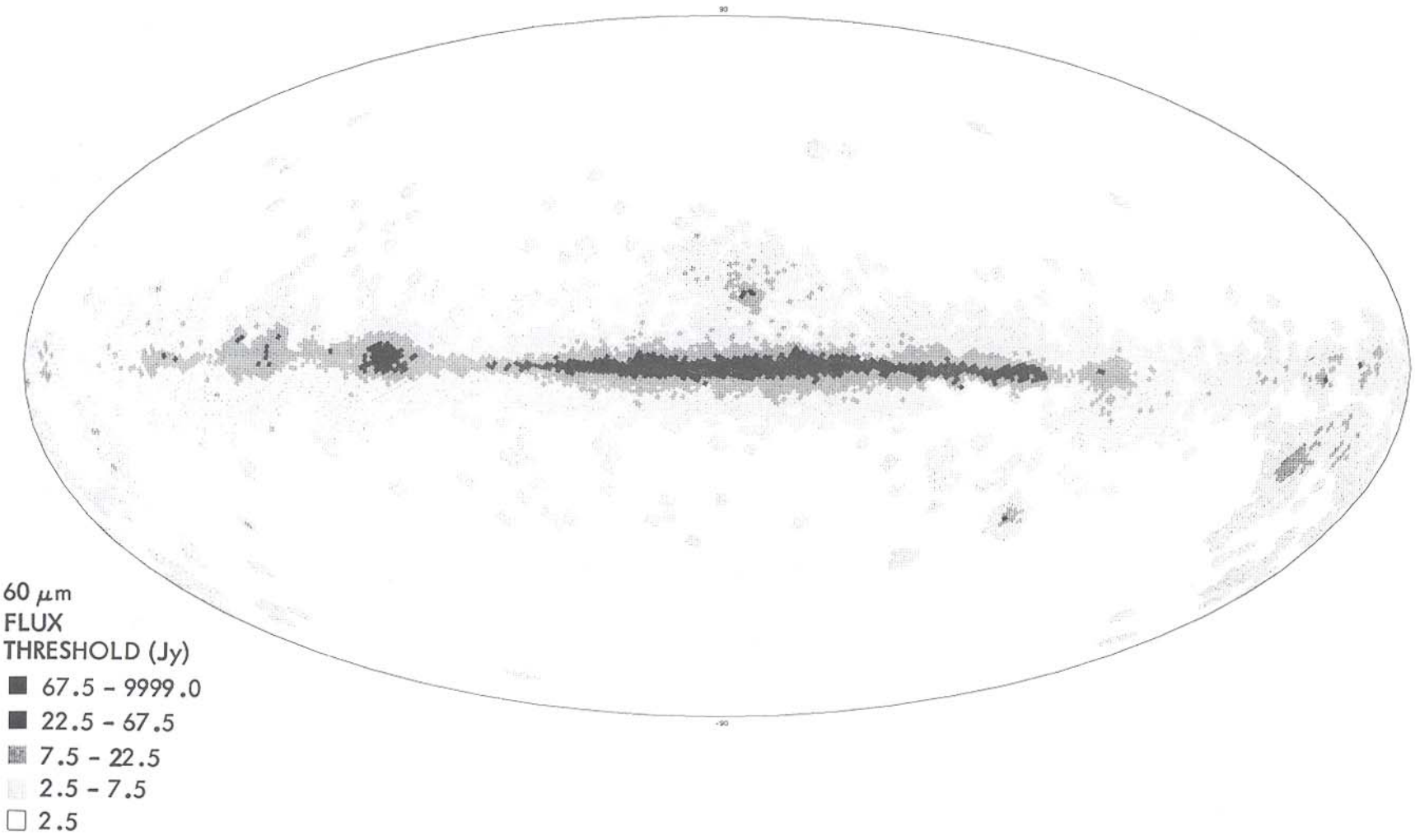

Figure IV.A.3 All-sky maps in Aitoff projection of Galactic coordinates showing the flux density threshold used at 60 μm as part of the flux test.

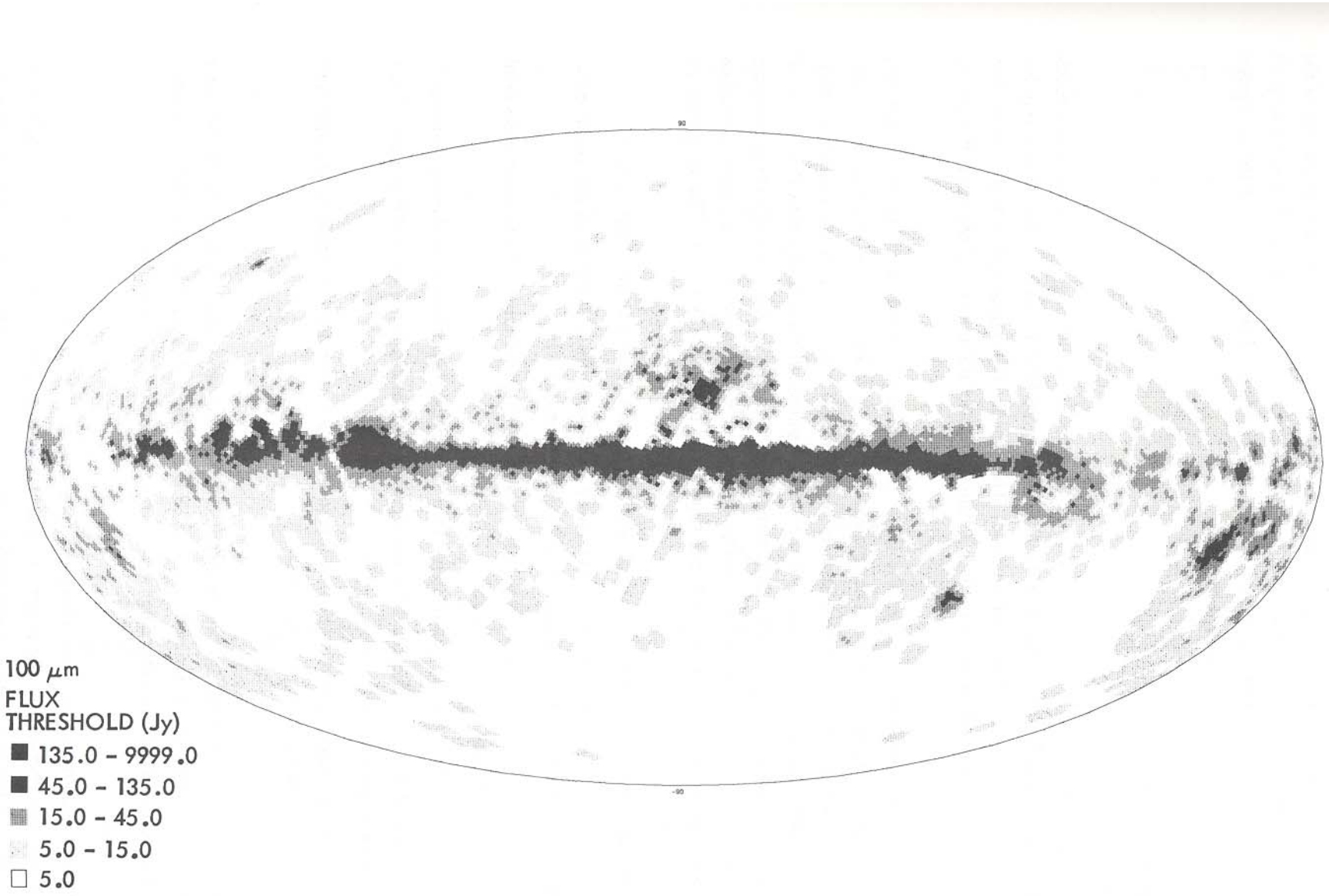

Figure IV.A.4 All-sky maps in Aitoff projection of Galactic coordinates showing the flux density threshold used at 100 μm as part of the flux test.

examined in detail. In three cases, the *detection* processor had failed to return a detection on one of the three coverages; one of these cases corresponded to a tight group of point sources. The remaining 13 sources had been detected three times each, but *cluster analysis* had taken away one of the coverages; about half of these entries could be described as cirrus.

B. Rules and Discussion

B.1 *Final Catalog Selection*: Overview

The last step in processing (Chapter II) was the selection from among weeks-confirmed, band-merged entries those acceptable for inclusion in the Catalog. Figure IV.B.1 represents the testing and flux quality assignment scheme designed for that purpose. The scheme is summarized in this section, then the individual rules are discussed in detail in III.B.2 below. A brief discussion follows in III.B.3 on the significance of flux quality.

Several points were considered in rating the *fluxes* in each band-merged candidate entry, each test intended to deal with one or more of the problems outlined in IV.A above. This resulted in a quality class (high, intermediate, or low) assigned separately to each band represented in the candidate entry. Candidate *sources* were accepted for inclusion in the Catalog unless all their component fluxes were of low quality. Accepted sources had *all* their component fluxes included in the Catalog with appropriate quality flags attached. A small number of sources which had experienced *band merging* difficulties (Suppl.V.E.6) were subjected to a slightly different source selection rule (IV.B.3.a). The tests may be summarized as follows:

i) Cross-talk: could this flux be a result of optical cross-talk from a nearby bright source?

ii) Source repeatability (or N/M test): how many weeks-confirming sightings in this component, and on how many survey coverages should it have been detected?

iii) Average detection count: on average, how many seconds-confirming detections are associated with each sighting of this component?

iv) Flux test: how bright is the flux relative to the local background filtered to the relevant scale?

In addition, one more test was applied for information only and did not enter the process of flux quality evaluation or source selection:

v) Double point source: is it *possible* that this source is no more than the result of two appropriately spaced and oriented point sources?

B.2 Details of Rules

The following five sub-sections discuss the details of implementation for specific tests, in the order in which these tests were applied, as outlined in Figure IV.B.1. The N/M rule was also called the "extrinsic" test, whereas detection count and flux rules were together called the "intrinsic" test.

B.2.a Cross-talk

As each potential detection was identified and passed on to *seconds confirmation* (II.A, Suppl.V.E.1), it was also checked for the possibility that it might be optical cross-talk, i.e. a detection of the diffraction image of the secondary support spider. The check was entirely analogous to the method

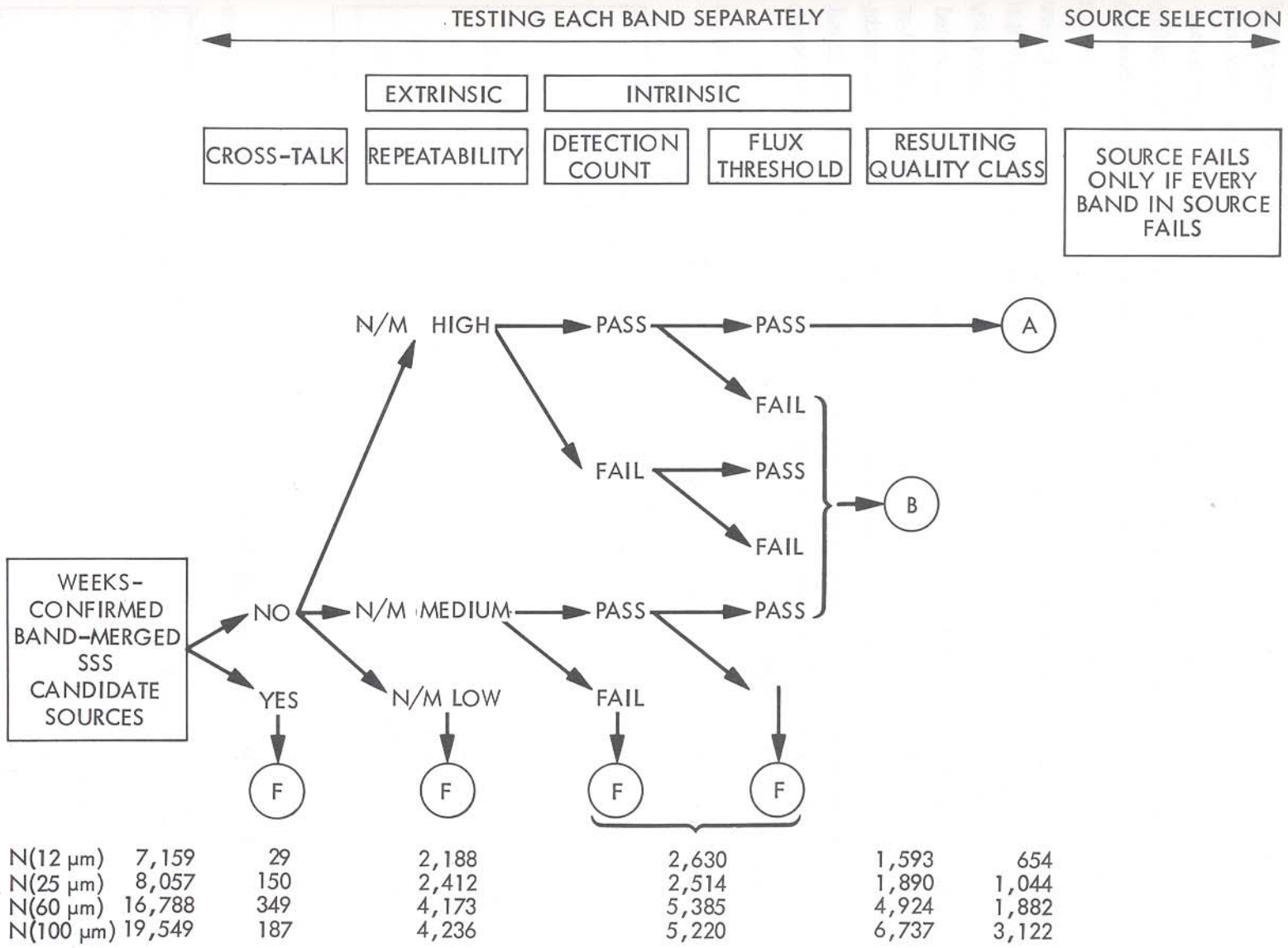

Figure IV.B.1 Schematic of the *final source selection* processor, with the number of components flagged at each stage. A, B, and F denote the flux quality (high, intermediate and failed) assigned to each measurement of a source as a result of these tests.

used for Point Sources (Suppl.V.D.2.c), so that potential detections were flagged only in the vicinity of point sources with a signal-to-noise ratio greater than 5000, 1200, 300, and 200, respectively at 12, 25, 60, and 100 μm. Then as a potential source was being constructed (Suppl.V.E.3) a count was kept of all individual detections tagged as possible cross-talk and contributing to this source. The count was then accumulated through *cluster analysis* and *weeks confirmation.* If the final count was not zero for a component in a candidate source, then that component was considered cross-talk and labeled as a low quality flux. Note that the test may have been be too severe, since a component was failed even if it had, for example, only 10% of its detections tagged as cross-talk.

However, just as with Point Sources (Suppl.VII.E.2), a few SSS entries due to cross-talk were in fact found unflagged, being located just beyond the flagging contours. Two new look-up tables (Table IV.B.1 and IV.B.2) were then created, one each for the 12 and 25 μm bands, establishing the radial range (as a function of brightness) over which a bright point source in that band might conceivably have generated cross-talk detections. As with Point Sources, there was no evidence of unflagged cross-talk at either 60 or 100 μm. An exhaustive search was then performed around all 12 and 25 μm Point Sources bright enough to be relevant to the new look-up tables; if a component from a candidate SSS entry was found within the indicated radius from the bright Point Source and with a lower flux than the Point Source in the same band, then it was considered cross-talk and labeled as a low quality flux.

TABLE IV.B.1 Cross-Talk Suppression Rules for 12 μm Band

Point Source Flux Density (Jy)	Search Radius (arcmin)
$100 \leqslant f_\nu < 300$	2
$300 \leqslant f_\nu < 1000$	3
$1000 \leqslant f_\nu < 2500$	4
$2500 \leqslant f_\nu < 6000$	5
$6000 \leqslant f_\nu < 12000$	10
$12000 \leqslant f_\nu$	25

TABLE IV.B.2 Cross-Talk Suppression Rules for 25 μm Band

Point Source Flux Density (Jy)	Search Radius (arcmin)
$100 \leqslant f_\nu < 300$	3
$300 \leqslant f_\nu < 1000$	4
$1000 \leqslant f_\nu < 2500$	5
$2500 \leqslant f_\nu < 10000$	7
$10000 \leqslant f_\nu$	20

There were 20, 135, 349 and 187 fluxes flagged as cross-talk in the course of *detection* processing at 12, 25, 60 and 100 μm respectively. The additional test (Tables IV.B.1 and IV.B.2) labeled as cross-talk nine and 15 previously unflagged fluxes at 12 and 25 μm respectively.

B.2.b Repeatability

The reliability of each band component was assessed by estimating the number of survey coverages carried out over that position and comparing it to the number of sightings recorded for that component. Once expected (M) and actual (N) number of coverages were known, Table IV.B.3 was used to decide the fate of that component as one of three outcomes: Low N/M caused unconditional failure and a low quality label for the flux. High N/M caused unconditional passage and guaranteed inclusion in the Catalog. Intermediate N/M caused no immediate decision and left the flux quality determination to later testing.

M, the expected depth of coverage, was not accurately known at an arbitrary position on the sky. The technique used to estimate it has been determined to be correct approximately 95% of the time, and within plus or minus one of the correct value about 98% of the time. Thus, some sources were incorrectly lost from the Catalog, and some entries incorrectly included, due to uncertainty about the depth of coverage. This effect was determined to be acceptably low.

The repeatability rule was responsible for failing roughly half the candidates that did not appear in the final Catalog.

TABLE IV.B.3 Repeatability Rule (N/M)

		M: Number of Expected Sightings				
		2	3	4	5	⩾6
N:						
Number	2	Med	Med	Low	Low	Low
of	3	High	High	Med	Med	Low
Actual	4	High	High	High	High	Med
Sightings	⩾5	High	High	High	High	High

B.2.c Detection Counts

The total number of detections contributing to a flux was divided by the number of sightings for that band. If the resulting average number of detections per sighting was less than four, then the component failed this test. The detection counts rule affected a rather small fraction of all candidates. The final quality class assigned to the flux was not uniquely determined by this test's outcome (see Figure IV.B.1); the same is also true for the flux test.

B.2.d Flux Test

Each flux was compared to the local threshold defined with one square degree resolution over the whole sky, described in IV.A.3 above, and illustrated in Figures IV.A.1-4. The minimum thresholds in low source density sky were set to 3, 3, 2.5 and 5 Jy at 12, 25, 60 and 100 μm. Fluxes below the threshold failed the test.

The flux test was responsible for failing about half the deleted entries. While clearly justified, this test was probably the least discriminating in the sense that it failed good as well as bad entries, in a ratio of more than five to one just below the threshold (IV.A.3). Because high signal-to-noise ratio radiation hits contributed to unreliable detections, flux threshold levels could not discriminate effectively between signal and noise, as they would have in the presence of a Gaussian noise distribution.

B.2.e Double Point Source Flagging

As demonstrated in III.B, two appropriately positioned point sources could be detected as a single extended source. To warn the reader about this possibility, a flag is set if a Catalog source has (at least) two weeks-confirmed IRAS point sources (not necessarily in the Point Source Catalog) detected in the same band, and satisfying the following geometry:

i) the angle defined by the positions of the two point sources and the small extended source, with the latter at the vertex, is greater than 90°,

ii) the two point sources are within $5'$ of each other in a direction normal to the line joining the small extended source and the closest point source, and

iii) the two point sources are within $7.1'$ of each other.

If all three conditions are met, then it is (almost) always possible to find one scan direction for which the two point sources are within $5'$ of each other both in the in-scan and cross-scan directions, and the extended source is "between" the point sources in both directions. This was precisely the situation (III.B) when two point sources generated an extended source. Therefore when all three conditions were met the flag was set to indicate the *possibility* that the source is no more than the sum of two nearby point sources. No more certain determination could be made because scan directions were neither unique nor known to the *final selection* processor.

B.3 Flux Quality and Source Selection

Each flux in a candidate source was thus assigned a quality, related to the reliability of that band component, as indicated on Figure IV.B.1. Grade A fluxes passed all tests, and should point to the most reliable sources. Grade B fluxes belonged to either one of two quite different categories: (i) free of cross-talk and highly repeatable, but failing either the detection count or the flux test, or both; or (ii) free of cross-talk, above detection count and flux thresholds, but of insufficiently tested repeatability. Grade F, or low quality fluxes, were those suspected of cross-talk, displaying low repeatability, or uncertain repeatability but low detection count or low flux.

To appear in the Catalog, a candidate had to have at least one flux with grade A or B. Grade F fluxes in a Catalog source were allowed to appear along with the other band components in the source because the latter were considered additional confirmation for them. Grade F fluxes in a source might be interpreted either as measurements of poor reliability, or as upper limits in those bands.

The detailed interpretation of a grade B flux depends on its category. Sources passing the extrinsic (N/M) test but failing the intrinsic test (e.g., below flux threshold) may be of questionable quality only regarding the estimate of their flux or other parameters. Sources with inconclusive N/M (e.g., 2/3) that passed the intrinsic test may not be true extended sources, but point sources broadened by radiation or

noise, especially if their flux is just above the threshold. As discussed in IV.A.4, grade B fluxes well above the threshold result mostly from *cluster analysis*, and often associate with cirrus.

It should be noted that the triple valued outcome of the extrinsic test left the fate of more than half the candidate sources entirely up to the intrinsic test. In particular, that part of the sky surveyed only twice was left devoid of single band sources below the flux thresholds since sources with $N/M = 2/2$ always ended up in the low quality class if they were below the flux threshold.

B.3.a *Band Merging* Failures

Sources with *band merging* complications (Suppl.V.E.6) presented themselves to the testing scheme with at least two components in one of the bands. Each individual component was tested and flagged normally as per Figure IV.B.1. The source was then reassembled, discarding all failed components. If the new candidate source still contained multiple components from the same band, it was rejected from the Catalog. If the conflict had disappeared, and at least one component was of high or intermediate quality, the source was included in the Catalog.

Because *band merging* had been allowed to chain, each component did not necessarily merge with all other components in a source (Suppl.V.E.6). After the modified source selection procedure described above had been applied, the accepted sources were all checked to ascertain that the surviving components in each source belonged together; only one source was found, X2018+380, consisting of a 12 μm component and a 100 μm component that would not have band-merged on their own. This source was retained unaltered in the Catalog.

V. ANALYSIS OF SMALL SCALE STRUCTURE CATALOG

This chapter presents a statistical overview of the Small Scale Structure Catalog. Statistics on the Catalog entries are given in Section A, including histograms of fluxes, flux ratios and sizes. Section B compares SSS processing results to other IRAS products, namely Point Sources, Sky Brightness Images, and Additional Observations. Section C discusses the uncertainties on the quantities listed in the Catalog. The rms error on fluxes is somewhat less than 50% in general, and about 30% in unconfused sky. There is some inconclusive evidence that flux densities (at least at 12 and 25 μm) are systematically overestimated by an amount between 0.5 and 1 Jy. Positional errors are on the order of 1 arcminute (rms) for a single band determination. Indicative sizes are accurate to half a beam width (rms). Section D provides a detailed look at the results of SSS processing in a small area of the Galactic plane, and displays raw detector output to illustrate the types of sources found in the Catalog.

A. Source Statistics

All SSS Catalog sources are displayed in Figure V.A.1, where each source is represented by a point. Figures V.A.2, 3, 4 and 5 display those sources in the Catalog that have a high or intermediate quality flux at 12, 25, 60 or 100 μm respectively. On these maps each source is represented by a symbol denoting the band combination and the flux density in that source. Most sources are clearly Galactic in origin, in spite of the severe confusion rejection criteria imposed in *cluster analysis* (Figure Suppl.V.E.5). Counting only high and intermediate quality fluxes, 31% of 12 μm fluxes fall in areas of the sky that are considered high source density at 12 μm in the sense of Point Source clean-up processing (Suppl.V.H.6). The corresponding fractions are 25%, 16%, and 57% respectively at 25, 60 and 100 μm. Only 35% of SSS Catalog sources fall in areas of the sky which are *not* considered high source density regions at *any* band. That fraction is about 50% in the Point Source Catalog. Apart from a few hundred resolved galaxies at high Galactic latitudes, it is clear that most of the structure at scales of interest to this Catalog arises in regions where the IRAS data is confusion limited or close to it (Suppl.V.H.6, Suppl.VIII.C).

The asymmetry in Figure V.A.1 about the Galactic plane is due to instability and lag in the noise estimator (Suppl.XI.B and II.A), enhanced by the rules in *final source selection*. The asymmetry is more evident at 60 and 100 μm, where the Galaxy is brighter, affecting more severely the noise estimator. The noise estimator lag results in different flux distributions in the file of intermediate small extended sources (FISES, Suppl.V.E.3) on either side of the plane, with more high fluxes on the side of the plane with a lower source density. This asymmetry is propagated into the local flux thresholds (IV.A.3) used in *final source selection*, resulting in higher thresholds on the more sparsely populated side of the plane. Thus the selection rules enhance the asymmetry by deleting more sources where the source density is lower to start with (Figure IV.B.1).

The Galactic plane stands out on Figures V.A.2 and 3, highlighted by multi-band sources which correspond to star clusters, reflection nebulae, HII regions, planetary nebulae, stars embedded in molecular clouds, and other Galactic objects. Orion, Ophiuchus, and the Large and Small Magellanic Clouds are also visible here. At high Galactic latitudes galaxies appear, usually detected at 12, 25 and 60 μm. On Figure V.A.4, more galaxies can be found, detected only at 60 μm. The Virgo Cluster of galaxies can be seen around Galactic longitude = 80°, and latitude = 75°. Unlike Point Sources, SSS sources detected

SMALL SCALE STRUCTURE CATALOG:
ALL SOURCES

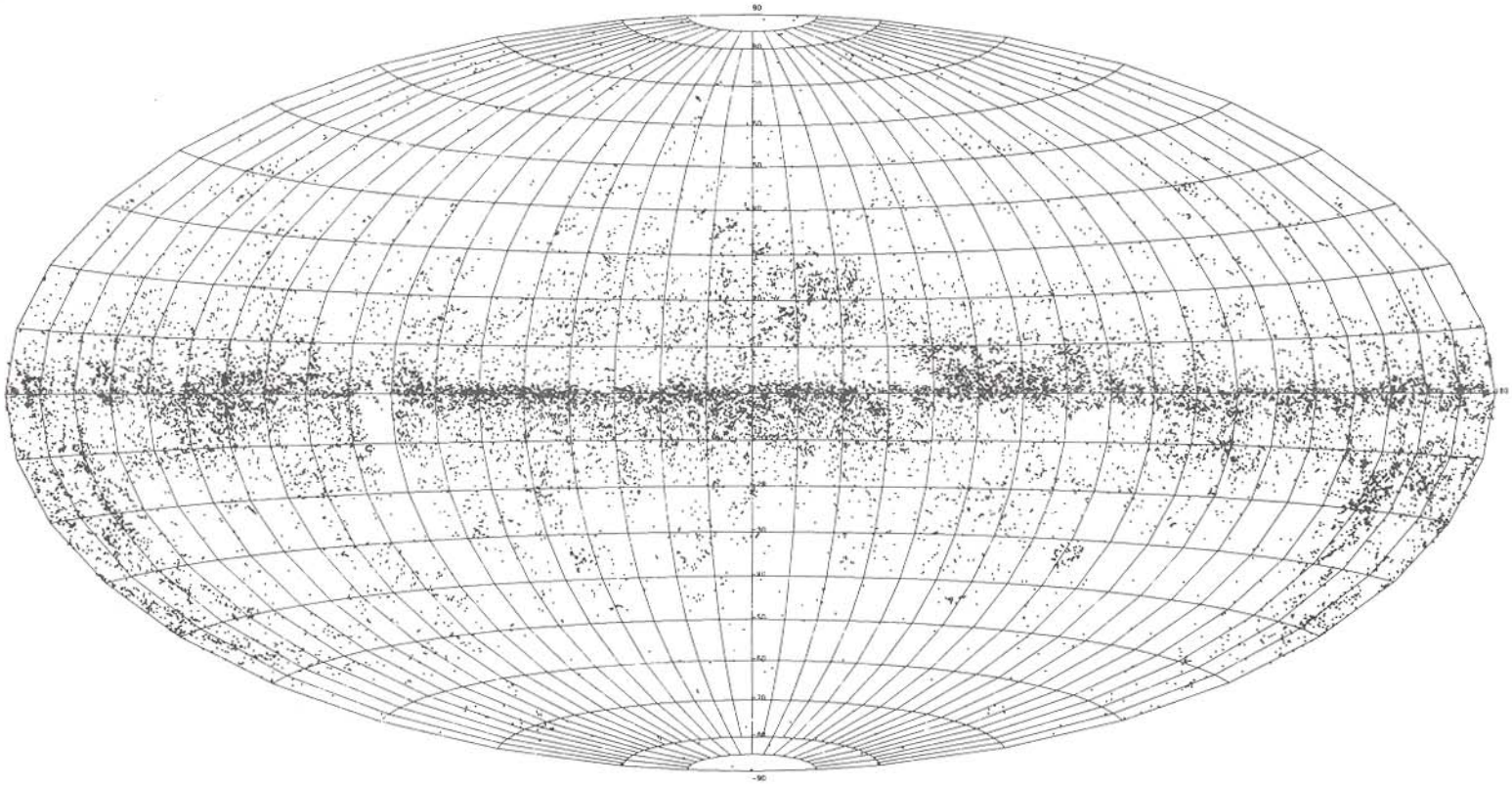

Figure V.A.1 All-sky map in Aitoff projection of Galactic coordinates showing all SSS Catalog sources.

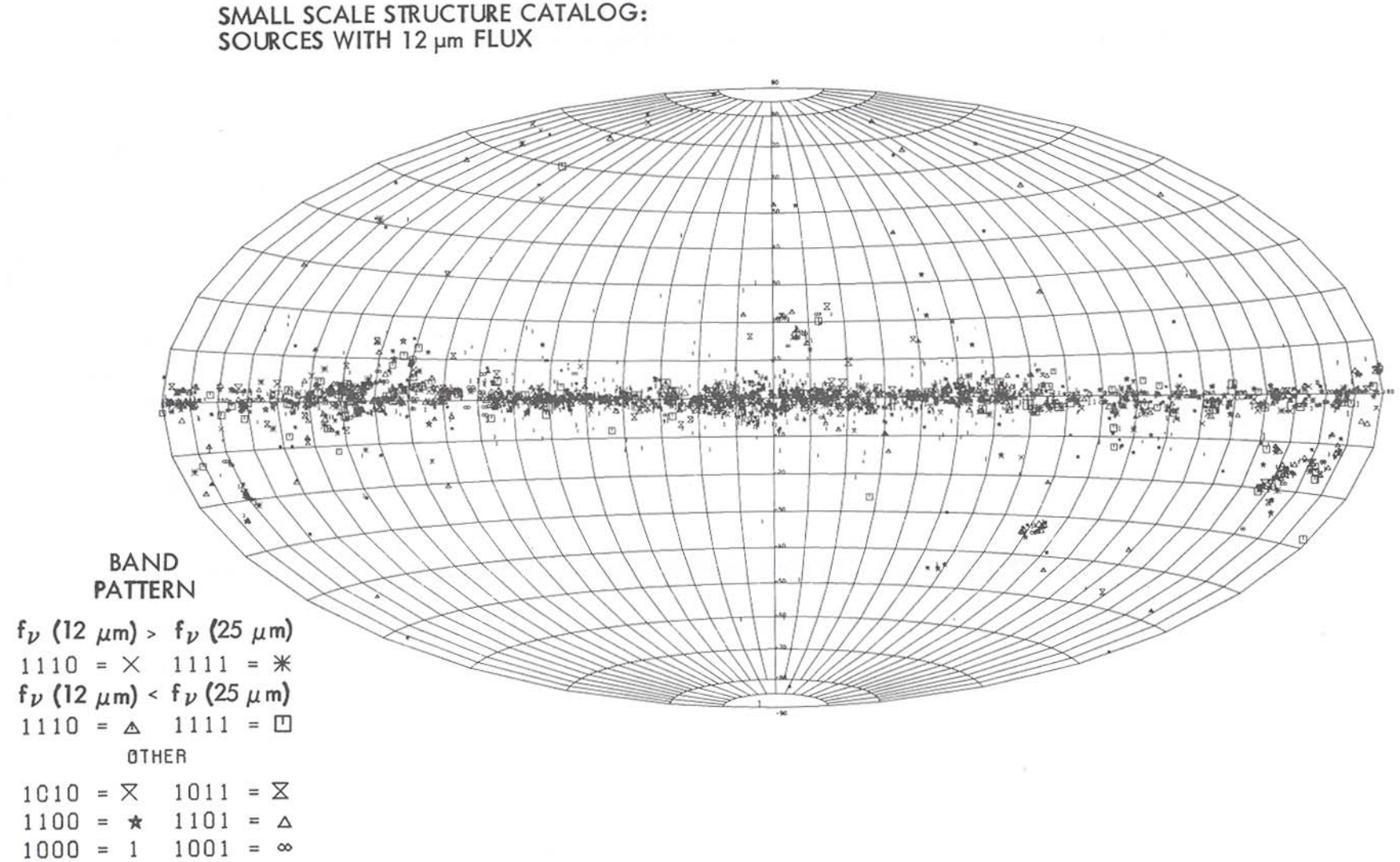

Figure V.A.2 All-sky map in Aitoff projection of Galactic coordinates showing the 12 μm component of the Catalog. Symbols refer to different band combinations, with a 12 μm only source symbolized by a "1". Symbol size is proportional to $\log(f_\nu(12\ \mu m))$.

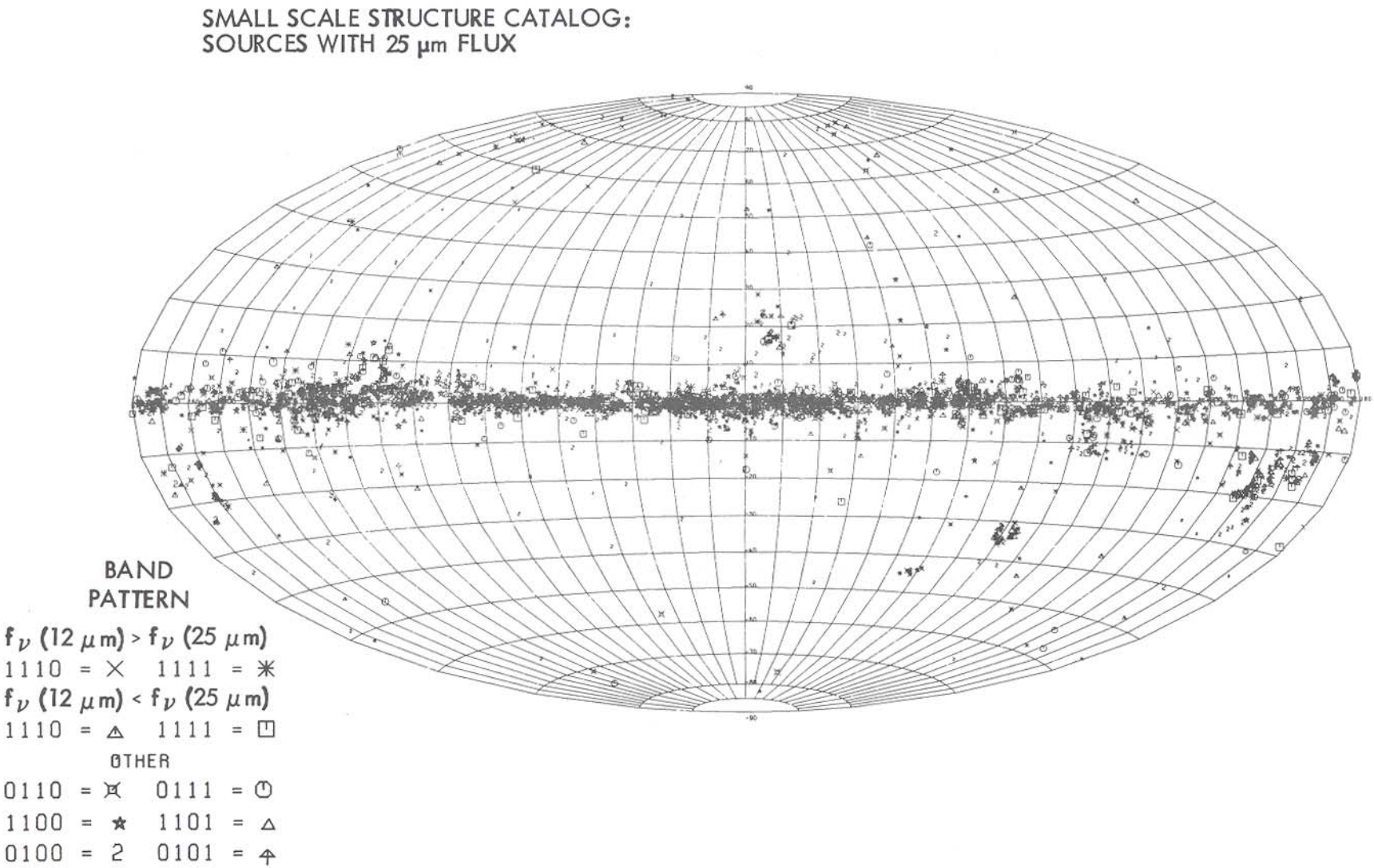

Figure V.A.3 All-sky map in Aitoff projection of Galactic coordinates showing the 25 μm component of the Catalog. A 25 μm only source is symbolized by a "2".

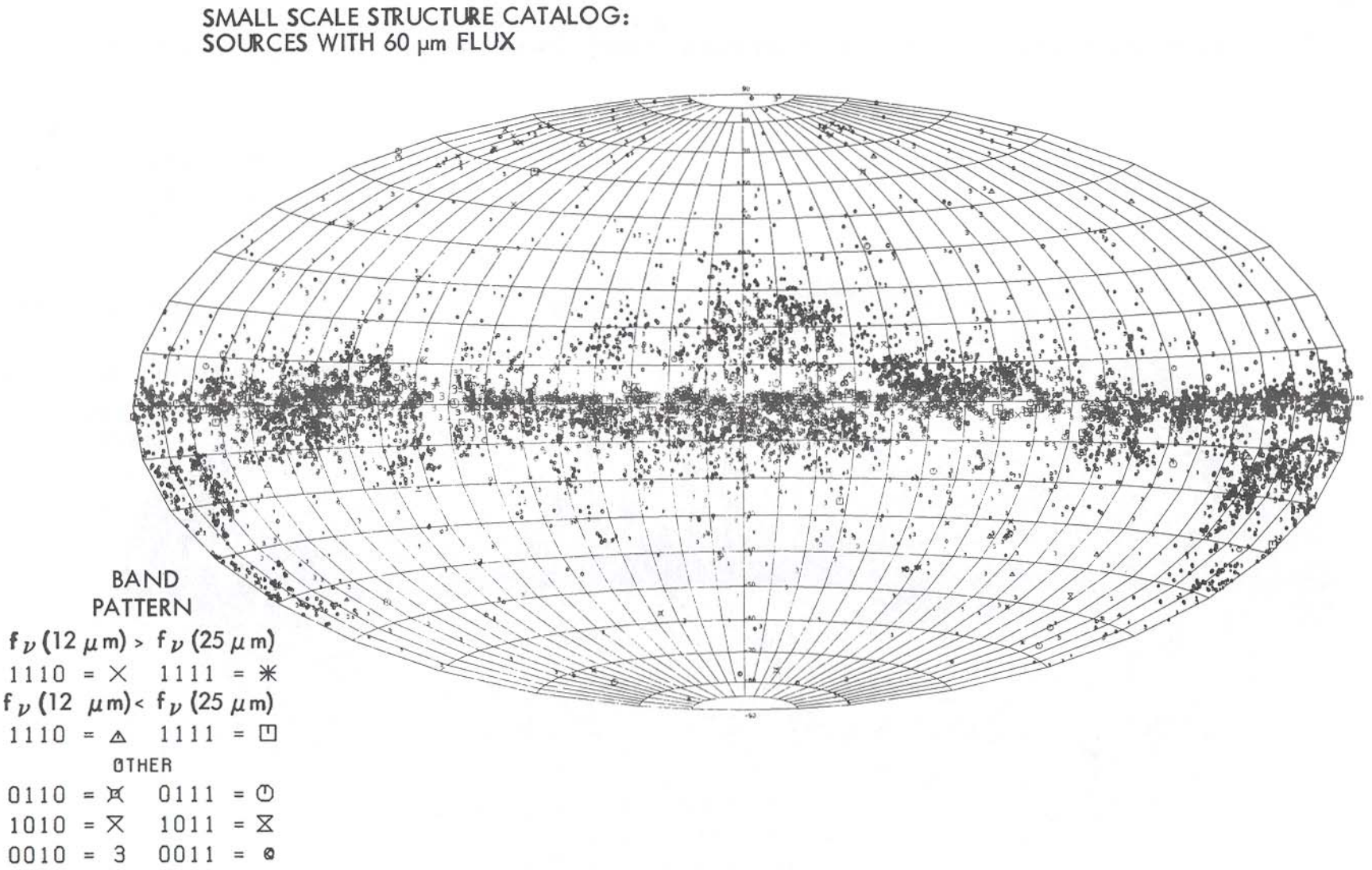

Figure V.A.4 All-sky map in Aitoff projection of Galactic coordinates showing the 60 μm component of the Catalog. A 60 μm only source is symbolized by a "3".

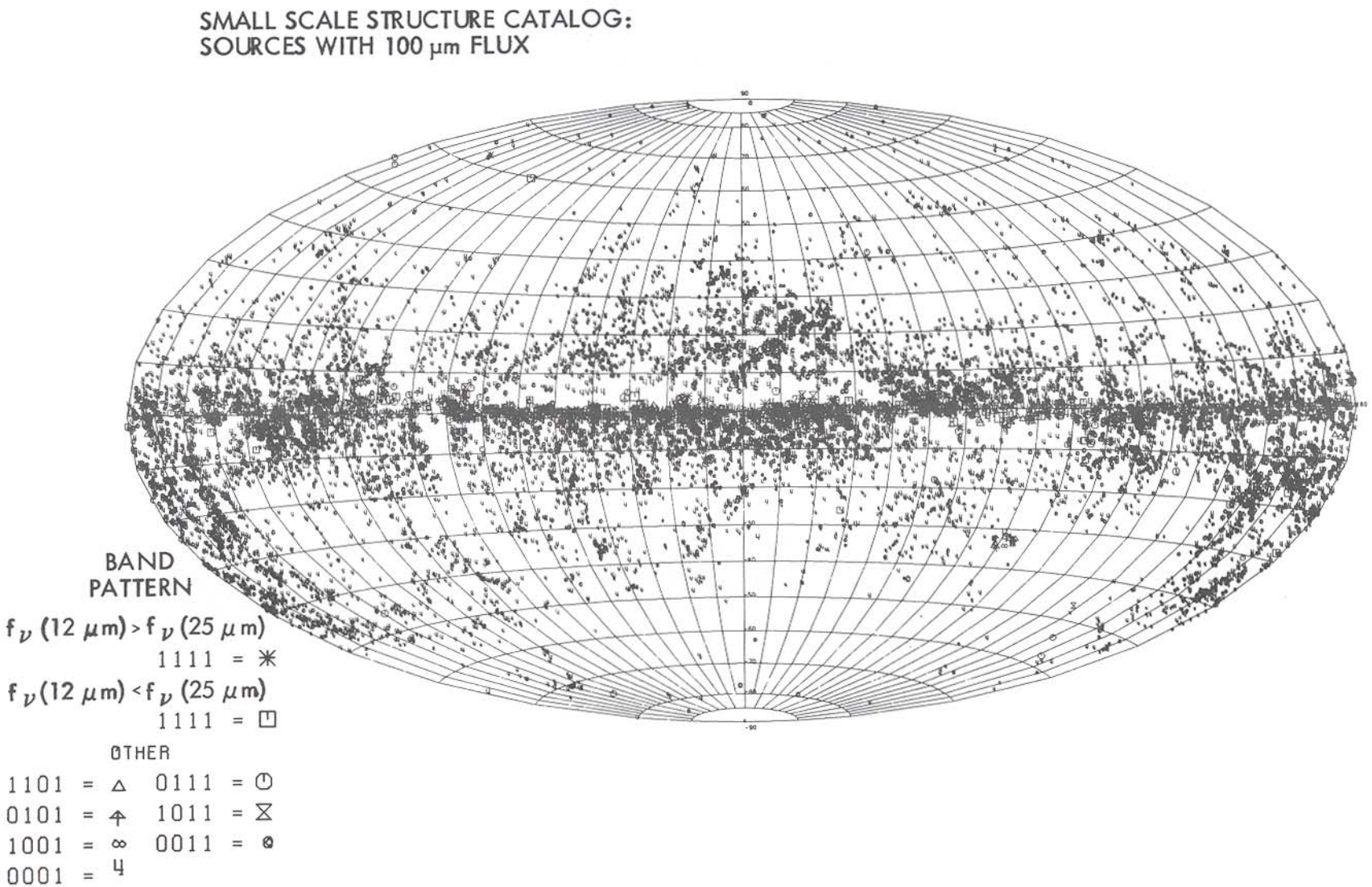

Figure V.A.5 All-sky map in Aitoff projection of Galactic coordinates showing the 100 μm component of the Catalog. A 100 μm only source is symbolized by a "4".

at 60 and 100 μm are typically due to Galactic cirrus, since few galaxies are resolved at 100 μm. Figure V.A.5 is dominated by 100 μm only sources, except within a few degrees of the Galactic plane. Orion and Ophiuchus become quite prominent in Figures V.A.4 and 5, whereas the Magellanic Clouds are barely discernible. The 100 μm component of the Catalog represents primarily Galactic cirrus.

Figure V.A.6 shows the flux distribution for Catalog sources with high (hatched histograms) and intermediate flux qualities. The flux distributions depend little on flux quality class, except for the absence (by definition) of high quality fluxes below the default flux thresholds, 3, 3, 2.5 and 5 Jy at 12, 25, 60 and 100 μm respectively. At 12 and 25 μm there are relatively more high quality grades at higher flux densities, but this is not the case at 60 and 100 μm. A reasonable power law approximation to the flux distribution above 10 Jy is $N(f_\nu)\, df_\nu = f_\nu^{-2}\, df_\nu$ for all bands, as would be expected for a population of Galactic sources.

Figures V.A.7 shows the distribution of flux density ratios (before color correction; see Suppl.VI.C) among the three pairs of adjacent bands. $f_\nu(12\ \mu m)/f_\nu(25\ \mu m)$ remains mostly below one, as might be expected for emission from nebulae, with a tail approaching photospheric colors presumably due to closely spaced stars whose combination is detected as extended sources (III.B). $f_\nu(25\ \mu m)/f_\nu(60\ \mu m)$ remains always below one, characteristic of color temperatures below 100 K. $f_\nu(60\ \mu m)/f_\nu(100\ \mu m)$ ranges from a color temperature around 25 K (cold cirrus) to around 100 K (compact HII regions).

Tables V.A.1, 2, 3 and 4 give basic statistics on the 12, 25, 60 and 100 μm components of the SSS Catalog. Each table shows for each band the total number of fluxes in that band, the number of sources with a flux in that band only, the number of fluxes with two, three, or more weeks-confirming sightings and the number of fluxes with a Point Source counterpart in the same band. The numbers are shown for each quality class separately, high (A), intermediate (B), and low (F), and for all of them combined (last column). The percentages in parentheses are with respect to the totals appearing at the top of the corresponding column, whereas percentages in square brackets are in comparison to the total in the last column of the corresponding line.

The relative frequencies of fluxes with two, three, or more sightings remain roughly constant from band to band as one might expect, since this is primarily a function of sky coverage.

About half of all SSS Catalog sources have counterparts in the Point Source Catalog (see VII.A for a precise definition). In all four bands, high quality fluxes have point source counterparts *in the same band* more often than intermediate quality fluxes. There is a higher incidence of same-band counterparts at the shorter wavelengths: about 60% at 12 and 25 μm, against roughly 35% at 60 and 100 μm. The fraction of fluxes flagged as possible double point sources (IV.B.2.e) is also higher at the shorter wavelengths: respectively 37%, 35%, 11% and 17% at 12, 25, 60 and 100 μm, excluding low quality fluxes.

When a Point Source counterpart is identified for a Catalog source, an indicative size, called PSIZ is computed (V.B.1 and V.C.3). Figure V.A.8 displays the PSIZ distribution in each band for Catalog sources with high (hatched histogram) and intermediate flux qualities. In each band the lower limit to the distribution corresponds to the width of a point source response, indicating that the SSS flux is always greater than the flux of the Point Source counterpart. As with flux densities, PSIZ distributions seem to be the same for high and intermediate quality fluxes.

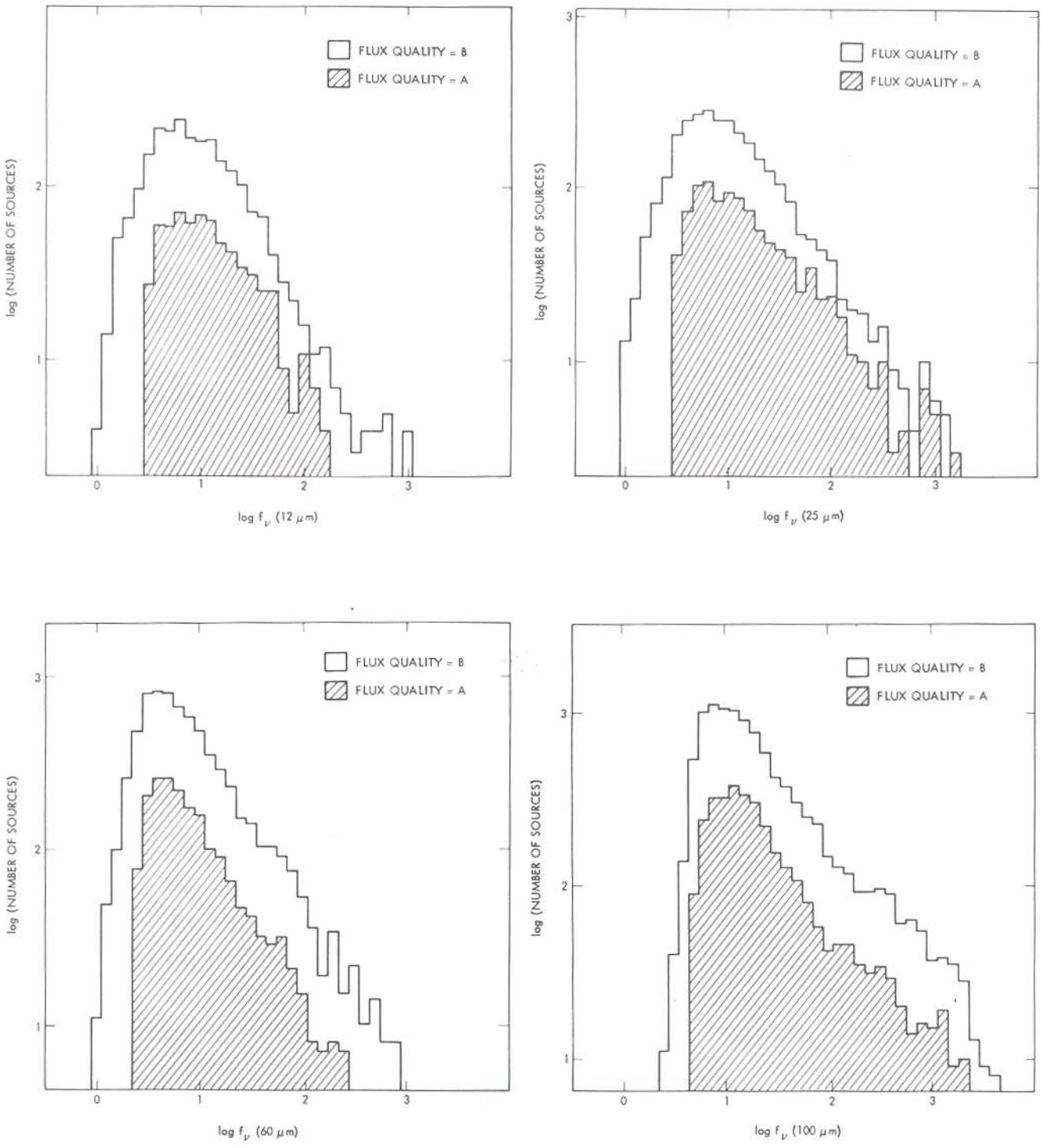

Figure V.A.6 Flux density histograms for high (A) and intermediate (B) quality components of Catalog sources.

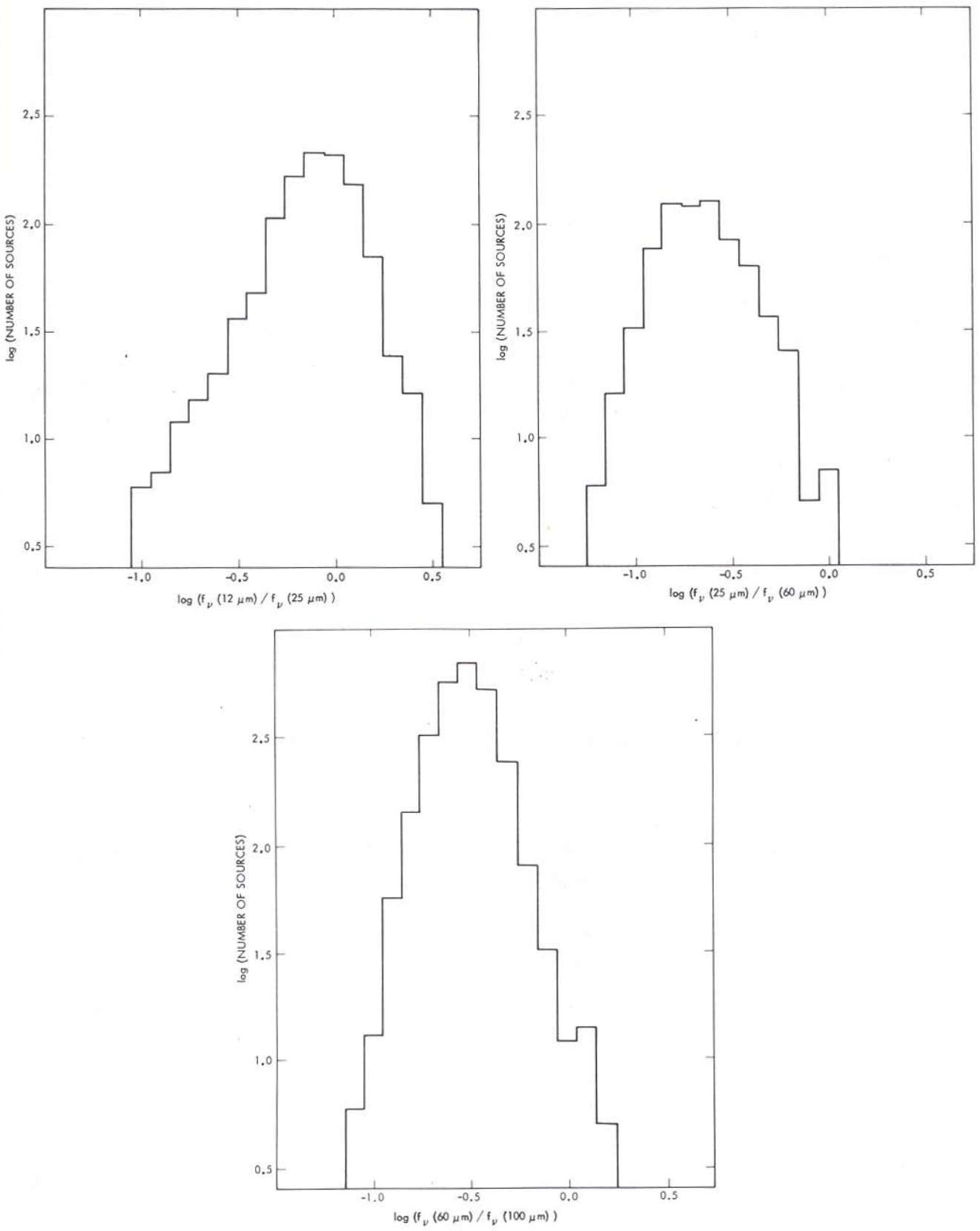

Figure V.A.7 Flux density ratio histograms for all Catalog sources, using only high and intermediate quality fluxes.

TABLE V.A.1 Statistics for 12 μm Fluxes in SSS Catalog

Quality class	A	B	F	All
Number of components in Catalog	654 [21%]	1,593 [52%]	824 [27%]	3,071
Number of 12 μm only sources in Catalog	85 (13%)	541 (34%)	0 0	626 (20%)
Number of components with 2 sightings	0 0	802 (50%)	728 (88%)	1,530 (50%)
Number of components with 3 sightings	488 (75%)	652 (41%)	87 (11%)	1,227 (40%)
Number of components with >3 sightings	166 (25%)	139 (9%)	9 (1%)	314 (10%)
Number of 12 μm Point Source counterparts	482 (74%)	972 (61%)	375 (46%)	1,829 (60%)

TABLE V.A.2 Statistics for 25 μm Fluxes in SSS Catalog

Quality class	A	B	F	All
Number of components in Catalog	1,044 [28%]	1,890 [50%]	828 [22%]	3,762
Number of 25 μm only sources in Catalog	190 (18%)	670 (35%)	0 0	860 (23%)
Number of components with 2 sightings	0 0	967 (51%)	717 (87%)	1,684 (45%)
Number of components with 3 sightings	788 (75%)	784 (41%)	91 (11%)	1,663 (44%)
Number of components with >3 sightings	256 (25%)	139 (7%)	20 (2%)	415 (11%)
Number of 25 μm Point Source counterparts	771 (74%)	1,128 (60%)	421 (51%)	2,320 (62%)

TABLE V.A.3 Statistics for 60 μm Fluxes in SSS Catalog

Quality class	A	B	F	All
Number of components in Catalog	1,882 [23%]	4,924 [59%]	1,528 [18%]	8,334
Number of 60 μm only sources in Catalog	483 (26%)	2,272 (46%)	0 0	2,755 (33%)
Number of components with 2 sightings	0 0	3,039 (62%)	1,247 (82%)	4,286 (51%)
Number of components with 3 sightings	1,500 (80%)	1,603 (33%)	245 (16%)	3,348 (48%)
Number of components with >3 sightings	382 (20%)	282 (6%)	36 (2%)	700 (8%)
Number of 60 μm Point Source counterparts	864 (46%)	1,609 (33%)	440 (29%)	2,913 (35%)

TABLE V.A.4 Statistics for 100 μm Fluxes in SSS Catalog

Quality class	A	B	F	All
Number of components in Catalog	3,122 [29%]	6,737 [62%]	1,023 [9%]	10,882
Number of 100 μm only sources in Catalog	1,307 (42%)	4,000 (59%)	0 0	5,307 (49%)
Number of components with 2 sightings	0 0	4,598 (68%)	843 (82%)	5,441 (50%)
Number of components with 3 sightings	2,401 (77%)	1,781 (26%)	160 (16%)	4,342 (40%)
Number of components with >3 sightings	721 (23%)	358 (5%)	20 (2%)	1,099 (10%)
Number of 100 μm Point Source counterparts	1,301 (42%)	2,256 (33%)	445 (43%)	4,002 (37%)

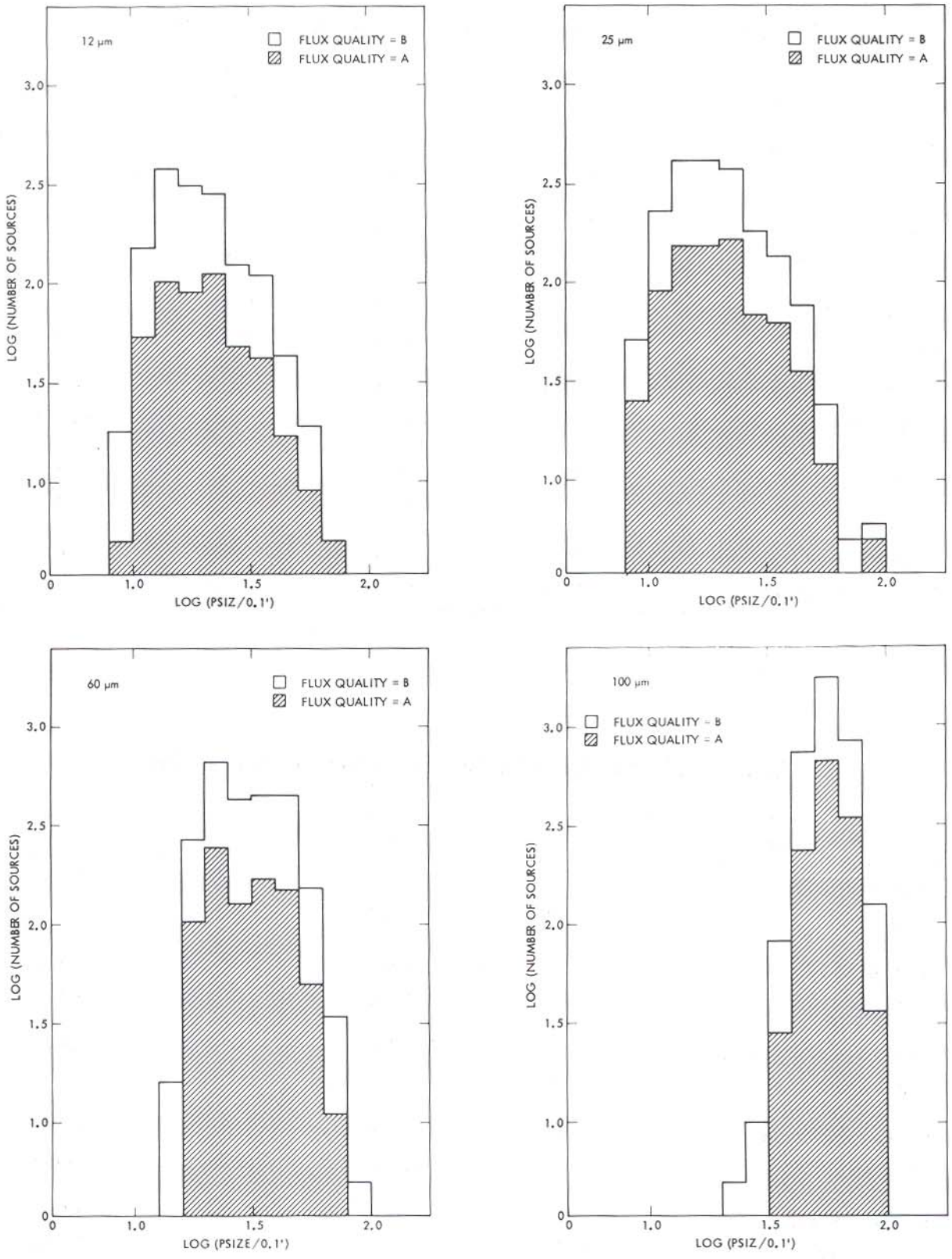

Figure V.A.8 Histograms of indicative sizes in each band for high (A) and intermediate (B) quality components in Catalog sources.

Table V.A.5 gives the frequency of occurrence of sources with all possible band combinations in two cases: counting all bands represented in each source (second column), and excluding low quality bands (last column). In the latter case, about 75% of all sources are single band sources, 21% are two-band sources, 3% have three bands, and 1% have four bands. Among the three-band and four-band sources, well over 90% are "mutually confirmed mergers" (Suppl.V.E.6), meaning that every band "merges" with every other band in the source. Here again, high quality fluxes from all bands belong to multi-band sources more often than to single-band sources; and the fraction of high quality fluxes belonging to multi-band sources is larger in every band than the fraction of intermediate quality fluxes doing the same (Tables V.A.1 to 4).

Some 16% of all Catalog sources are positionally associated with objects in one or more of the 31 astronomical catalogs listed in Table Suppl.V.H.1, including about 400 sources associated with galaxies. Not all of these associations are physically significant; many are simply due to a line-of-sight coincidence, especially with Galactic cirrus. On the other hand, more galaxies were detected and resolved than those appearing in the Catalog; see chapter VI for a discussion of completeness.

TABLE V.A.5 Band Combinations in Catalog Sources

Band Combination				Number of Sources with Combination	
				All Fluxes	A or B Fluxes Only
12 μm	25 μm	60 μm	100 μm		
1	0	0	0	626	932
0	1	0	0	860	1,283
0	0	1	0	2,755	3,671
0	0	0	1	5,307	6,674
1	1	0	0	784	541
0	1	1	0	386	249
0	0	1	1	3,849	2,308
1	0	1	0	103	59
1	0	0	1	196	112
0	1	0	1	268	181
1	1	1	0	344	146
0	1	1	1	244	127
1	1	0	1	365	211
1	0	1	1	142	50
1	1	1	1	511	196

B. Comparison with Other IRAS Data

B.1 Comparison with Point Sources

About half of the SSS Catalog entries coincide with an IRAS Point Source (see VII.A for a precise definition), providing two complementary descriptions of the emission. It turns out in these cases that the Point Source flux is a good measure of the peak amplitude of the emission. For roughly circular sources therefore, the ratio of total flux (as estimated by SSS processing) to point source flux is expected to scale with the square of the detection width. This is in fact verified in Figure V.B.1 for about 70 sources selected as explained in V.C.1 below for Figure V.C.1. Based on the evidence in Figure V.B.1, the following quantity is listed in the Catalog as an estimate of the in-scan full width at half maximum of the emission in each band i (see V.C.3 for more details):

$$PSIZ_i = FWHM_i \times [SSSFLUX_i/PTSRCFLUX_i]^{0.5}$$

where $FWHM_i$ is the width of the point source response, 0.82′, 0.84′, 1.44′, and 3.14′ at 12, 25, 60 and 100 μm, respectively.

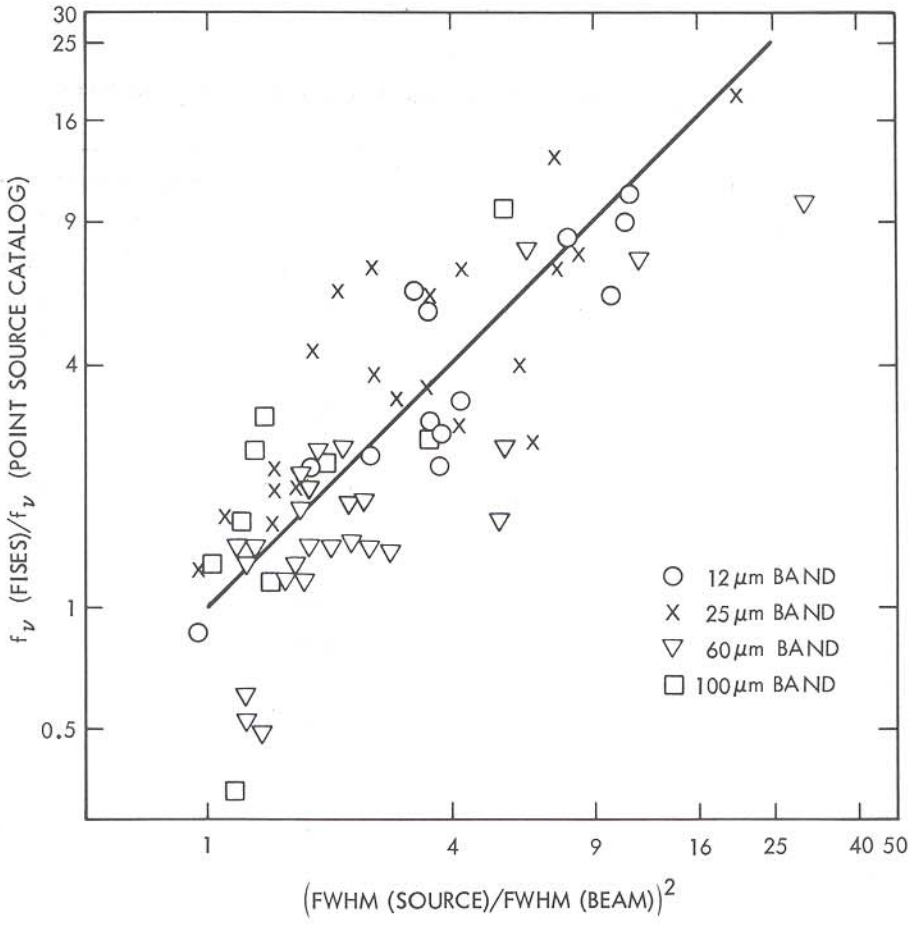

Figure V.B.1 Correlation between source size (width at half maximum in-scan) and ratio of SSS flux to flux from Point Source Catalog. "Beam" refers to the IRAS point source response in-scan at each band.

B.2 Comparison with Sky Brightness Images

As part of the verification procedure of the SSS Catalog in relatively uncrowded regions of the sky, Plate 25 of the Atlas of Sky Brightness Images was searched at the positions of Catalog sources; the search was made for all sources above 10 Jy in the 12 and 60 μm bands and within the plate boundaries. All 35 sources were found. The emission from each source was then measured on the Plate in a square area 10′ on a side, thus mimicking the SSS flux estimation. Figure V.B.2 shows the comparison between the fluxes measured from the Plate and those in the Catalog. There is clearly good agreement, with a standard deviation on the flux ratio of about 27%. In Section V.D below a detailed comparison is shown of a Sky Brightness Image with the SSS entries in the same area of the sky.

B.3 Comparison with Additional Observations

For areas of the sky targeted by Additional Observations, maps are available with substantially higher sensitivity than the survey. For details see *A User's Guide to IRAS Additional Observation*

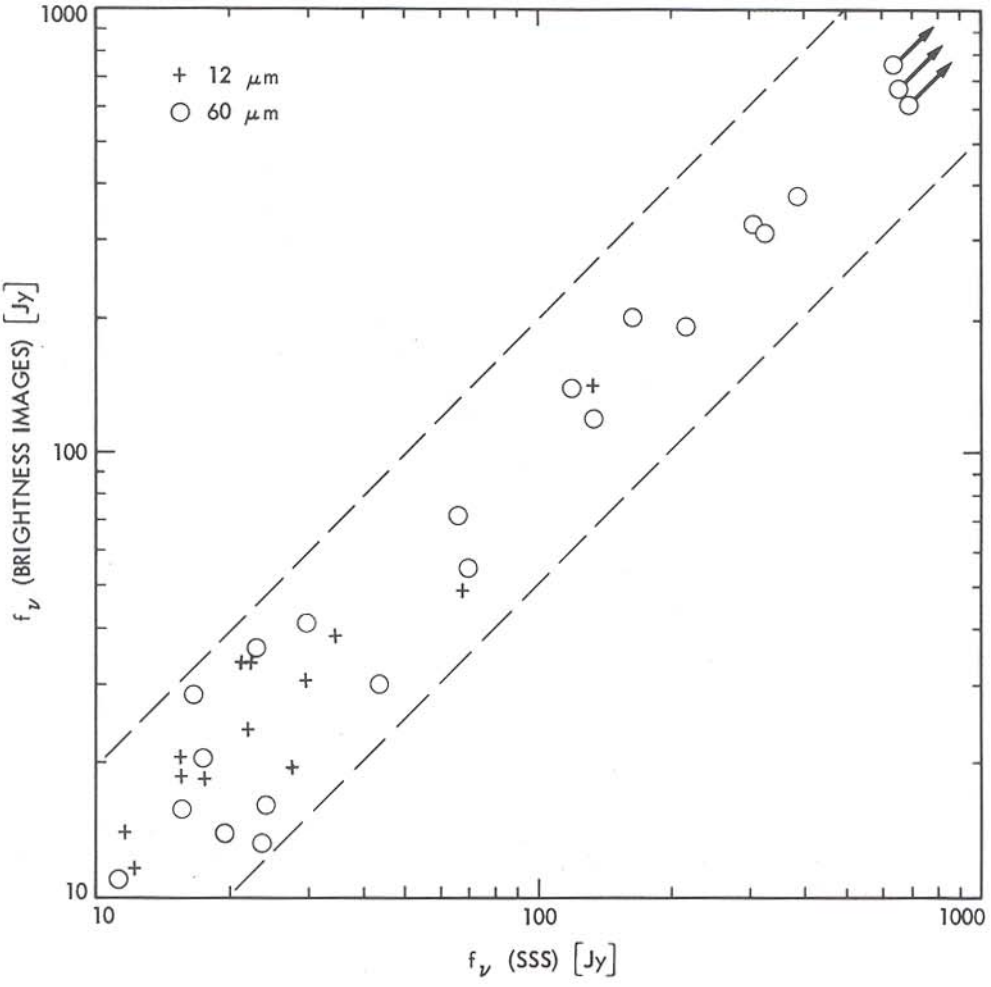

Figure V.B.2 Comparison between SSS fluxes and fluxes estimated from Sky Brightness Images. The two broken lines correspond to a factor 2 disagreement between the two measurements of the same source.

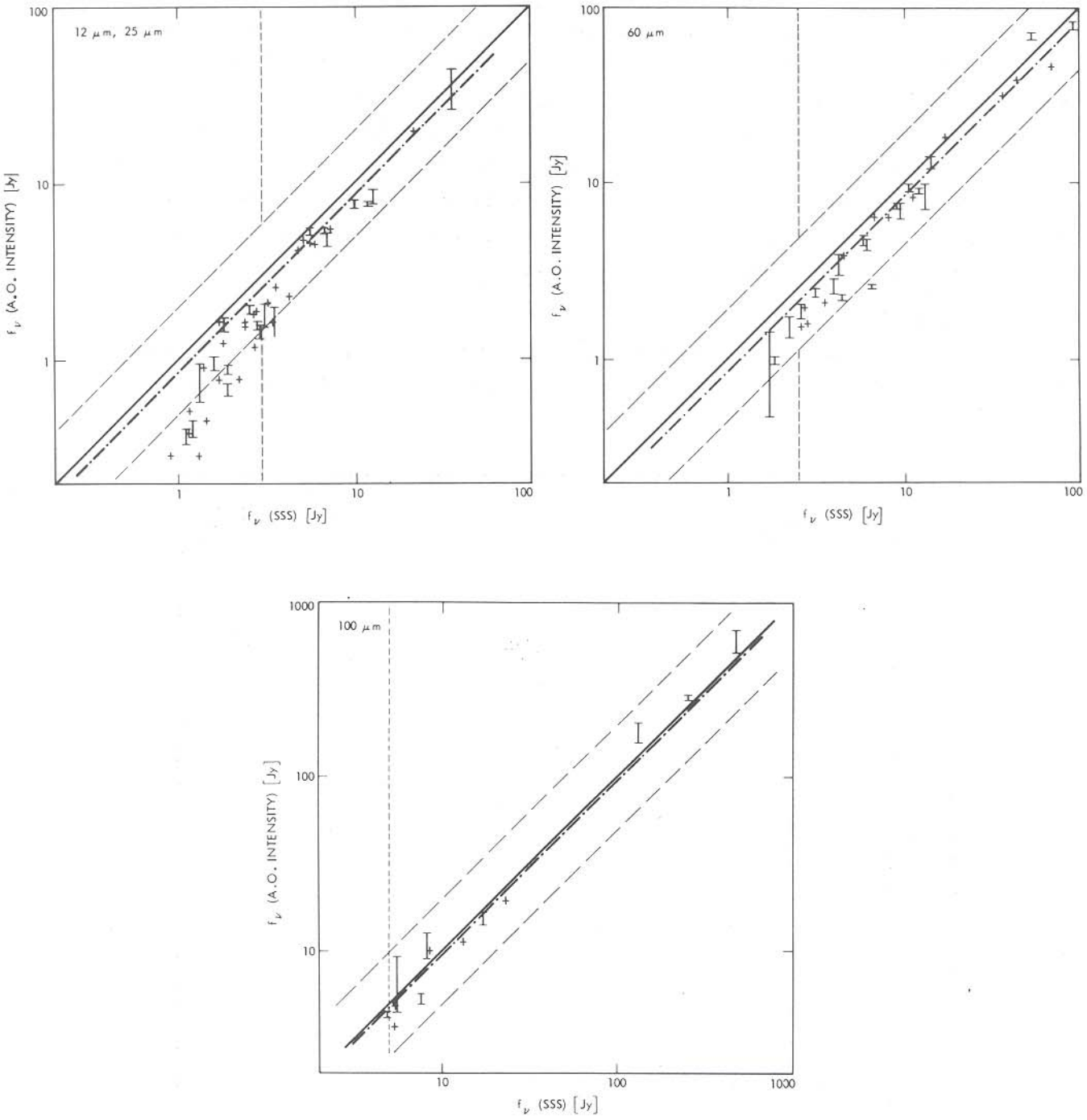

Figure V.B.3 Comparison between SSS fluxes and fluxes extracted from Additional Observations "intensity mode" maps.

Programs, Young *et al.* 1986. These maps are searched for sources using a two-dimensional algorithm. The "intensity mode" maps used here are specifically designed to allow correct measurement of extended emission rather than point sources. Sources thus found and extracted are completely independent of the SSS Catalog both in the origin of the data and the method of analysis. A list of extractions from a random set of maps was compared to SSS Catalog entries to assess the results of SSS processing near the detection limit. The flux comparison between the two data sets is shown in Figure V.B.3. In each panel of that Figure, the abscissa has flux densities from the Catalog, and the ordinate from the extractions; when there are extractions from several Additional Observations of the same source, a vertical bar is drawn joining the lowest and highest flux densities extracted. The vertical line at a few Jy indicates the flux threshold away from confused areas (IV.A.3). The solid line represents a flux ratio of unity, and the lighter broken lines on either side of it represent flux ratios of 1/2 and 2.

Because of the different calibration philosophies applied to the Catalog and to the "intensity mode" Additional Observations maps, agreement should result in a flux ratio not of unity, but a ratio indicated by the dotted line just below the solid line in each of the panels in Figure V.B.3. This different ratio takes into account two effects: (i) The maps used to extract extended sources are calibrated using detector responsivity at very long dwell times or "DC" responsivity (Suppl.IV.A and Suppl.VI.B), which is always higher than survey rate responsivity; SSS calibration assumes survey rate responsivity with a partial adjustment for source size (II.C and Suppl.IV.B). (ii) In addition effective detector areas used in obtaining the "intensity mode" maps are slightly (0 to 4%) larger than the geometric areas used in SSS *source construction* (Suppl.V.E.3).

The agreement between SSS and Additional Observations is quite good above 5 Jy, with the data more consistent with the dotted line than the solid one. Compared to Additional Observations, SSS seems to over-estimate the flux density systematically by 0.5 to 1 Jy at 12 and 25 μm; the 60 μm data is consistent with this trend but inconclusive. The over-estimation may occur at all flux levels, for it would not be noticeable above 5 Jy. This trend apart, the two flux estimates always agree to better than a factor 2. Above 5 Jy the standard deviation on the ratio between the two estimates is about 20%. If SSS flux densities are corrected for over-estimation by 0.7 Jy, the resulting flux ratio has a standard deviation of about 30% for all the data at 12 and 25 μm shown in Figure V.B.3. Caution is required in applying a correction for this apparent over-estimation, because the "intensity mode" extractions are not understood in fine detail. To justify a correction, an over-estimation trend would have to be established for SSS fluxes compared to the raw detector output measured by the SSS processor. As shown in V.C.1, such a trend could not be convincingly established.

C. Uncertainties

In estimating uncertainties on the Catalog source parameters, we have compared these sources to the corresponding raw detector data, to their description in other IRAS products, and to the corresponding entries in other astronomical catalogs.

C.1 Flux Uncertainties

The largest contributors to flux uncertainties in the Catalog were the SSS processor's measurement of the size of an excursion associated with a source above the baseline in the detector output (III.A), and

the source assembly resulting in a FISES entry (Suppl.V.E.3). In order to estimate those errors, detector data were examined in detail for about 90 sources. The sources were chosen in two independent ways from FISES; about half were found by searching near large spiral galaxies, and the rest selected to represent a wide range of total fluxes and sizes, including objects with complex background. For each source, detector output was integrated numerically to obtain the total emission and the width at half maximum of the source above a local linear baseline. The results are shown on Figure V.C.1, where the ratio of FISES flux to flux from direct integration is shown as a function of source size. The size (full width at half maximum) is normalized so that a point source at any wavelength appears at an abscissa of zero, and an 8′ source is at an abscissa of 1. This same sample of sources is used for the size comparison in V.B.1.

In more than 90% of the cases, the FISES flux agrees with the more accurate direct measurement to within a factor of 2. For sources with a signal to noise ratio above 20, the same agreement holds in more than 95% of the cases. For the entire sample, the mean ratio between the two flux estimates in Figure

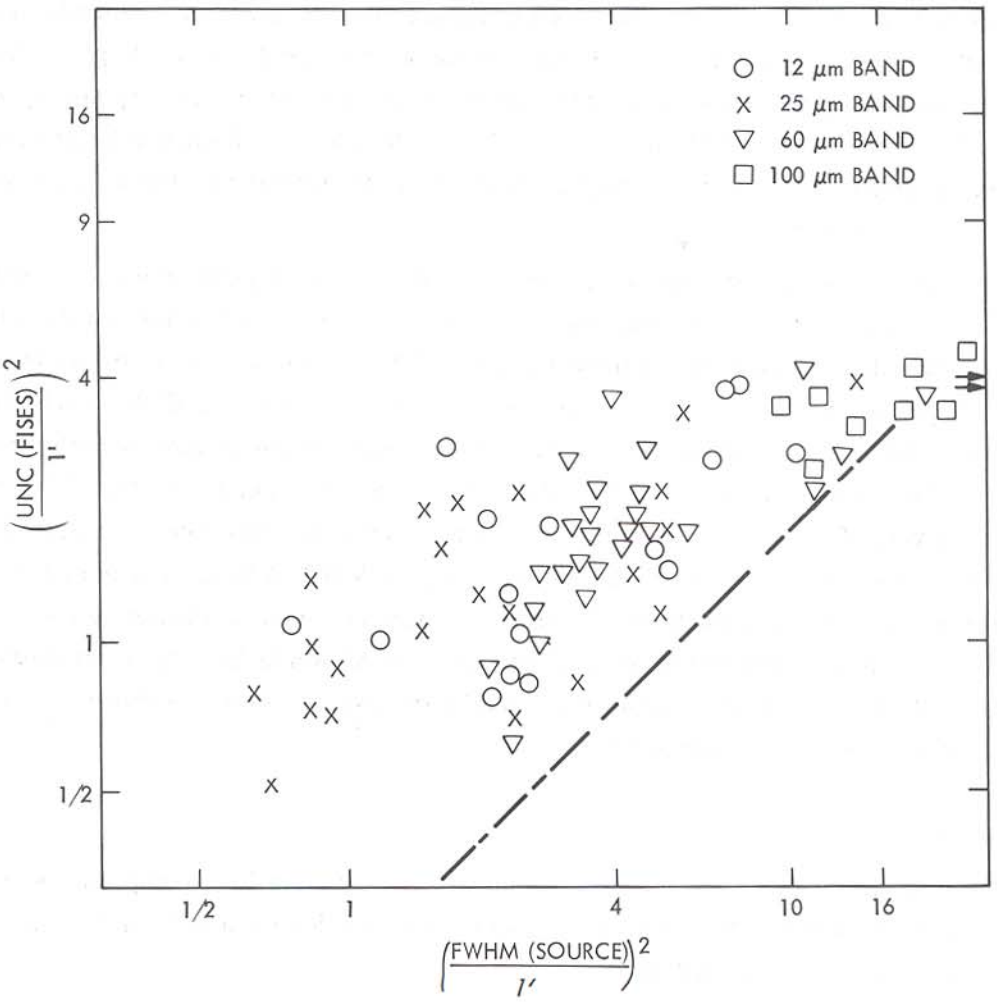

Figure V.C.1 Comparison between FISES fluxes and fluxes obtained by direct integration of detector output.

V.C.1 is one. The population dispersion in the flux ratio is about 50%, roughly the same for sources at high and low signal to noise ratios, and in all bands. Figure V.C.1 also reveals a tendency in the SSS processor to over-estimate flux for sources close to the resolution limit, and a lesser effect in the other direction for large sources.

The same check for flux accuracy was repeated for SSS Catalog entries associated with galaxies; 25 fluxes at 60 μm, and five at 100 μm were estimated from the detector data directly and compared with Catalog fluxes (Figure V.C.2). The heavy line corresponds to exact agreement, and the dashed lines to disagreement by a factor 2. The vertical dashed lines indicate the flux thresholds (2.5 Jy at 60 μm and 5 Jy at 100 μm) in this part of the sky. The dispersion in flux ratio is about 33%. The difference between the accuracy of fluxes in intermediate and low quality classes is not significant. Figure V.C.2 provides at best meager support to the over-estimation trend discussed in connection with Figure V.B.3, with only low quality fluxes possibly affected. Given the conflict between the evidence here and in Figure V.B.3, no blanket correction was applied to Catalog fluxes.

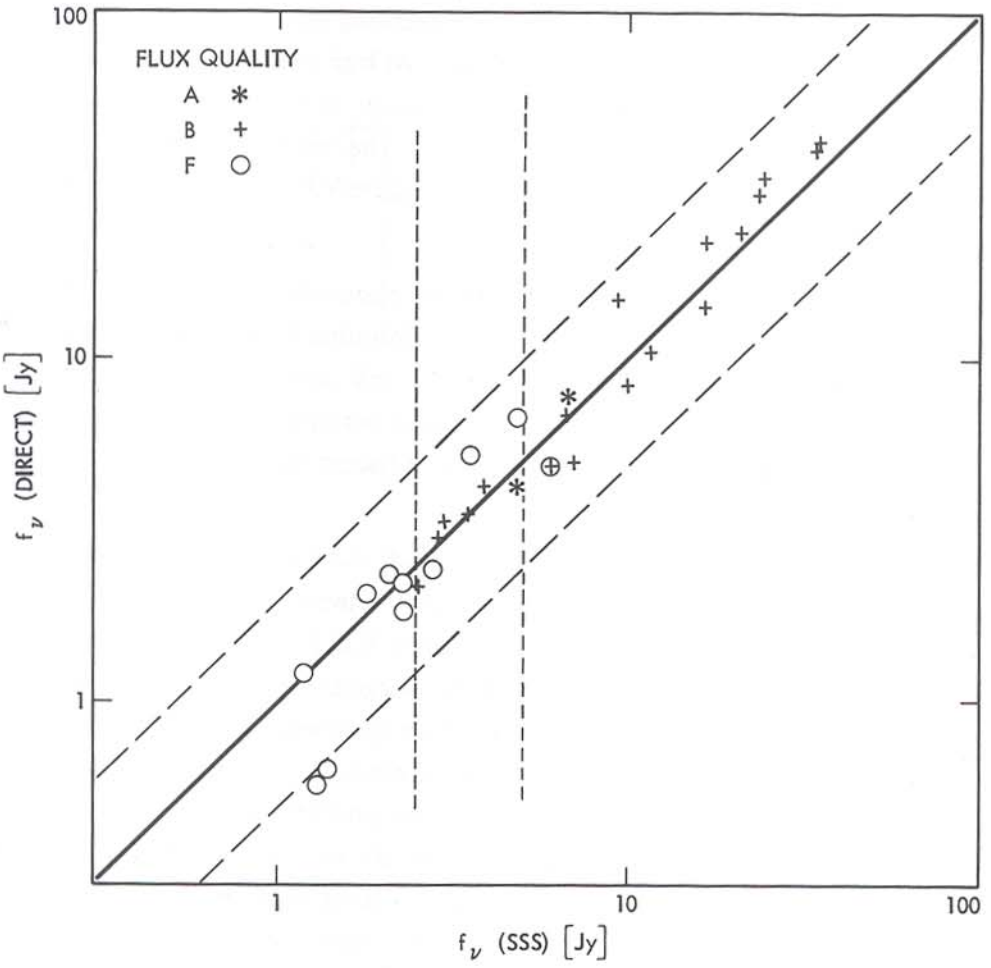

Figure V.C.2 Comparison between SSS Catalog fluxes and fluxes at 60 and 100 μm obtained by direct integration of detector output.

Repeatability of the processor was also tested by examining the various flux estimates present in FISES for the same source. As *weeks confirmation* proceeded, a histogram was accumulated of the flux ratio in each pair of weeks-confirming FISES entries. The standard deviation in this flux ratio on a log scale is equivalent to 54%, 53%, 49% and 43% respectively at 12, 25, 60 and 100 μm. This implies a scatter in each flux measurement about the final value with a standard deviation equivalent to 36%, 35%, 33% and 29% respectively at each wavelength. If in the limit of a large number of sightings SSS flux estimation converges to the true flux, the expected rms error in Catalog fluxes (with at least two sightings) should be better than 24%, 24%, 22% and 20% respectively at 12, 25, 60 and 100 μm. But this is not the case, as both single measurement errors and Catalog flux errors are larger than predicted from repeatability. This implies that the mean SSS flux estimate does not necessarily approach the true flux as the number of sightings approaches infinity, and that flux accuracy does not improve with the number of sightings as fast as $N^{-0.5}$. The reason for that behavior is related to the fundamental limitation of filtered amplitudes as signal estimators, as illustrated in Figure III.A.1.

Based on these results and Figures V.B.2 and V.B.3, flux estimates in the SSS Catalog are assigned an uncertainty between 30% and 50%, completely overshadowing possible errors in absolute calibration which are on the order of a few percent to 10% at 100 μm. At high signal to noise ratio and in clean sky, the uncertainties are near 30%, whereas larger errors may occur in crowded regions. Figure V.B.3 provides the most convincing validation of these numbers. The tendency it points out toward overestimation of fluxes (by less than 1 Jy) is not confirmed by Figure V.C.2 and thus remains questionable.

C.2 Positional Uncertainties

Because of the degraded resolution in SSS processing, positional errors here were expected to arise mostly in *source construction* (Suppl.V.E.3) rather than in Pointing Reconstruction (Suppl.V.B), and to be on the order of one arcminute, since this was the cell size on the *source construction* grid (Suppl.V.E.3). To assess positional uncertainties, positional agreement was analyzed in two contexts: First, band to band in Catalog sources with detections in adjacent bands, and second, between Catalog sources and associated astronomical objects.

All Catalog sources containing only two adjacent bands were *assumed* to represent spatially coincident emission at those two wavelengths, and disagreement between the positions measured in each of the two bands was ascribed to positional uncertainty. Table V.C.1 summarizes the results of positional comparisons for all three pairs of adjacent bands, with the disagreement broken down into rms separation in declination and right ascension. There is clearly more disagreement (25% to 50% roughly) in the R.A. than in the declination direction. This reflects greater uncertainty in localizing the source in the cross-scan direction than in the scan direction, since the latter was generally along Ecliptic meridians. Assuming independent errors along and across the scan direction, the two can be combined to obtain the rms vector amplitude of the separation between the two adjacent band components given in the third line of Table V.C.1. If positional determinations in each band are again independent, the expected rms positional error in a single band source is $60''$ to $70''$.

Another test for positional accuracy comes from analyzing the positional associations with objects in the ESO/Uppsala Survey (Catalog number 14 in Table Suppl.V.H.1). The rms amplitude of the vector separation between Catalog entries (both with single and multiple bands) and associated objects is about

TABLE V.C.1

Band-to-Band Positional Offsets in Adjacent-Band Sources

Band Pair	12 μm/25 μm	25 μm/60 μm	60 μm/100 μm
Number of Sources	784	387	3849
RMS Dec Difference	58″	61″	48″
RMS R.A. Difference	79″	75″	73″
RMS Separation	98″	96″	88″

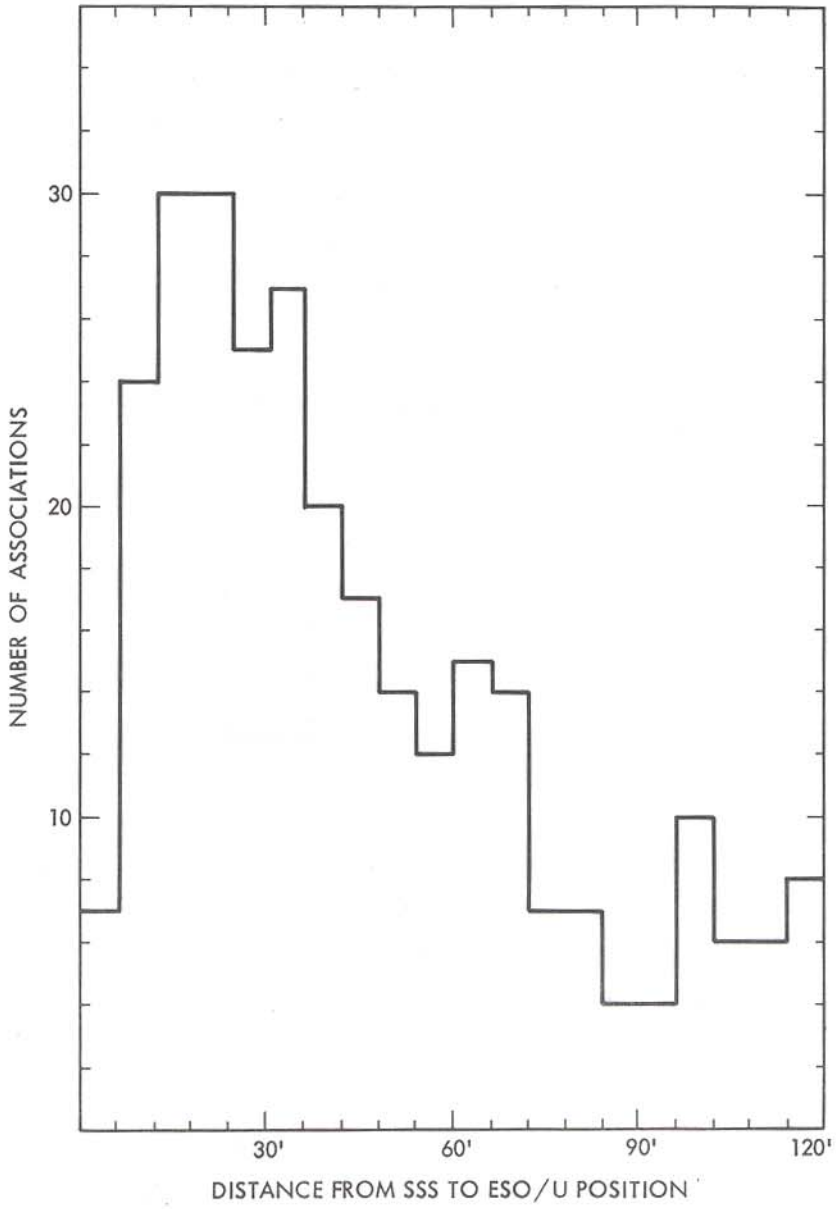

Figure V.C.3 Histogram of the distance between SSS Catalog sources and their associated objects in the ESO/Uppsala Catalog.

55″ (Figure V.C.3); two thirds of the 288 associated objects are within 54″ of the corresponding source. This may be taken as a conservative estimate of the positional accuracy since some of the associations are fortuitous (cirrus, line of sight coincidence, etc.) and optical positions are not perfect. Using the same associations, no anisotropy is detected in the positional errors: the distribution of position angles from SSS to associated objects is uniform to statistical accuracy (Figure V.C.4).

The accuracy of a SSS position determined from a single band is therefore estimated at about one arcminute for the rms amplitude of the error vector. The positional uncertainty attached to each band component in a source, UNC (defined in Chapter VII; see V.C.3 below), has a median of about 3.6′, 3.6′, 4.1′, and 4.4′, respectively, at 12, 25, 60, and 100 μm. In the Gaussian approximation UNC can therefore be interpreted as the 95% confidence diameter within which the emission centroid may be found.

C.3 Sizes

The inferred sizes PSIZ obtained from a comparison of SSS fluxes with Point Source Catalog fluxes (see V.B.1 above) should be interpreted as rough indicative sizes since they are not direct measurements. Clearly, PSIZ is a valid estimator only for simply shaped sources completely contained within ten

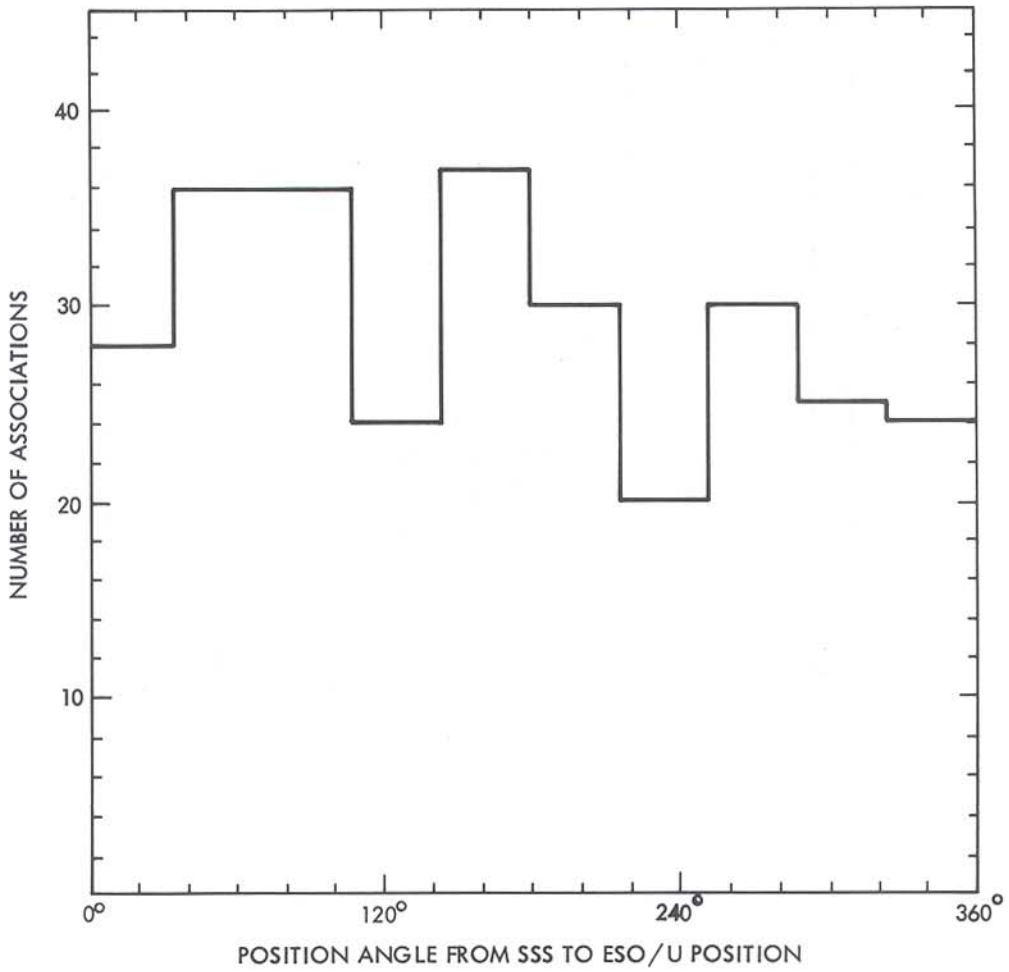

Figure V.C.4 Histogram of position angles from SSS Catalog sources to their associated objects in the ESO/Uppsala Catalog.

arcminutes or so. In these cases, PSIZ is affected by uncertainties in the flux estimate and to a lesser extent by variations in source shape. For all but one of the sources plotted on Figure V.B.1, PSIZ agrees with the measured source width at half maximum to within one point source width. From this and the roughly Gaussian dispersion, the uncertainty on PSIZ can be stated as an expected rms error of about 0.4′, 0.4′, 0.8′ and 1.5′ at 12, 25, 60 and 100 μm respectively, or as ± one beamwidth for the 95% confidence interval. PSIZ is also useful as a record of the associated Point Source flux.

Originally, it had been hoped that the second moment of the modeled flux distribution might be useful as a size estimator (Suppl.V.E.3). But this could be the case only if the source was substantially larger than the one arcminute grid cells, had a high signal to noise ratio, and was constructed from a large number of detections. Most sources detected proved to be near the resolution limit, thus rendering useless the covariance matrix as a size estimator. Most often, the second moment reflected the construction algorithm, i.e. was determined by the sizes of detection filters and grid cells. This can be seen directly on Figure V.C.5, where UNC is plotted against the half power width of each source, measured directly off the detector data, for the same sources that appear in Figure V.C.1. The heavy dashed line corresponds to perfect agreement between the two measurements. Although there is a general positive correlation between the two quantities, UNC is more adequately thought of as the positional accuracy with which the processor could localize the source.

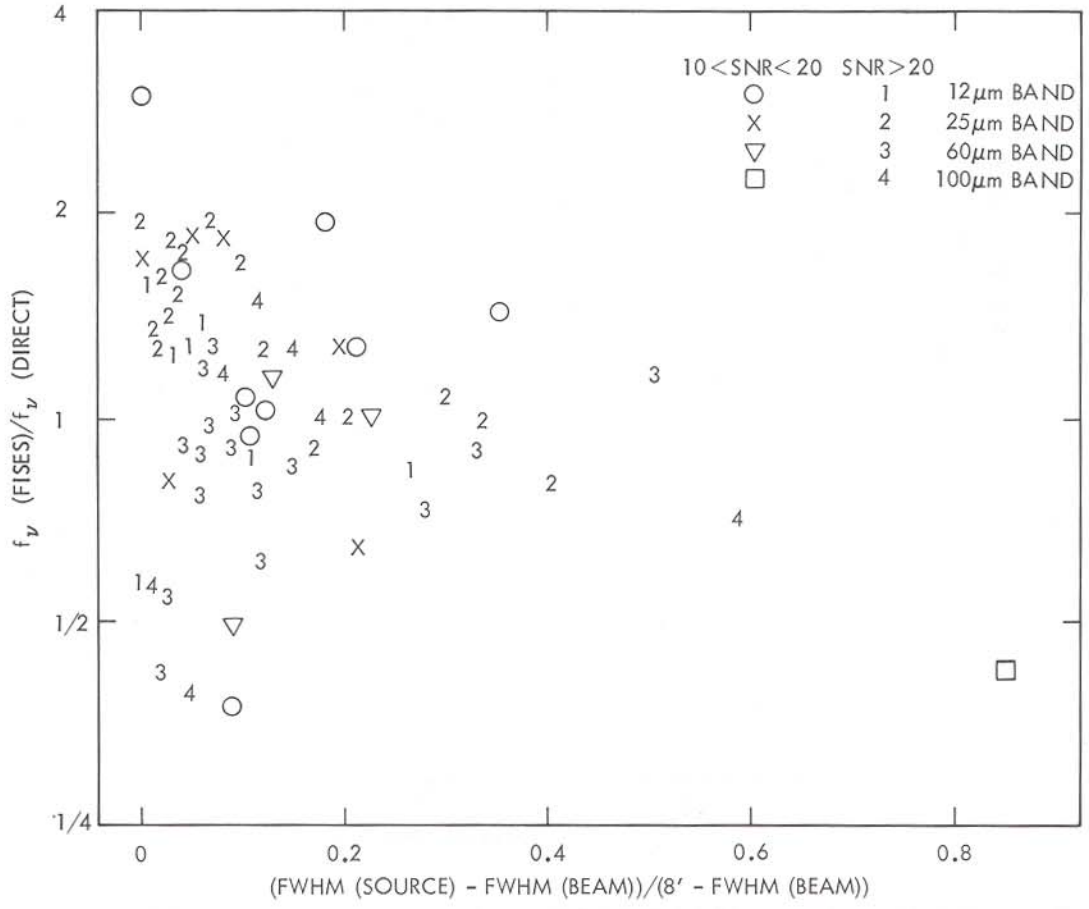

Figure V.C.5 Comparison of UNC with the in-scan width at half maximum measured directly on the detector output.

D. Performance in the Galactic Plane

This Section presents a detailed examination of the IRAS data in a small region of the Galactic plane, comparing the various final products and checking in particular the performance of SSS processing in an area rich with complex structure. Data at all bands from the Point Source Catalog, the SSS Catalog, and the Sky Brightness Images are displayed as maps. A deeper level of detail is explored at 25 μm, where the FISES contents and some raw detector output are also displayed.

Figure V.D.1 shows all Point Source Catalog entries in the part of the sky chosen for this analysis, a square area 4° on a side, centered at Galactic coordinates (l,b)=(60°,0°), and surveyed three times in the course of the mission. Figure V.D.2 presents all SSS Catalog sources in the same region. On both maps,

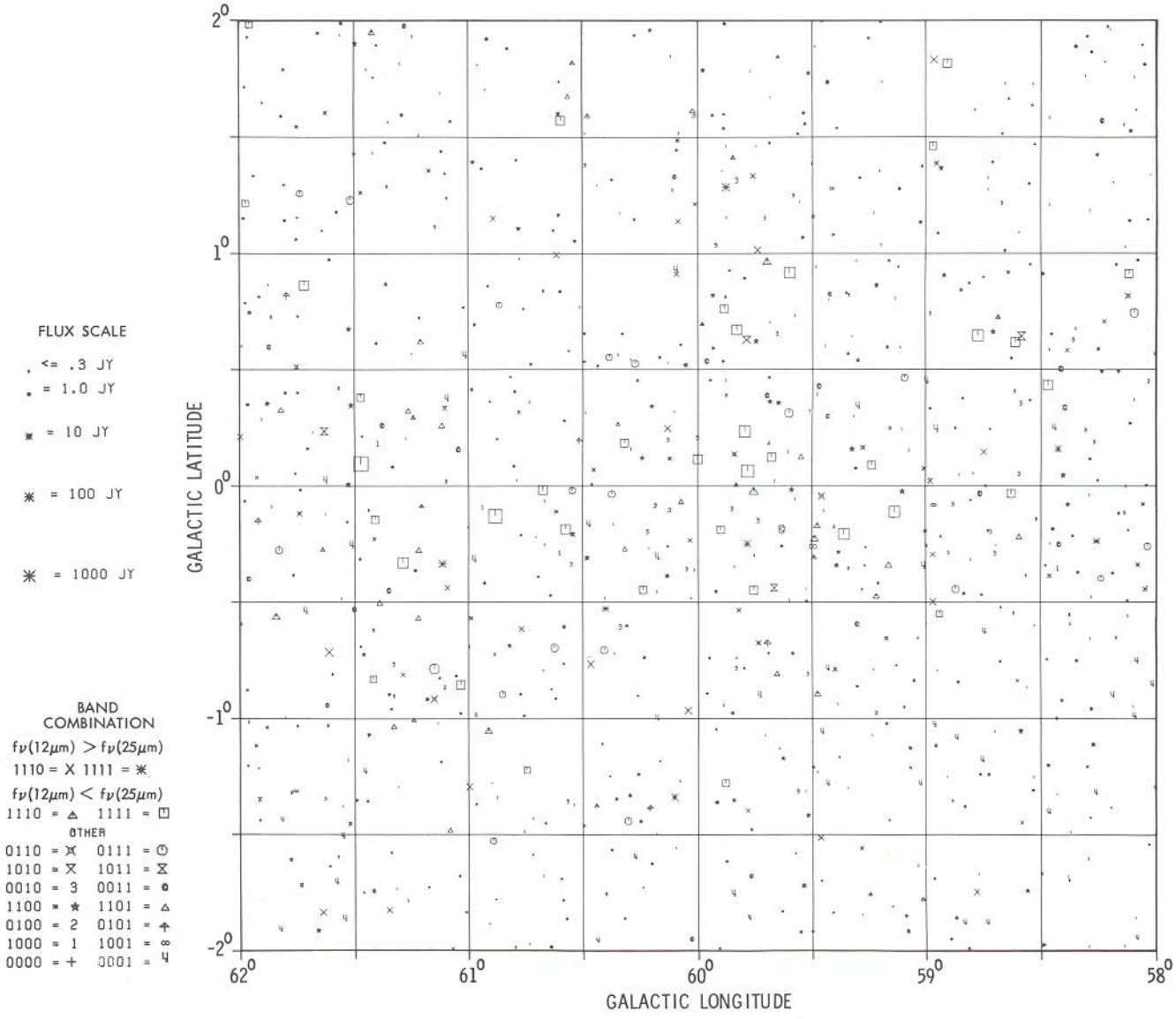

Figure V.D.1 The distribution of IRAS Point Sources in the test area of the Galactic plane. Each symbol represents one source and indicates the bands in which it was detected, and the flux density in the brightest band.

each source is shown as a symbol denoting the combination of bands at which the source is detected. Fluxes with low quality in SSS sources are not considered detections in their bands. Symbol size indicates source brightness on a logarithmic scale. The surface density of SSS sources remains below about 10 sources per square degree, and is almost ten times smaller on average than the density of Point Sources which ranges from 40 to 60 per square degree. This is a direct result of *cluster analysis*. There is no direct correspondence between Point Sources and SSS sources, although the Point Source density is so high that most SSS sources fall near or at the position of a Point Source.

Figure V.D.3 displays the 12 μm contour map of the Sky Brightness Image and the 12 μm data in the SSS Catalog. The contour steps correspond to equal steps of 0.1 in the log of surface brightness. In

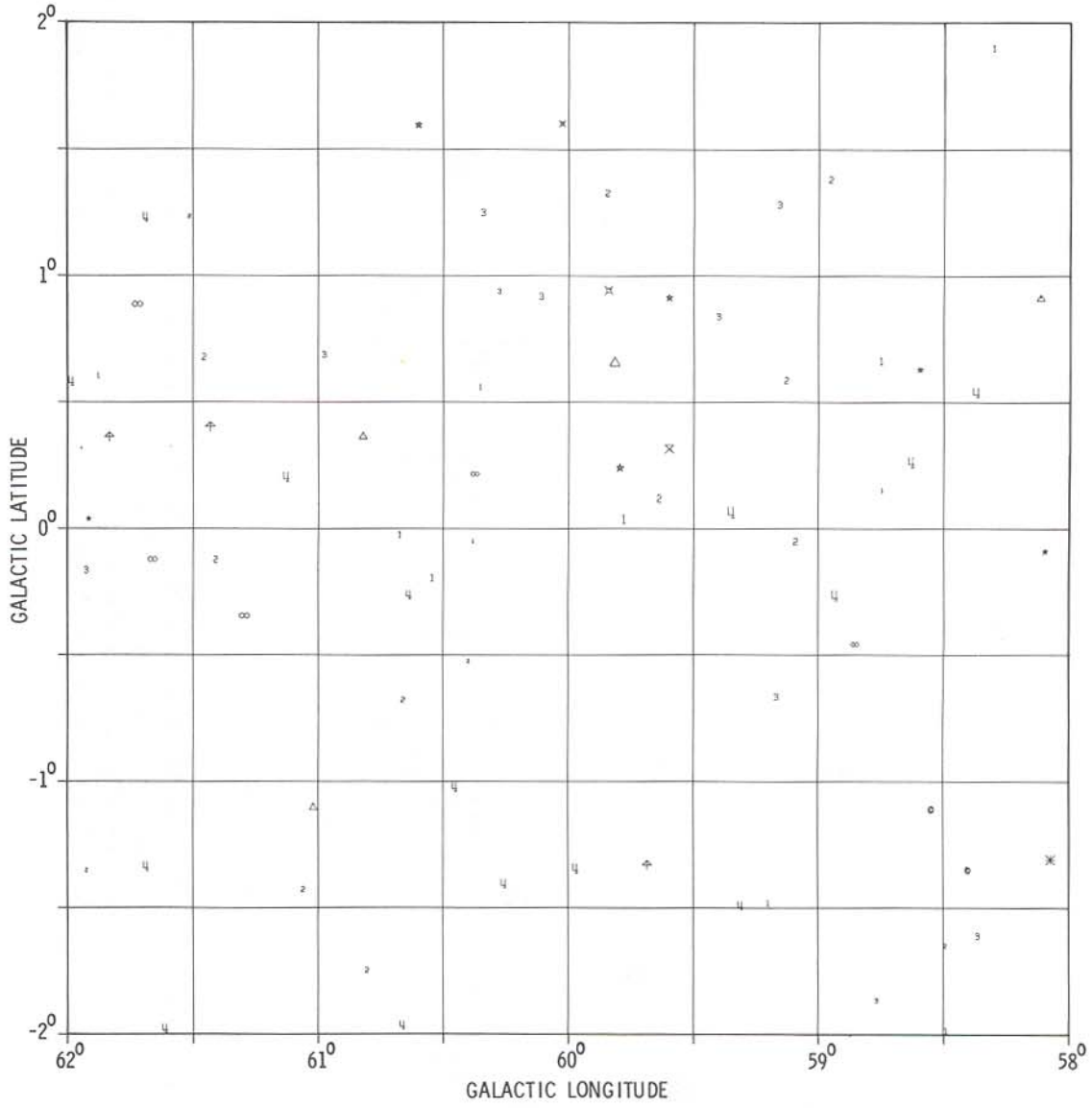

Figure V.D.2 The distribution of sources from the SSS Catalog in the test area of the Galactic plane. See Figure V.D.1 for interpretation of symbols.

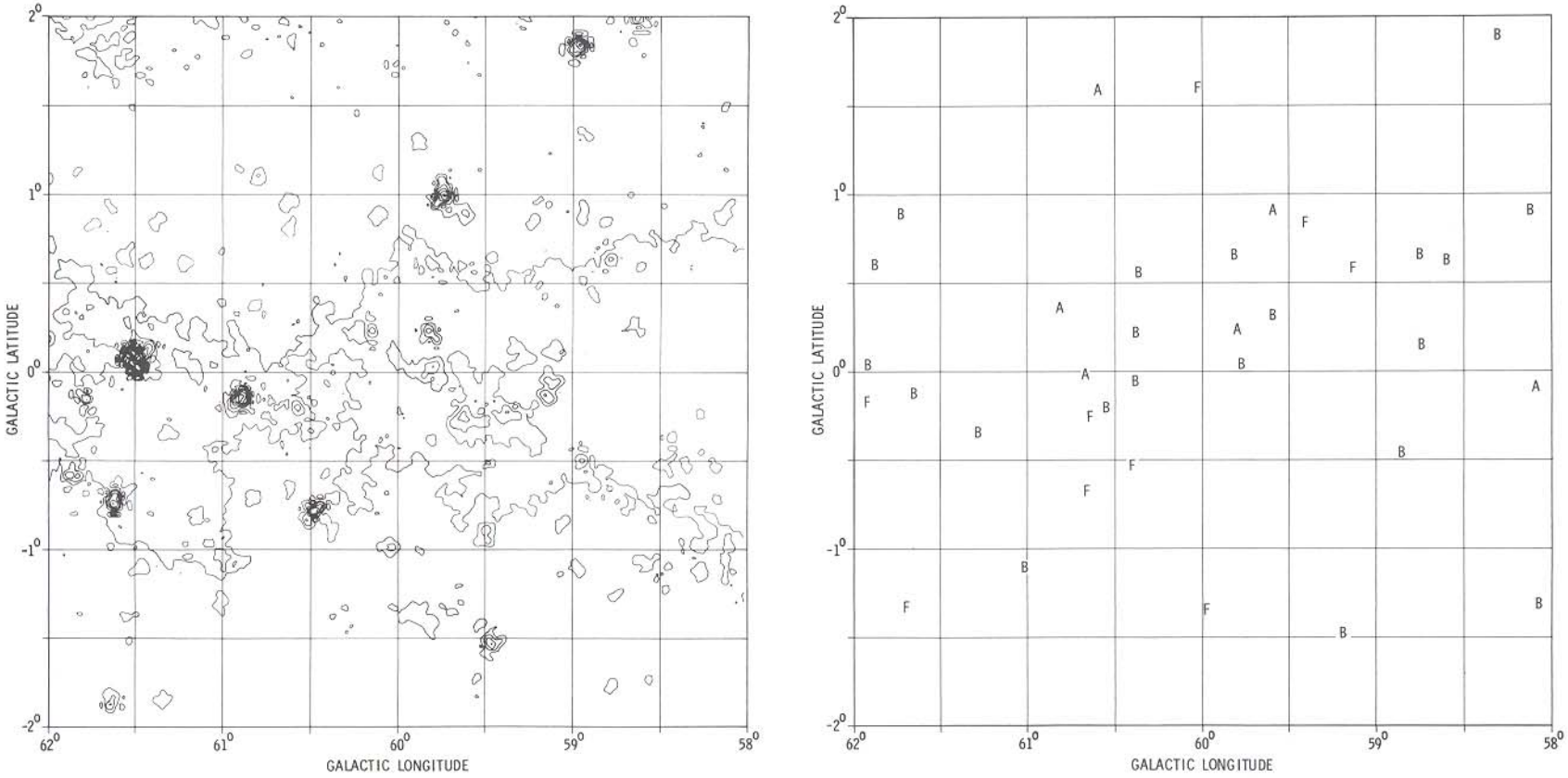

Figure V.D.3 Left: The Sky Brightness Image for the test area of the Galactic plane, shown as a contour map where contour steps correspond to +26% steps in surface brightness. Right: The distribution of 12 μm fluxes from the SSS Catalog in the same area. Each flux is represented by a letter corresponding to its quality class, "A" for high quality, "B" for intermediate, and "F" for low quality or failed flux.

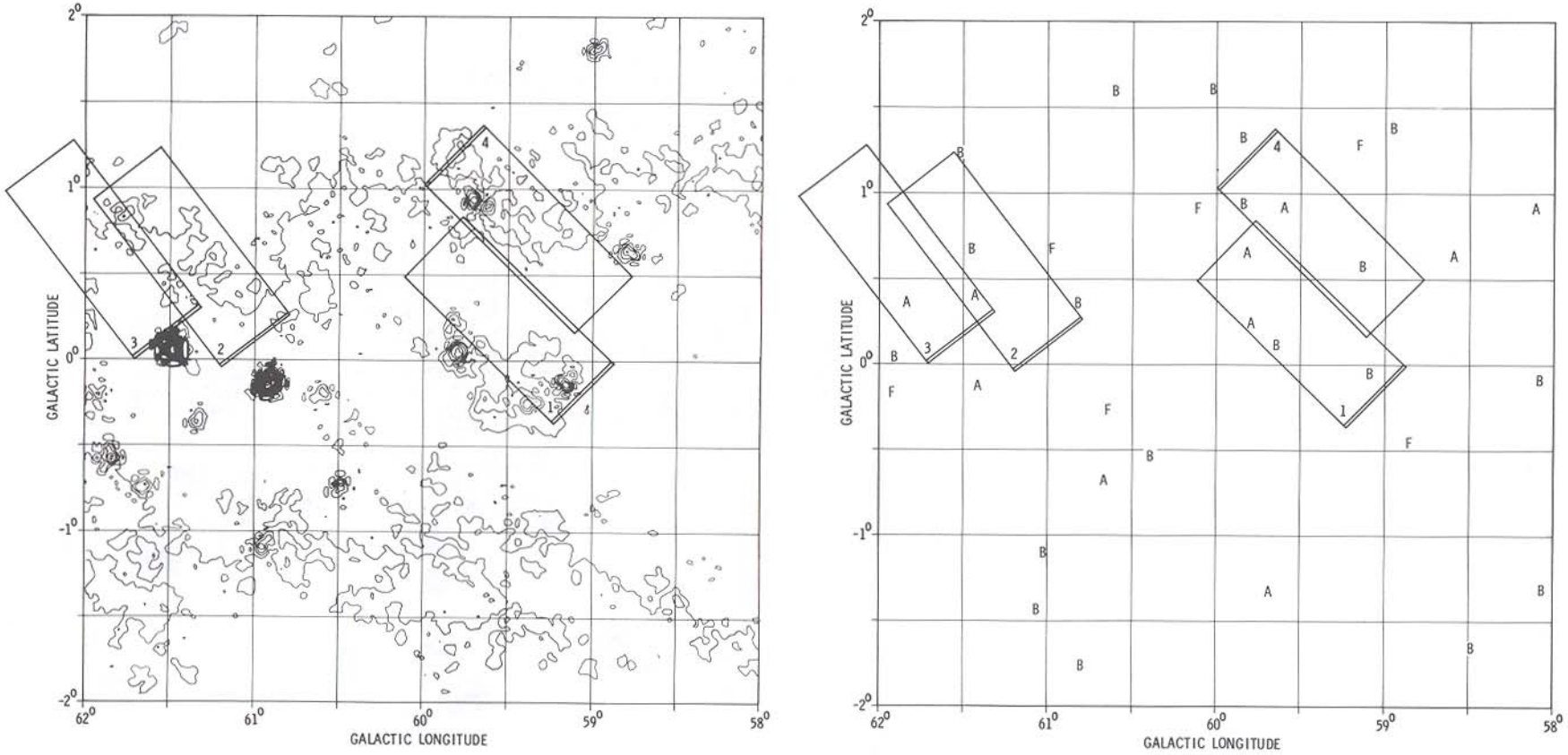

Figure V.D.4 Same as Figure V.D.3, but for 25 μm data. Each rectangular frame superposed on the map outlines a field for which the raw detector data are displayed in V.D.8. The focal plane scanned these fields proceeding from the side of the field marked by a double line toward the opposite side.

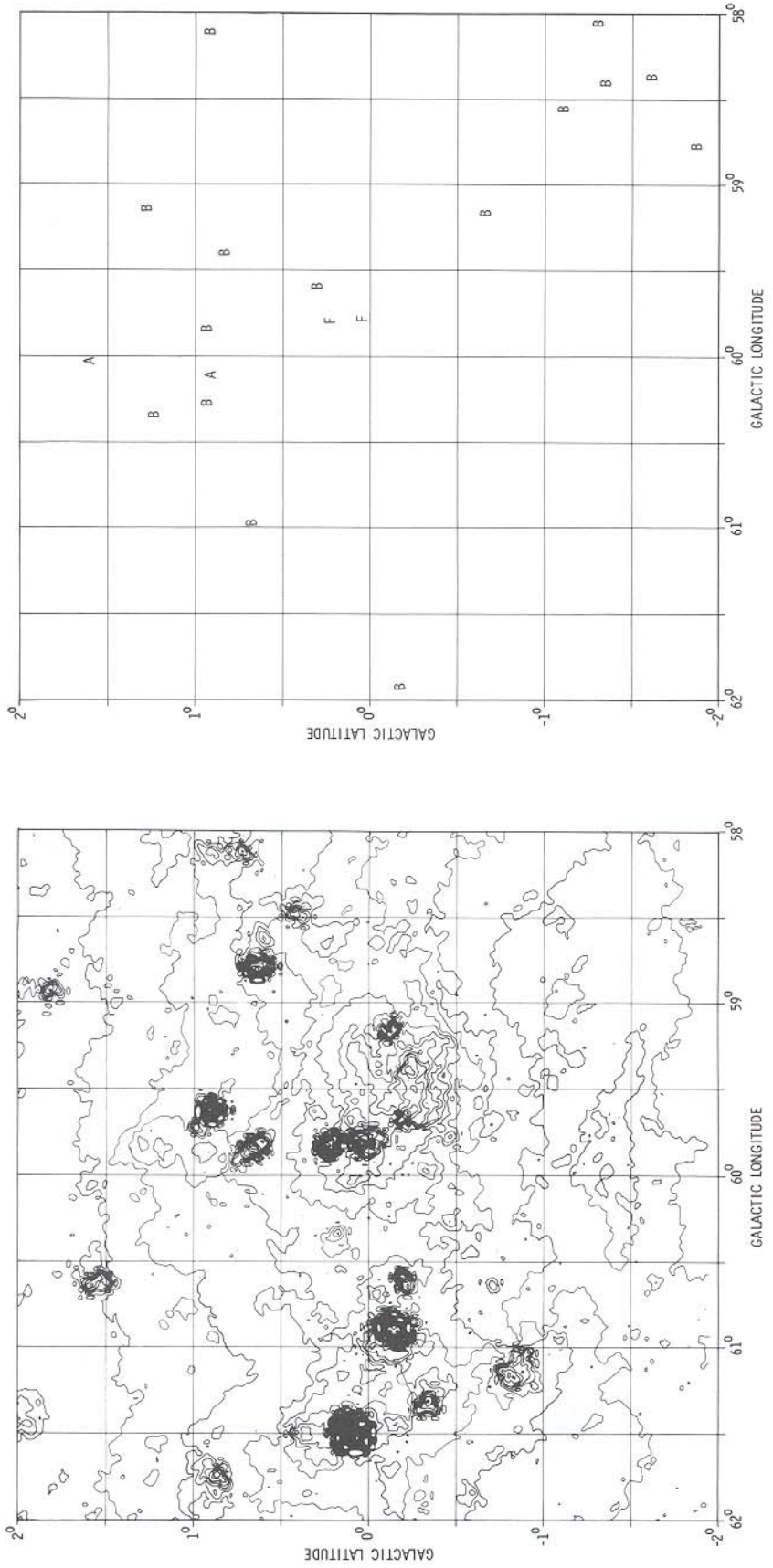

Figure V.D.5 Same as Figure V.D.3, but for 60 μm data.

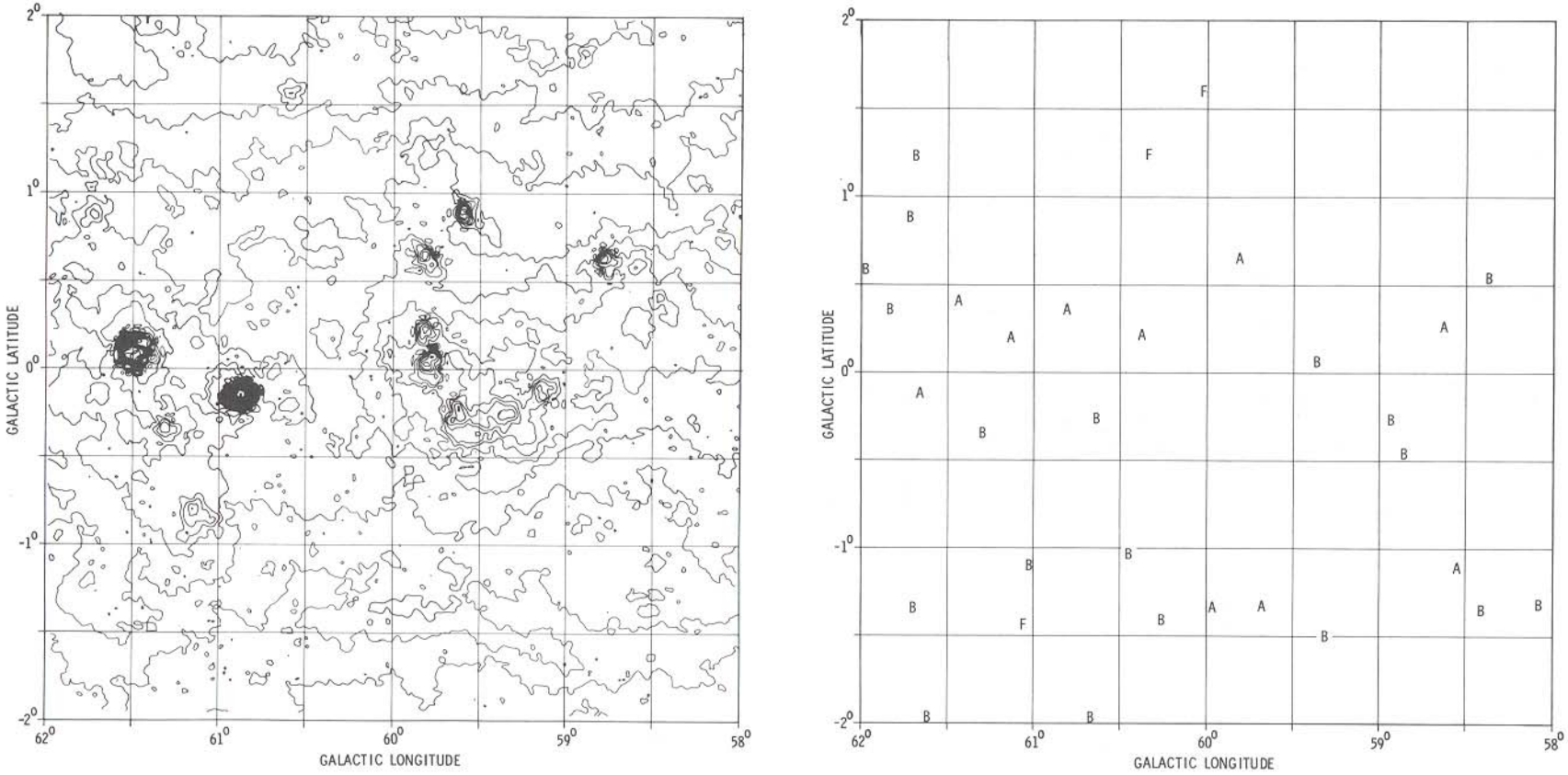

Figure V.D.6 Same as Figure V.D.3, but for 100 μm data.

the frame at the right, each 12 μm flux is shown as a letter corresponding to its quality class, "A" for high quality, "B" for intermediate, and "F" for low. The equivalent data for 25, 60 and 100 μm are shown in Figures V.D.4, 5 and 6. Figure V.D.7 shows all 25 μm FISES entries in the region of interest. Each symbol corresponds to an hours-confirmed sighting, with multiple symbols at the same location indicating weeks confirmations for the source. For the fields labeled 1 to 4 outlined on Figures V.D.4 and V.D.7, the raw IRAS data are displayed in Figure V.D.8 as the output from all 25 μm detectors when the focal plane scanned these fields on one of the survey coverages (see Suppl.II.C.4 and Figure Suppl.II.C.6 for a definition of detector numbers). On Figure V.D.8 the detections relevant to a SSS source are framed in dashed lines and labeled with a Greek letter which identifies that source. Catalog data on the sources thus identified appear in Table V.D.1 which lists for each source its IRAS name, approximate position in Galactic coordinates, flux density and quality class at 25 μm. The detector data in Figure V.D.8 are arranged such that if the scan proceeds towards East on the sky, then detectors at the Northern edge of the focal plane appear at the top of the frame. This is the reverse of the usual convention adopted for all the maps displayed in this Chapter. The signal amplitude (in inches) as plotted in Figure V.D.8 must be multiplied by the corresponding scaling factor shown to the right of the frame to obtain the signal amplitude on the same arbitrary scale for all detectors. Failed detectors are labeled with "F" instead of an amplitude scaling factor.

The first impression from Figures V.D.3 to 6 is that there is little if any correspondence between the features seen on the Sky Brightness Image and the data in the SSS Catalog. As will be shown in this discussion, this impression is due to a combination of incompleteness in the SSS Catalog, coarse resolution in the images, and limitations in the image display method.

TABLE V.D.1 Identification of SSS Sources Appearing in Figure V.D.8

Source Identifier	Source Name	Galactic Longitude (degree)	Galactic Latitude (degree)	f_ν (25 μm) (Jy)	Flux Quality
α	X1937+238	59.6	0.9	38	A
β	X1937+233	59.1	0.6	12	B
δ	X1937+241	59.8	0.9	7	B
γ	X1938+239	59.8	0.7	54	A
ε	X1939+229	59.1	-0.1	18	B
ζ	X1940+237	59.8	0.2	77	A
η	X1940+235	59.6	0.1	17	B
θ	X1942+253	61.5	0.7	10	B
ι	X1943+252	61.4	0.4	27	A
κ	X1944+255	61.8	0.4	25	A

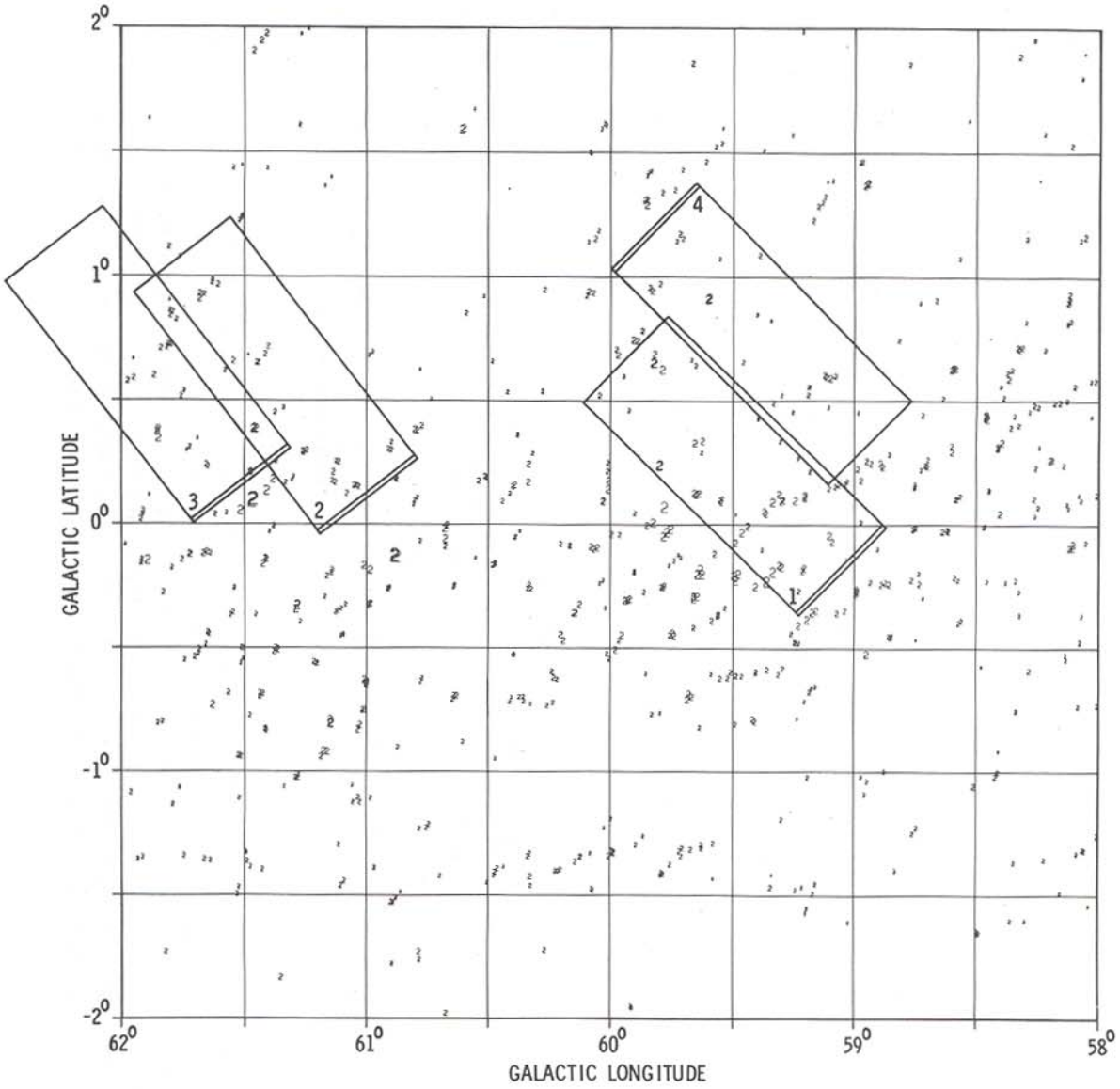

Figure V.D.7 The distribution of FISES entries at 25 μm in the test area of the Galactic plane. Each symbol represents an hours-confirmed sighting; symbol size is proportional to $\log f_\nu$ (25 μm). Each rectangular frame superposed on the map outlines a field for which the raw detector data are displayed in Figure V.D.8.

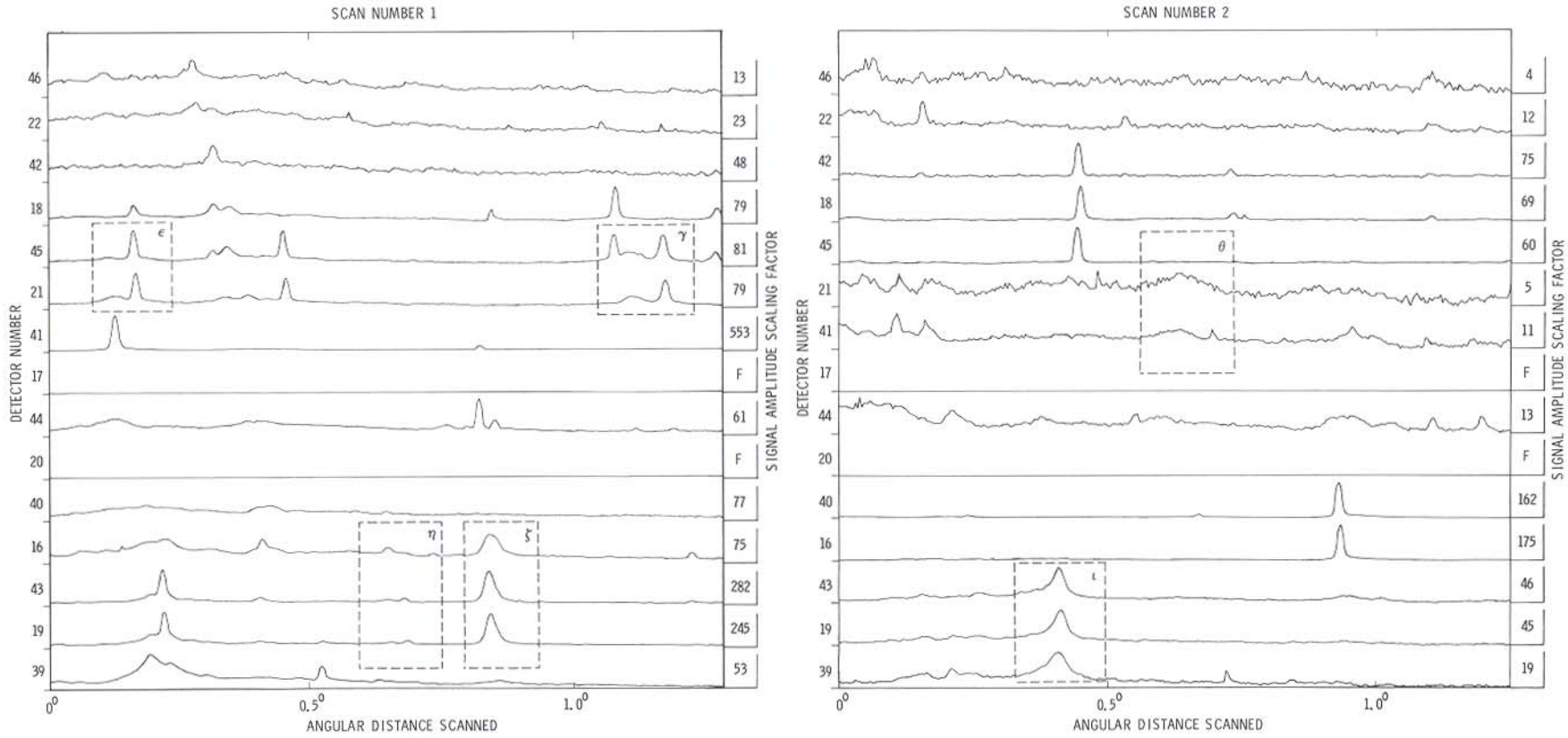

Figure V.D.8 The raw detector output from scans over the fields outlined on Figures V.D.3 and V.D.7. The scan starts at that end of the rectangular frame marked by a double line. In this Figure only, East is to the right if North is up. Output signal amplitude is plotted for each detector at each position; the plotted amplitude multiplied by the scaling factor at left gives the output amplitude in the same arbitrary units for all detectors. The distance scanned applies to each detector individually, so on this plot a source is seen on all the detectors it illuminates at the same abscissa, even though the detectors are illuminated at different times.

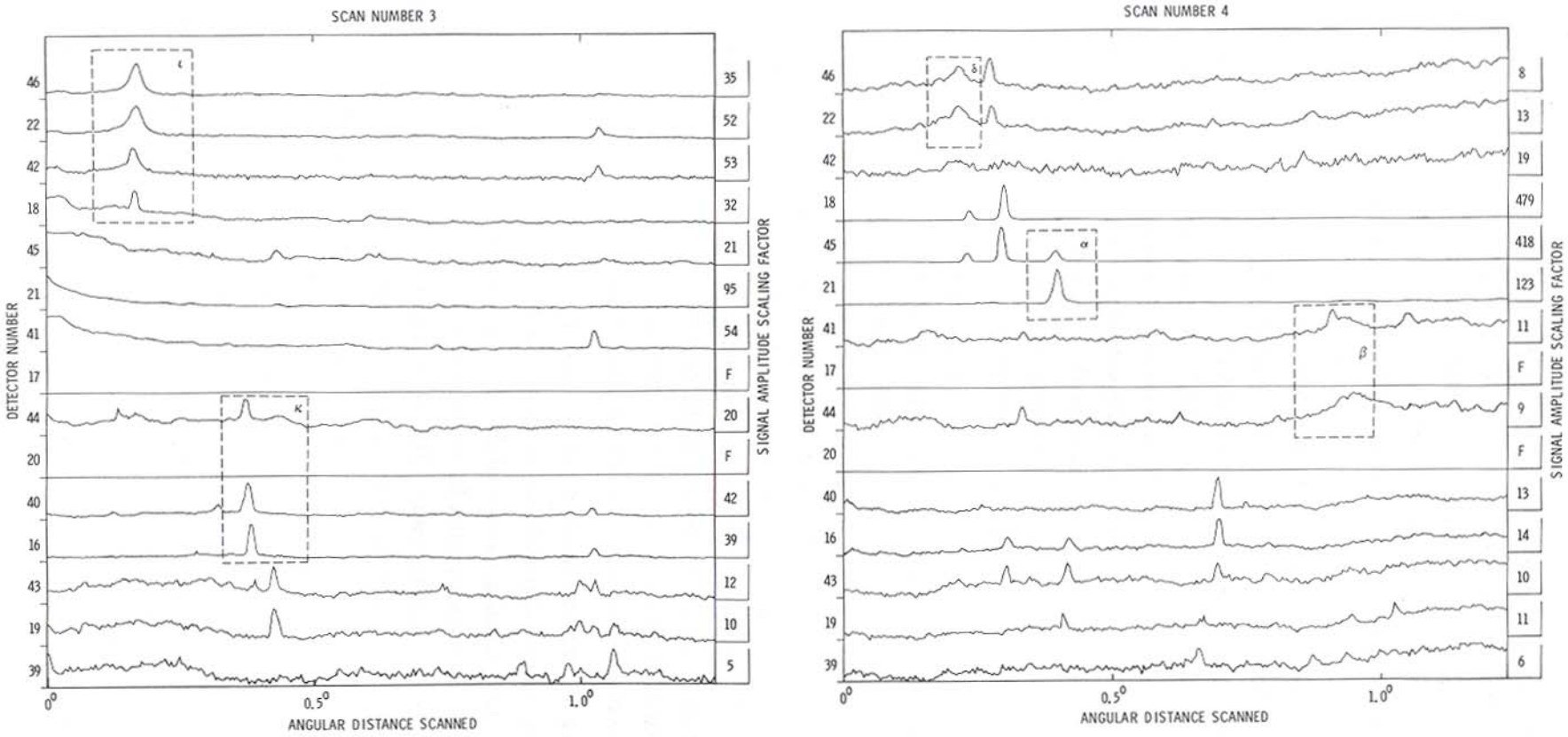

Figure V.D.8 Continued

The contour maps should indicate the presence of sources and thus might be used to investigate the completeness of the Catalog. Extended emission visible on these maps is expected to appear as SSS sources. It is clear from a casual inspection of Figures V.D.3 to 6 that not all prominent features in the contour maps have counterparts in the SSS Catalog. There are several reasons for this lack of Catalog entries; if the emission features are larger than about 10′, confused with neighbors, or details in larger structures, they were probably discarded by *cluster analysis* (Suppl.V.E.4), as they should have been. An example of too large a source at 25 μm is the prominent feature near (l,b)=(61.5°,0°) in the contour map in Figure V.D.4. It contains at its center a tight group of point sources that combined to cause detections in FISES (Fig. V.D.7). The trailing wing of the emission is just visible at the edge of scan field number 3, where it already covers more than 10′ (detectors 45, 21 and 41, left hand side of third panel in Figure V.D.8). An example which can be interpreted as either confusion or extended complex structure can be found in scan field number 1 in Figure V.D.4, as the feature extending towards the North-West starting from near (l,b)=(59.5°,0°) in the contour map. The corresponding string of detections can be easily seen on Figure V.D.7, and the corresponding signals can be found on detectors 21, 45 and all those above them roughly 20′ beyond the starting point of the scan on the first panel in Figure V.D.8.

In connection with emission features on the Images that do not appear in the SSS Catalog, it should be pointed out that the resolution of the Images is low enough (about 4′)that it is impossible to discriminate between point sources and true extended sources smaller than twice the point source template in width . This is well illustrated by the close pair of sources at (l,b)=(59.6°,0.9°) within scan field number 4 in the contour map in Figure V.D.4. Both components of the pair appear in the Point Source Catalog. The SSS Catalog contains only the component to the West, which appears to be the less extended of the two. Even FISES (Figure V.D.7) contains no trace of the component to the East. Examination of detector output clearly vindicates the Catalog, indicating that the detected component (Figure V.D.8, fourth panel, source α) is in fact extended, whereas its neighbor (immediately to the left from α, detectors 18 and 45) is unresolved. This example illustrates the complementary nature of the various IRAS products.

The inverse test of trying to verify the reliability of the Catalog by looking at the Images for features corresponding to SSS Catalog sources also leads to apparent inconsistencies that are resolved only by inspection of the detector output. Catalog sources labeled β, δ, γ, ι and κ are all good illustrations of positions where the Sky Brightness Images cannot be interpreted to contain sources, but where detector data provide ample justification for a Catalog entry. The main reason for sources not to appear on the contour maps is one of display; the choice of contours cannot be optimized for all sources on a map when there are substantial variations in the background level. Another reason is that visibility of a source on the images is more affected by its maximum surface brightness than by its total flux. This makes it easier to spot a point source than an extended source of equal total flux.

Figure V.D.8 illustrates clearly the wide variety of sources present in the SSS Catalog. Sources like α, ζ and ι are examples of well behaved, simply shaped extended sources. β, δ and θ are less well defined though no less real, and show a transition towards more diffuse, cirrus-like emission. ε, η and κ are examples of double point sources detected as extended emission. All three are flagged in the Catalog as possibly due to a double source at 25 μm. Finally, γ is a well defined extended source confused with two nearby point sources.

Even a casual examination of Figure V.D.7 reveals that Catalog sources correspond almost always to relatively isolated sources with successive sightings that coincide closely. Areas with a large number of FISES detections spread around betray complex emission structure which yields detections that vary with scan angle. These detections are removed mostly by *cluster analysis*. But in spite of this confusion processing, some chains of sources remain in the SSS Catalog which are a result of Galactic cirrus. An example of such a chain can be found at 100 μm (Figure V.D.6) running from near (l,b)=(60.3°,-1.5°) to near (l,b)=(59.3°,-1.5°).

In summary, the SSS Catalog has identified true extended sources and double point sources of acceptable quality in this area of the Galactic plane. It provides an incomplete census of such sources because of the restrictions imposed by confusion. Completeness and reliability are discussed in Chapter VI. It should be abundantly clear that absence of a SSS Catalog entry in no way implies absence of emission. The IRAS Catalogs and Images provide complementary descriptions of the infrared sky and they should all be considered, especially in confused regions.

VI. COMPLETENESS AND RELIABILITY

The *reliability* of a source is defined here as the probability that a Catalog entry describes emission from an inertially fixed astronomical source of a size resolvable by IRAS. Ideally, an entry in this Catalog gives the position of a resolved source and its flux as measured in an aperture of about $8'$ diameter after removal of the local sky brightness. The fundamental goal in producing the SSS Catalog was to generate a list of highly reliable objects at the necessary expense of completeness. The average reliability of the Catalog is estimated to be 97% (Section A).

The *completeness* of the Catalog at a given flux density is defined as the fraction of all real sources in the part of the sky surveyed by IRAS that are included in the Catalog. Because of the inhomogeneous nature of the sky, the survey, and the data analysis procedures, it is impossible to estimate the completeness of the Catalog. As discussed in Section B, the completeness appears to be uniform at high flux densities and to drop rapidly below flux densities of 10 Jy at 12, 25, and 60 μm and below 20 Jy at 100 μm. These limits can be considerably higher in the vicinity of the Galactic Plane.

Users should be aware that reliability is a function of source parameters such as flux and quality class. An entry with a high quality 50 Jy flux at 25 μm is clearly more than 97% reliable, whereas an intermediate quality 4 Jy flux may be closer to the 90% reliability characteristic of entries at the threshold.

A. Reliability

The estimation of reliability was based on a careful analysis of a sample of Catalog entries which were inspected individually to decide on their reliability. From these inspections a simple model was constructed for the incidence of spurious sources as a function of brightness. The number of unreliable sources was integrated over the flux distribution to yield a total unreliability for the Catalog.

Unbiased observers familiar with IRAS raw data inspected detector output streams from scans over the position of each entry in the sample. They estimated whether these data justified a Catalog entry, or whether the entry should be dismissed as unreliable (See also IV.A.3). Since reliability problems were expected to be worse at the detection thresholds, the entries to be inspected were chosen to be of marginal quality, i.e., selected to have an intermediate repeatability (IV.B.2.b) with N/M = 2/2 or 2/3, and relatively low flux densities; such entries would appear in the Catalog only if they passed the intrinsic (flux threshold) test (IV.B.2), and would always carry an intermediate quality flag. The results of the detailed inspection of about 300 candidate SSS entries are shown in Table VI.A.1, which gives for each band and flux density the number of sources inspected and of those found unreliable. Note that barely resolved double or multiple sources and well defined hot spots in cirrus were deemed acceptable for the purposes of this test since they represent recognizable, fixed, resolved features on the sky.

Six of 102 sources at the threshold (3, 3, 2.5 and 5 Jy at 12, 25, 60 and 100 μm) were deemed unreliable. The number dropped rapidly with increasing brightness. The flux dependence of unreliability was approximated by the flux distribution of the rejected low N/M entries, which went like $N(f_\nu)df_\nu \sim f_\nu^{-2.5}df_\nu$. Assuming, conservatively, an unreliability at the threshold of 10%, and a number

TABLE VI.A.1 Data Used in Reliability Estimate

Band (μm)	Flux Density (Jy)	Number Inspected	Number Unreliable
12	2.0	33	13
12	3.0	26	2
12	6.0	24	0
25	2.0	21	4
25	3.0	20	1
25	10.0	22	0
60	2.5	27	2
60	3.5	27	0
60	30.0	16	0
100	5.0	29	1
100	6.5	30	0
100	85.0	16	0

of unreliable entries dropping like $f_\nu^{-2.5}$ resulted in an estimate of 97% for the reliability of all sources with intermediate N/M. There is evidence in Table IV.A.1 that unreliability drops off more rapidly than in the model, leading to even higher estimates for the integrated reliability. The reason for these high estimates is in the flux distribution of Catalog sources (Figure V.A.6) which falls off slowly just above the flux threshold and contains relatively large numbers of bright sources which are highly reliable. Since only half the Catalog entries have intermediate N/M and the remaining, high N/M entries must be more reliable, the global reliability of the Catalog should be better than 97%.

B. Completeness

Completeness was not a primary concern in the generation of the Catalog. No estimate is given here for completeness except for some comments on the shape of the flux distributions. These distributions, as can be seen in Figure V.A.6 cannot be described simply in terms of a power law. In the range between roughly 10 and 100 Jy, the power law approximation would have the form $N(f_\nu)df_\nu \sim f_\nu^{-2}df_\nu$ in all bands, as might be expected for a population of Galactic sources (Suppl.VIII). The distributions fall away from this power law approximation at about 10, 10, 7 and 20 Jy respectively for the 12, 25, 60 and 100 μm bands, indicating these flux densities as the levels below which severe incompleteness sets in. Above those levels, it is reasonable to expect, at least at high latitudes, a uniform completeness of unknown value. It is important to note however that completeness is a strong function of position on the sky, as may be clearly seen for instance on Figure V.A.1 where a strong asymmetry in source density near the Galactic plane is quite evident. See discussion in V.A.1 and Suppl.VII.D.6.

In addition to the Galactic plane shadow, several other factors militated against a high or uniform completeness. *Cluster analysis* deleted entries in all regions with source densities exceeding a few per square degree (Suppl.V.E.7). Because *cluster analysis* was carried out before *weeks confirmation*, spurious entries may have linked to reliable sources and caused their deletion. Some relatively isolated pairs of sources could have been deleted as well if they had linked into a large "cluster". *Final source selection* complicated the picture further, deleting many reliable sources along with the unreliable ones. In particular, it deleted (or flagged as low quality) all detections below the flux threshold in that part of the sky surveyed only twice; it deleted half the detections below threshold in the rest of the sky. The damage to completeness was irretrievable because of the variable flux thresholds. See V.D for a detailed examination of the SSS processor performance in a confusion limited region.

VII. FORMATS

The Small Scale Structure Catalog is available in two media, on tape and in print. On tape the Catalog is contained in one file ordered by right ascension, and by declination in case of conflict. The printed version has essentially identical contents to the tape copy, but is organized and formatted differently and shows only one association. In both versions and for each source, data are shown only for those bands where detections have been found and have survived processing through *weeks confirmation.* No upper limits are given where no detections were found; none are given where detections were dropped because of confusion (*cluster analysis*). Absence of data from this Catalog at a given position in a given band does not imply absence of emission, but simply lack of information (see Chapter VI for a discussion of completeness). On the other hand, flags NEARPS, SES1 and HD, which depend only on position in the sky, are always estimated for all four bands, at the mean position of each source.

A. Tape Version

In general, the data for each source is organized in three 80-byte records followed by a variable number of association records; Table VII.A.1 shows the detailed organization. The first two records contain basic parameters and warning flags referring to the band-merged source, whereas the third record is made up of four 20-byte components containing position and quality flags for each of the bands. When present, the 12 μm data is inserted into the first 20 bytes of the record; the 25, 60, and 100 μm data go into the second, third, and last block of 20 bytes in the record, respectively. Quarters corresponding to bands absent from the source are filled with blanks. The fourth and subsequent records contain data on positional associations between the Catalog source and objects in a variety of astronomical catalogs listed in Suppl.V.H.9. Each record holds data on two associations, in two 40-byte blocks. All data entries for each source are described below in their order of appearance in Table VII.A.1.

Source Name: NAME

The letter "X" prefixes all names in this Catalog to distinguish them from Point Source names. The name is then derived from the position by combining the hours and minutes from the right ascension with the sign, degrees, and decimal fraction of degrees from the declination. In case of name duplication the letters "A", "B", etc. are appended to the name in order of increasing right ascension, and of increasing declination in case of a tie.

Band Merging Flag: BMFLG

The *band merging* flag gives the number of bands in which the source has an entry in the third record (regardless of flux quality in these bands), together with indications on the *band merging* processing history for that source. BMFLG=C or D indicates 3 or 4 mutually confirming (Suppl.V.E.6) components in the source. BMFLG=I, J, K or L indicates 1, 2, 3 or 4 components in a source having experienced *band merging* complications and having survived the modified *final selection* discussed in IV.B.3.a.

Position: RAHR, RAMIN, RASEC, DSIGN, DECDEG, DECMIN, DECSEC

Source position is the simple mean of the positions of all the individual band components in the source regardless of the individual flux quality flags. It is given in equatorial coordinates for the 1950 equinox. Positional accuracy is discussed in V.C.2.

Number of Sightings: NH(4)

The number of survey coverages contributing a sighting to the weeks confirmed source is given for each band as a single character. The order for this and similar arrays in the Catalog is from 12 μm (subscript = 1) to 100 μm (subscript = 4).

Flux Density: FLUX(4)

An estimate of the spatially integrated flux density from the source is given in Jansky for each band, with three digit precision. This is transformed from the fluxes in the IRAS bands assuming a spectrum with $\nu \times f_\nu$ = constant (see Suppl.VI.C). To obtain the actual flux density at the nominal wavelength for each band, FLUX must be corrected according to the prescription in Suppl.VI.C, or by using Table VI.C.6, which is reproduced at the end of this volume. The estimation algorithm is described in Suppl.V.E.3, 4 and 5; calibration in II.C. Accuracy is discussed in V.C.1.

Optical Cross Talk Flag: XTALK(4)

This quantity indicates the extent and kind of cross-talk for which each component in the source was flagged (the printed version gives only a summary described under "FCAT" below). As discussed in IV.B.2.a above, the processor accumulated the number NXT of detections that might have been caused simply by optical cross-talk, along with the number NS of detections. If NXT=0 then XTALK=0 for that band. If NXT>0, and either (i) (NS-NXT)>2, or (ii) (NXT/NS)<2/3 then XTALK=1 for moderate cross-talk. If NXT>0, and neither (i) nor (ii) is true then XTALK=2 for severe cross-talk. If in addition a band component was flagged for cross-talk at the level of *final source selection*, then XTALK is increased by 4. Note that the component is given a low quality rating if XTALK>0.

Near-by Point Sources: NEARPS(4)

This flag gives a count of all weeks-confirmed point sources (regardless of whether or not they are included in the Point Source Catalog) in each band within a 9′ radius of the mean position of the SSS Catalog source. NEARPS=1 indicates most often that the emission has been detected as a point source as well as here. Larger values are a warning of possible confusion affecting the source, or an indication that this source combines emission from two or more barely resolved point sources (see DBLPS below). NEARPS is given as a single character per band, and denoted by a letter when it exceeds 9 ("A" for 10, "B" for 11, etc.).

Near-by Intermediate Small Extended Sources: SES1(4)

This flag gives a count in each band of all hours-confirmed entries in FISES (Suppl.V.E.3) within a 9′ radius of the mean position of the source. In clean sky, SES1 would be equal to NH; larger values implying a higher density of detections, either spurious or due to complex structure, point to areas where *cluster analysis* was active. Large values of SES1 for a band not represented in the source may indicate reliable extended detections discarded in subsequent processing. SES1 appears as a single character per band in the same notation as NEARPS.

Cirrus Indicator: CIR

This cirrus flag gives the number of point source detections at 100 μm only, hours confirmed but not necessarily weeks confirmed, within a 30′ radius of the SSS source. Cirrus is rich in structure on all

scales, and may supply a 100 μm or a 60 μm component to a source detected at other wavelengths, or may combine with the 100 μm or 60 μm emission from a source and severely compromise its flux measurement. Values of CIR above six invite caution in interpreting both 60 and 100 μm detections.

High Source Density Flag: HD

This single character flag denotes whether the source falls in a region of high source density in the sense of Point Source clean-up processing (Suppl.V.H.6). This flag was not used in SSS processing, but warns against confusion by pointing out areas where point source density may exceed the resolving capability of the instrument. When the flag is written out in binary notation the least significant bit refers to the 12 μm band, and is set to one in high density regions. The next bit refers to the 25 μm band, and so on. Values greater than 9 are denoted by letters as for NEARPS (see Table Suppl.X.B.2).

Double Point Source Flag: DBLPS

This flag indicates the possibility that this Catalog source is the combination of two point sources (see IV.B.2.e for definition). The indication is given for each band, encoded as for HD, with the bit set to one when the possibility exists for the corresponding band. This flag is estimated only for bands represented in the source, regardless of the flux quality in these bands.

Coincident Point Source: PTSRC

A small extended source will often trigger the point source detection processor, either because it is still small enough to produce an acceptable fit to the template (bright point sources with low correlation coefficients are examples of this), or because it actually contains one or more point-like components. When an entry from the Point Source Catalog lies within a distance D of the SSS Catalog source position it is identified as a point source counterpart to the SSS Catalog source, and its IRAS name is entered in this column. The distance D used is half the largest value of UNC (V.C.3) among the bands in the source. When two or more counterpart candidates are found, the nearest one is chosen, and an asterisk precedes PTSRC as a warning. Clearly, the source descriptions here and in the Point Source Catalog are complementary, and neither can be ignored.

Inferred Source Size: PSIZ(4)

An estimate of the source size is given in deci-arcminutes for those bands where the Point Source counterpart is detected. The estimate is obtained from

$$\mathrm{PSIZ}_i = \mathrm{FWHM}_i \times (\mathrm{SSSFLUX}_i/\mathrm{PTSRCFLUX}_i)^{1/2} \ ,$$

where FWHM_i is the full width at half maximum of a point source in band i, namely 0.82′, 0.84′, 1.44′, and 3.14′, respectively, at 12, 25, 60, and 100 μm; SSSFLUX and PTSRCFLUX are the fluxes in the two catalogs. See V.B.1 and V.C.3 for details and a discussion of accuracy.

Positional Associations: NID, IDTYPE

Positional associations between objects in the Small Scale Structure Catalog and objects in astronomical catalogs were obtained following the same strategy used for Point Sources (Suppl.V.H.9). The only difference is that the search radius around sources in this Catalog is never less than 120″. NID is the total number of matches found. IDTYPE ranges from 1 to 4 to indicate an association found in an

extragalactic catalog (1), a stellar catalog (2), other catalogs (3), or matches in multiple types of catalogs (4). Data on each associated object appear in a 40 byte block whose format is detailed further below. Each record starting with the fourth data record for the source contains two of these blocks. The format for the association data is almost identical to the Point Source Catalog (see Suppl.X.B.1).

Flux Quality Flag: FQLT

This is the quality class assigned to the band component by the scheme described in Chapter IV and Table IV.A.1. High, intermediate and low qualities are denoted, respectively, by A, B, and F. Starting with this flag, data for each band appear separately in the corresponding quarter of the third data record for the source.

Final Catalog Selection Flags: FCAT

The results of the three main stages of *final selection* (Figure IV.B.1) are presented in this flag which appears in the tape version as a single character ranging from 0 to V, and is decomposed in the printed version into three parts (VII.B). When FCAT is written out in binary notation, the least significant bit indicates the result of the flux test (IV.B.2.d), and is set if failed; the next bit refers to the detection count test (IV.B.2.c), and is set if failed. The next two bits refer to the repeatability test (IV.B.2.b), and signal one of four possible outcomes: 00 for intermediate values of N/M except $N/M = 2/2$; 01 for low N/M; 10 for high N/M; and 11 for $N/M = 2/2$ (Table IV.B.3). The most significant bit in FCAT is set if the detection is flagged for cross-talk of any kind (IV.B.2.a). Table VII.A.2 shows all possible values of FCAT, their representations both on tape and in print, and their meaning.

Right Ascension Offset: DRA

This gives in seconds the amount to add to the mean right ascension of the source (shown in the first record) to obtain the right ascension measured for the emission in this band.

Declination Offset: DDEC

This gives in arcseconds the amount to add to the mean declination of the source (shown in the first record) to obtain the declination measured for the emission in this band.

Positional Uncertainty from Intensity Distribution: UNC

The second moments about major and minor axes of the roughly modeled intensity distribution are estimated as explained in Suppl.V.E.3, and their geometric mean is given here as a diameter in deci-arcminutes. Because of the coarse grid used in the definition, UNC is best interpreted as a positional uncertainty, namely the 95% confidence diameter for the position in this band (see V.C.3 for a discussion).

Number of Detections: NS

This total number of seconds-confirmed detections in the source is accumulated through *cluster analysis* and *weeks confirmation*, and includes detections that failed to seconds-confirm because of a failed detector.

Association Record: CATNO, SOURCE, TYPE, RADIUS, POS, FIELD1, FIELD2, FIELD3

For each match in an astronomical catalog, CATNO is the number identifying that catalog in Tables Suppl.V.H.1 and Suppl.X.B.4. SOURCE is the name of the object in that catalog, and TYPE its

character or spectral or morphological type if available. RADIUS is the distance in arcseconds from the IRAS position to the associated object. POS is the position angle measured in degrees East of North of the direction from the IRAS source to the associated object. FIELD1-3 carry values depending on the catalog in question (Table Suppl.X.B.4). Typically FIELD1 and FIELD2 contain magnitudes in decimag, and FIELD3 a size in arcseconds.

B. Printed Version

The printed version of the Small Scale Structure Catalog contains essentially the same data as the tape version, but the contents are reorganized for easy visual inspection. Each source occupies one to four lines of print, one line for each band component in the source. The first line holds data pertaining to the source as a whole, plus details for the shortest wavelength band, whereas additional lines provide details for the remaining bands. These details are: band identifier and *band merging* warning flag, flux density and flux quality flag, number of sightings, number of detections, right ascension and declination offsets, positional uncertainty, *final source selection* flags, and source size estimate. Specific quantities are always given in the same units in both versions, and usually printed with the format shown in Table VII.A.1, except where noted. Galactic coordinates are given only in the printed version. When associations have been found in more than one astronomical catalog, only one of the matches is printed, following the rules detailed in Suppl.X.B.2. Figure VII.B.1 illustrates the printed format of the Catalog. All data entries are given below, in their order of appearance in print from left to right, with comments on differences between printed and tape versions.

Source Name: NAME

Equatorial Coordinates: RAHR, RAMIN, RASEC, DSIGN, DECDEG, DECMIN, DECSEC

Galactic Coordinates: GLON, GLAT

These are given in degrees to a precision of 1°.

Band Identifier and Band Merge Warning Flag: BAND

On each line, at the beginning of the band component block, the band is identified by its nominal wavelength in micrometers. The *band merging* flag BMFLG does not appear explicitly in print, but a warning flag is printed whenever BMFLG=J, K, L, 3 or 4, to indicate an unsatisfactory outcome of *band merging*. The warning flag is an asterisk instead of a blank following the band identifier for each band in the source.

Flux Density and Quality Class: FLUX DENSITY

The total emission is given as a flux density estimated to a precision of 1 Jy or three significant digits. The flux quality flag follows immediately, denoted by a blank, "B", and "F" respectively for high, intermediate, and low.

Number of Sightings: NH

Number of Detections: NS

Right Ascension and Declination Offsets: DRA and DDEC

Positional Uncertainty from Intensity Distribution: UNC

Final Catalog Selection Flags: FCAT

This flag summarizes the results of the three main stages of *final selection*, using the notation detailed in VII.A and Table VII.A.2. In the printed version, FCAT appears in three columns labeled X, E, and I. I combines the two least significant bits in FCAT and ranges from 0 to 3 to signal the result of the intrinsic test; the next two bits in FCAT are combined into E to signal the result of the extrinsic test; finally cross-talk (i.e. XTALK>0) is signaled by an "X" instead of a blank in the X column. This flag marks the end of the block which is repeated for each band component; PSIZ is the only remaining quantity that appears on multiple lines for multi-band sources.

High Source Density Flag: HD

Near-by Point Sources: NEARPS(4)

Near-by Intermediate Small Extended Sources: SES1(4)

Cirrus Indicator: CIR

Double Point Source Flag: DBLPS

Coincident Point Source: PTSRC

Inferred Source Size: PSIZ

Positional Associations Block: NID, CAT, NAME and TYPE, RAD, and MAG

Only one of the total number (NID) of associations found is printed, slightly shortened from the 40-byte association block appearing in the tape. CAT identifies the catalog (Tables Suppl.V.H.1 and Suppl.X.B.4); NAME identifies the object within that catalog, and TYPE gives its spectral or morphological type as available there. RAD is the distance from IRAS source to associated object in arcseconds. FIELD1 (usually a magnitude in deci-mag units) appears as MAG when available, for all catalogs except 2 and 19, from which FIELD2 appears in MAG. When NID is greater than one, the association printed is chosen according to the priority scheme specified in Suppl.X.B.2.

TABLE VII.A.1 Format of the Small Scale Structure Catalog Tape

Start Byte	Name	Description	Units	Format
0	NAME	IRAS source name	---	10A1
10	BMFLG	Number of bands in source and *band merging* warning flag	---	A1 [1]
11	RAHR	Right Ascension (1950)	Hours	I2
13	RAMIN	Right Ascension (1950)	Minutes	I2
15	RASEC	Right Ascension (1950)	Seconds	F4.1
19	DSIGN	Declination (1950)	---	A1
20	DECDEG	Declination (1950)	Degrees	I2
22	DECMIN	Declination (1950)	Arcminutes	I2

TABLE VII.A.1 Format of the Small Scale Structure Catalog Tape (Continued)

Start Byte	Name	Description	Units	Format
24	DECSEC	Declination (1950)	Arcseconds	I2
26	NH(4)	Number of hours-confirmed sightings	---	4A1
30	FLUX(4)	Averaged, spatially integrated flux density (no color correction)	Jy	4E8.2 [1]
62	XTALK(4)	Cross-talk flag	---	4A1 [1]
66	NEARPS(4)	Number of near-by weeks-confirmed point sources	---	4A1
70	SES1(4)	Number of near-by FISES entries	---	4A1
74	CIR	Number of hours-confirmed, 100 μm only point sources	---	I2
76	BLANK	Four spare bytes	---	4A1
		(----------new record----------)		
80	HD	High source density flag (encoded, one bit per band)	---	A1
81	DBLPS	Possibility this is double point source (1 bit per band)	---	A1
82	PTSRC	Name of IRAS Point Source counterpart and conflict flag	---	12A1
94	PSIZ(4)	Size estimate from comparison of FLUX with PTSRC flux	Deciarc-minutes	4I3
106	NID	Number of associations	---	I2
108	IDTYPE	Type of objects associated	---	I4
112	BLANK	48 spare bytes	---	48A1
		(----------new record----------)		
160-179		(blank if no 12 μm component)		
160	FQLT	12 μm flux quality class	---	A1 [1]
161	FCAT	12 μm *final selection* flags	---	A1 [1]
162	DRA	Right ascension offset from mean position to 12 μm	Seconds	F6.1
168	DDEC	Declination offset from mean position to 12 μm	Arcseconds	I4
172	UNC	95% confidence diameter for position at 12 μm	Deciarc-minutes	I3

TABLE VII.A.1 Format of the Small Scale Structure Catalog Tape (Continued)

Start Byte	Name	Description	Units	Format
175	NS	Number of individual detections in 12 μm component	---	I3
178	BLANK	Two spare bytes	---	2A1
180-199		25 μm equivalent of bytes 160-179 (blank if no 25 μm component)		
200-219		60 μm equivalent of bytes 160-179 (blank if no 60 μm component)		
220-239		100 μm equivalent of bytes 160-179 (blank if no 100 μm component)		
		(----------new record----------)		
240-279		(blank if no associations found)		
240	CATNO	Catalog identifier	---	I2
242	SOURCE	Object ID in that catalog	---	15A1
257	TYPE	Object type in that catalog	---	5A1
262	RADIUS	Distance from IRAS source to associated object	Arcseconds	I3
265	POS	Position angle from IRAS source to object	Degrees E of N	I3 [1]
268	FIELD1	Object data field Nr 1 (magnitude or other)	[2]	I4 [1]
272	FIELD2	Object data field Nr 2 (magnitude or other)	[2]	I4 [1]
276	FIELD3	Object data field Nr 3 (magnitude or other)	[2]	I4 [1]
280-320		Repeat of 240-279 for second association (blank if only one association found)		
		(----------new record----------)		
etc.		Continue in 40 byte blocks until all NID associations have been shown.		

[1] This quantity appears with a different format or representation, or is omitted in the printed version of the catalog.

[2] The definition and units of the quantities in FIELD1-3 depend on the individual catalog in which the association is found. See Table Suppl.X.B.4.

TABLE VII.A.2 Interpretation of Final Source Selection Flag

Optical Cross-Talk	N/M Test [1]	Detection Count	Flux Threshold	Tape Version		Printed FCAT XEI	Binary Notation FCAT
				FQLT	FCAT		
NO	MED*	PASS	PASS	B	0	00	00000
NO	MED*	PASS	FAIL	F	1	01	00001
NO	MED*	FAIL	PASS	F	2	02	00010
NO	MED*	FAIL	FAIL	F	3	03	00011
NO	LOW	PASS	PASS	F	4	10	00100
NO	LOW	PASS	FAIL	F	5	11	00101
NO	LOW	FAIL	PASS	F	6	12	00110
NO	LOW	FAIL	FAIL	F	7	13	00111
NO	HIGH	PASS	PASS	A	8	20	01000
NO	HIGH	PASS	FAIL	B	9	21	01001
NO	HIGH	FAIL	PASS	B	A	22	01010
NO	HIGH	FAIL	FAIL	B	B	23	01011
NO	2/2	PASS	PASS	B	C	30	01100
NO	2/2	PASS	FAIL	F	D	31	01101
NO	2/2	FAIL	PASS	F	E	32	01110
NO	2/2	FAIL	FAIL	F	F	33	01111
YES	MED*	PASS	PASS	F	G	X00	10000
YES	MED*	PASS	FAIL	F	H	X01	10001
YES	MED*	FAIL	PASS	F	I	X02	10010
YES	MED*	FAIL	FAIL	F	J	X03	10011
YES	LOW	PASS	PASS	F	K	X10	10100
YES	LOW	PASS	FAIL	F	L	X11	10101
YES	LOW	FAIL	PASS	F	M	X12	10110
YES	LOW	FAIL	FAIL	F	N	X13	10111
YES	HIGH	PASS	PASS	F	O	X20	11000
YES	HIGH	PASS	FAIL	F	P	X21	11001
YES	HIGH	FAIL	PASS	F	Q	X22	11010
YES	HIGH	FAIL	FAIL	F	R	X23	11011
YES	2/2	PASS	PASS	F	S	X30	11100
YES	2/2	PASS	FAIL	F	T	X31	11101
YES	2/2	FAIL	PASS	F	U	X32	11110
YES	2/2	FAIL	FAIL	F	V	X33	11111

[1] In the repeatability test, "MED*" indicates that N/M is in the intermediate range (Table IV.B.2) excluding $N/M = 2/2$; this latter case is indicated by "2/2".

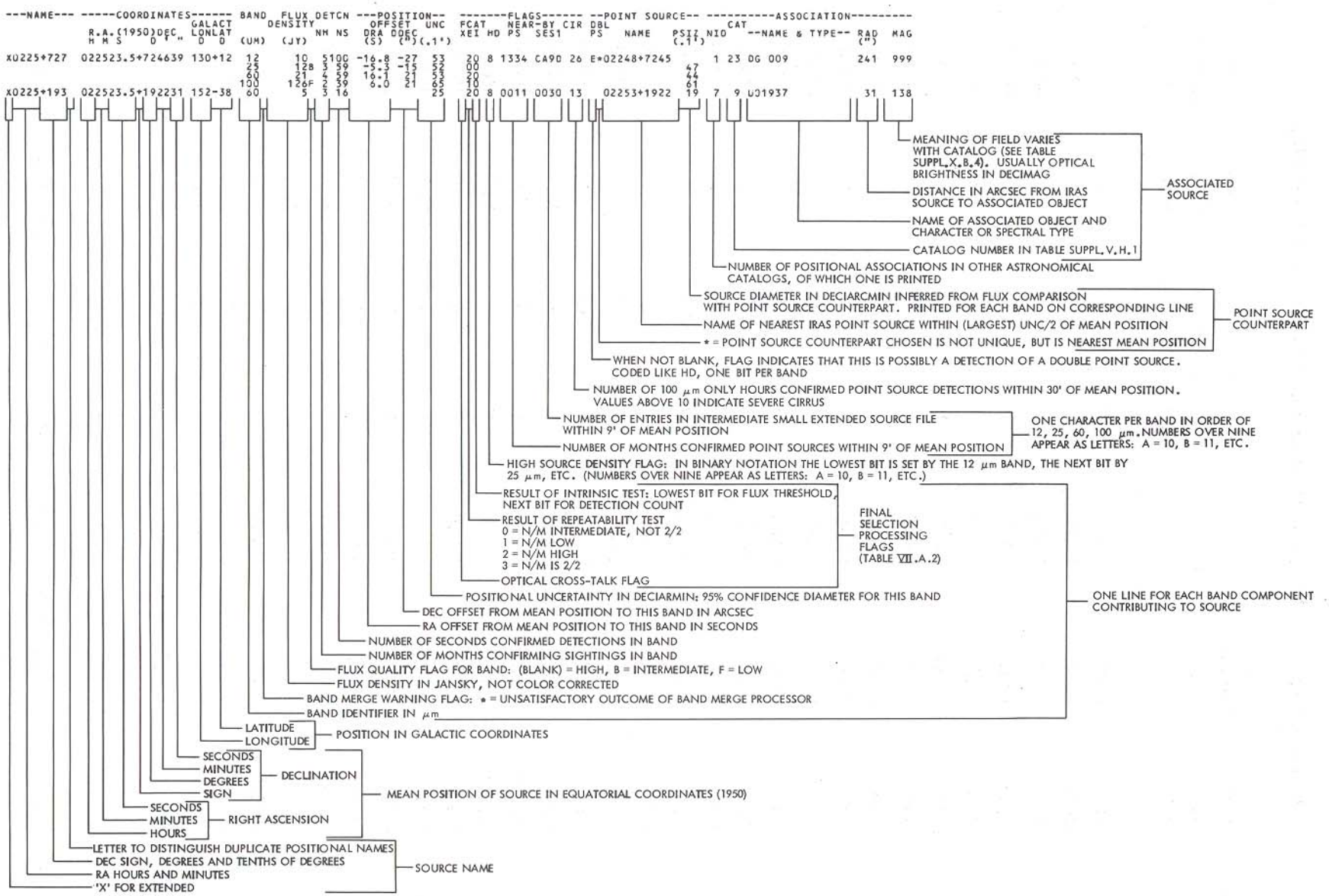

Figure VII.B.1 Explanation of format of printed version of Small Scale Structure Catalog.

VIII. ACKNOWLEDGEMENTS

Many people have contributed to the success of IRAS. They are acknowledged in Suppl.XII. This document was assembled with the assistance of J. Boyd Anderson and R. Dumas.

People whose contributions to the realization of this Catalog were of particular importance are: G. Kopan and E. Rolfe for *source detection* and *source construction*, J. Fowler for *cluster analysis* and *weeks confirmation*, C. Oken for *band merging*, J. Chillemi for associations, R. Benson and T. Conrow for *final source selection*, and T. Chester, J. Bennett, D. Gregorich and A. Leene for Catalog analysis.

Authors:

George Helou, C. Beichman, R. Benson, T. P. Conrow and D. Gregorich

TABLE Suppl.VI.C.6 Color Correction Factors, K[1]

INTRINSIC POWER LAW[2]	RATIO OF FLUX DENSITIES BEFORE COLOR-CORRECTION			CORRECTION FACTOR			
α	$\frac{f_\nu(12\ \mu m)}{f_\nu(25\ \mu m)}$	$\frac{f_\nu(25\ \mu m)}{f_\nu(60\ \mu m)}$	$\frac{f_\nu(60\ \mu m)}{f_\nu(100\mu m)}$	K(12 μm)	K(25 μm)	K(60 μm)	K(100 μm)
-3.0	0.113	0.063	0.21	0.91	0.89	1.02	1.02
-2.5	0.162	0.102	0.275	0.92	0.91	1.00	1.01
-2.0	0.232	0.164	0.355	0.94	0.93	0.99	1.00
-1.5	0.333	0.262	0.460	0.97	0.96	0.99	1.00
-1.0	0.480	0.417	0.600	1.00	1.00	1.00	1.00
-0.5	0.694	0.662	0.786	1.04	1.04	1.02	1.00
0.0	1.005	1.045	1.037	1.10	1.10	1.05	1.01
0.5	1.459	1.642	1.378	1.17	1.16	1.09	1.02
1.0	2.123	2.567	1.843	1.25	1.23	1.15	1.04
1.5	3.094	3.992	2.484	1.35	1.32	1.23	1.06
2.0	4.519	6.170	3.373	1.47	1.41	1.32	1.09
2.5	6.610	9.480	4.617	1.61	1.53	1.44	1.12
3.0	9.681	14.475	6.370	1.78	1.67	1.59	1.16

INTRINSIC	RATIO OF FLUX DENSITIES BEFORE COLOR-CORRECTION			CORRECTION FACTOR			
TEMP (K)	$\frac{f_\nu(12\ \mu m)}{f_\nu(25\ \mu m)}$	$\frac{f_\nu(25\ \mu m)}{f_\nu(60\ \mu m)}$	$\frac{f_\nu(60\ \mu m)}{f_\nu(100\ \mu m)}$	K(12 μm)	K(25 μm)	K(60 μm)	K(100 μm)
10000	4.345	6.050	3.350	1.45	1.41	1.32	1.09
5000	4.172	5.931	3.327	1.43	1.40	1.32	1.09
4000	4.086	5.872	3.316	1.42	1.40	1.31	1.09
3000	3.944	5.773	3.297	1.41	1.39	1.31	1.09
2000	3.666	5.578	3.259	1.38	1.38	1.31	1.09
1000	2.891	5.005	3.145	1.27	1.34	1.29	1.08
800	2.545	4.730	3.088	1.22	1.32	1.28	1.08
600	2.036	4.287	2.995	1.15	1.29	1.27	1.08
500	1.692	3.950	2.920	1.09	1.26	1.26	1.08
400	1.272	3.478	2.810	1.01	1.22	1.24	1.08
300	0.785	2.780	2.630	0.92	1.15	1.21	1.07
290	0.734	2.693	2.606	0.91	1.15	1.21	1.07
280	0.684	2.602	2.580	0.90	1.14	1.20	1.07
270	0.633	2.506	2.553	0.89	1.13	1.20	1.07
260	0.583	2.407	2.523	0.88	1.12	1.19	1.07
250	0.534	2.304	2.491	0.87	1.11	1.19	1.07
240	0.486	2.196	2.457	0.86	1.09	1.18	1.07
230	0.438	2.084	2.420	0.85	1.08	1.18	1.07
220	0.392	1.967	2.381	0.85	1.07	1.17	1.07
210	0.347	1.845	2.338	0.84	1.06	1.16	1.06
200	0.304	1.719	2.291	0.83	1.04	1.16	1.06
190	0.263	1.589	2.240	0.83	1.02	1.15	1.06
180	0.224	1.455	2.184	0.83	1.01	1.14	1.06
170	0.188	1.317	2.124	0.83	0.99	1.13	1.06
160	0.154	1.176	2.057	0.84	0.97	1.12	1.06
150	0.124	1.034	1.983	0.85	0.95	1.11	1.05
140	0.097	0.892	1.901	0.87	0.93	1.09	1.05
130	0.073	0.751	1.810	0.90	0.91	1.08	1.05
120	0.053	0.614	1.709	0.94	0.89	1.06	1.04
110	0.036	0.484	1.595	1.01	0.86	1.04	1.04
100	0.023	0.363	1.468	1.12	0.84	1.02	1.04
95	0.018	0.307	1.400	1.19	0.83	1.01	1.03
90	0.014	0.256	1.326	1.28	0.83	1.00	1.03
85	0.010	0.208	1.249	1.39	0.82	0.99	1.03
80	0.007	0.165	1.168	1.54	0.81	0.97	1.02
75	0.005	0.127	1.082	1.74	0.81	0.96	1.02
70	0.003	0.095	0.993	2.01	0.81	0.95	1.01
65	0.002	0.067	0.898	2.40	0.82	0.94	1.01
60	0.001	0.045	0.801	2.97	0.83	0.93	1.00
55	---	0.028	0.700	3.86	0.86	0.92	1.00
50	---	0.016	0.597	5.35	0.90	0.91	0.99
45	---	0.008	0.493	8.09	0.97	0.92	0.98
40	---	0.003	0.391	13.79	1.08	0.93	0.98

[1] f_{ν_0}[actual] = f_{ν_0}[quoted]/K (See Suppl.VI.C.3); spectral response given in Table Suppl.II.C.5.

[2] $f_\nu = \nu^\alpha$